POLITECNICO DI MILANO

Scuola di Ingegneria Industriale e dell'Informazione

Corso di Laurea Magistrale in Ingegneria Energetica

Dipartimento di Energia

SEMI-TRANSPARENT FLAT-PLATE PULSATING HEAT PIPE: EXPERIMENTAL STUDY IN MICROGRAVITY

Supervisor: Prof. Lucio Araneo

Thesis of:

Pietro Marzorati Matr. 801744

Academic Year 2014 – 2015

Acknowledgments

I would like to express a particular gratitude to Prof. Lucio Araneo who offered me a unique opportunity to join this ambitious project. His clever and decisive support helped me throughout this challenge.
This work has been carried out in the framework of the Institut P' CNRS-ENSMA, Université de Poitiers (France).
A special thanks goes to Dr. Vincent Ayel for his fruitful advice in the laboratory and for his care about my accommodation in a foreign country.
Finally, I thank Dr. Cyril Romestant and all the laboratory technicians of the Département Thermique for their essential help in the building process.

Riassunto esteso

In questa tesi viene descritta la progettazione, costruzione e test svolti su uno scambiatore di calore passivo a transizione di fase: una Pulsating Heat Pipe (PHP) semi trasparente a facce piane.
La PHP è un dispositivo in cui un canale, che può essere un tubo piegato più volte o ricavato all'interno di una piastra metallica come in questo caso, viene riempito parzialmente da un fluido. Una volta che si fornisce calore per mezzo di un riscaldatore, le instabilità generate durante l'evaporazione e la condensazione causano l'oscillazione del fluido (nel caso di canali ad anello anche la circolazione).
L'obiettivo è quello di visualizzare e registrare i diversi regimi di flusso del fluido termovettore (FC-72) in diverse condizioni di accelerazione gravitazionale.
Per poter eseguire questi studi, è stato necessario prender parte alla 62° campagna di volo parabolico organizzata dalla European Space Agency (ESA) ed eseguito da Novespace con sede a Bordeaux (Francia), in cui svolgere test in condizioni di microgravità, iper gravità (circa 1,8g) e gravità normale.
Si è dovuta sviluppare una particolare PHP costituita da una piastra di rame incollata ad un vetro. Nella piastra di rame è stato ricavato un canale ad anello, con un percorso ad "S" che forma 11 curve a U nella zona dell'evaporatore, tra rame e vetro il canale presenta una sezione quadrata di lato 2.5mm (vedi figura 3.4). Un riscaldatore elettrico (Thermocoax con una resistenza di 3,81Ω) è stato unito per brasatura sul retro della piastra di rame (vedi figura 3.9).
Il condensatore è composto da una piastra alettata di alluminio (su cui è fissata la PHP) e due ventole da 132 m^3/h ciascuna, che estraggono l'aria riscaldata dalla zona alettata (vedi figura 3.7).
Un sistema di videocamera ad alta frequenza e specchio è stato utilizzato per registrare il funzionamento della PHP.
La particolarità di questa PHP, oltre al fatto di avere una faccia completamente trasparente, è quella di avere una sezione di canale ampiamente maggiore di quella definita dal diametro critico. Quest'ultimo viene calcolato attraverso un criterio basato sul numero di Bond e per il fluido utilizzato, a una temperatura di 20°C, vale 1,66mm.
Si è fatta questa scelta per poter confrontare il differente funzionamento tra le condizioni di gravità normale e ipergravità (in cui si ha un effetto della capillarità trascurabile) rispetto al funzionamento in microgravità, dove l'effetto della capillarità è preponderante.

Oltre alla PHP, è stato anche indispensabile adattare l'apparato sperimentale contenente tutti gli apparecchi necessari al test, già utilizzato nelle campagne di volo parabolico 58, 59, 60 e 61, modificando o sostituendo alcune parti.
Durante la fase di progettazione, si è dovuto tener conto delle rigide regole di sicurezza imposte da Novespace (Rosier P., 2014) per potere svolgere gli esperimenti durante il volo.
L'incollaggio del vetro sulla piastra di rame è stata la fase costruttiva più delicata. La deposizione della colla sulla piastra è stata effettuata per mezzo di una macchina a controllo numerico, così da ottenere una distribuzione il più omogenea possibile (vedi figura 4.1).
Nella fase di sviluppo del progetto, si è scelto di costruire due PHP utilizzando due colle differenti.
In una è stata utilizzata una resina epossidica (Loctite 3609), caratterizzata da una ottima adesività, un basso degasaggio ma una scarsa elasticità una volta indurita. Questo ha causato, a seguito del processo di indurimento (quattro giorni di permanenza in forno a 70°C), una leggera concavità sulla faccia di rame a causa della sua maggiore dilatazione termica rispetto al vetro. Dato il colore di questa colla, questa PHP verrà definita "Rossa" (vedi figura 4.10).
L'altra PHP è stata invece costruita utilizzando la colla siliconica (Nusil CV7-2289-1P). In questo caso, a seguito del processo di indurimento (48 ore a 70°C), non è stata rilevata alcuna deformazione residua, grazie alla elevata elasticità della colla che assecondava la differente dilatazione termica tra vetro e rame. Dato il colore di questa colla, questa PHP verrà definita "Bianca" (vedi figura 4.13).
Entrambe le PHP sono state testate per quanto riguarda la tenuta al vuoto. La PHP rossa ha presentato una eccellente tenuta alle infiltrazioni. In quella bianca è invece stata rilevata la presenza di gas all' interno dovuta a leggeri trafilamenti d'aria o causata dal degasaggio della colla. E' stato comunque possibile eseguire i test senza influenzarne troppo le prestazioni.
Prima dei test della 62° campagna di volo parabolico, sono state eseguite alcune prove a terra, per una miglior caratterizzazione del dispositivo.
Durante il test con la PHP in posizione verticale ed evaporatore nella parte bassa del dispositivo, il funzionamento è stato equiparabile a quello di un termosifone a transizione di fase. E' stato possibile notare come il vapore generato si muove verso il condensatore al centro del canale, mentre il liquido condensato ritorna nella zona dell'evaporatore lungo le pareti, grazie all'azione della gravità (moto anulare) (vedi figura 5.3).
All'interno della PHP, le temperature erano fortemente disomogenee: passando dalle zone centrali più calde a quelle esterne più fredde (vedi figura 5.2). Questo è dovuto agli effetti di bordo nei lati della piastra di rame e dal forte effetto aletta della piastra di alluminio su cui la

PHP era fissata. Proprio per limitare questo ponte termico, sul supporto di alluminio sono state eseguite due scanalature ai lati della PHP (Vedi Figura 3.8).
Questa disuniformità termica influenzava la distribuzione del fluido all'interno dei canali. Ai lati, dove le temperature erano minori, si è rilevata una maggior presenza di liquido con la possibile situazione di canali completamente pieni di liquido o con una ebollizione di tipo nucleata. Spostandosi verso il centro, la quantità di liquido era sempre minore fino ad arrivare al canale centrale quasi completamente in dry-out, se non per la presenza di un sottile film di condensato (vedi figura 5.3). A causa della larga sezione di canale, il moto a tappi (slug and plug) non è mai stato rilevato.
Questo tipo di funzionamento è stato verificato a vari livelli di potenza e per entrambe le PHP. Con la PHP bianca è stato effettuato anche un test in posizione orizzontale. In questa configurazione l'evaporatore si è portato immediatamente in una condizione di dry-out a causa della gravità orientata perpendicolarmente alla PHP ed alle dimensioni del canale che non hanno permesso l'instaurarsi di un moto a tappi. Tuttavia, grazie alla differenza di pressione all'interno del canale tra la parte alta e la parte bassa del liquido e alla, se pur limitata pressione capillare, parte del liquido è stato spinto dalla zona condensatore alla zona evaporatore, evitando così la crisi termica che avrebbe causato un rialzo repentino delle temperature.
Per via di un problema a seguito dei test a terra sulla PHP rossa, durante i test in volo parabolico si è utilizzata unicamente la PHP bianca.
I test durante i voli parabolici sono stati svolti su tre giornate così suddivisi: test a potenza medio bassa, test a potenza medio alta, test partendo da potenze medie fino ad arrivare alla massima potenza che la PHP è in grado di sopportare prima dell'intervento dei controlli di sicurezza software (Vedi tabella 3).
Durante ciascuno di questi test si sono effettuate 31 parabole durante le quali, per ciascuna parabola, 22 secondi di microgravità sono stati preceduti e seguiti da una condizione di ipergravità (1.8g di accelerazione per 20 secondi ciascuno) (vedi figura 2.7).
Si è notato come il funzionamento in ipergravità sia analogo a quello registrato in condizioni di gravità normale.
Non appena si passava dalla condizione di ipergravità a quella di microgravità, il fluido si disponeva subito in Slug and plug, con l'alternanza di fase liquida e vapore. La zona dell'evaporatore si portava in dry-out, più o meno rapidamente a seconda della potenza fornita. La condizione di dry-out permaneva finché del liquido si portava nella zona dell'evaporatore ed evaporando generava una pressione che spingeva il liquido dei canali adiacenti nell'evaporatore (fase definita come attivazione della PHP) e così via fino all'instaurarsi di una nuova condizione di dry-out (Vedi figure da 6.8 a 6.10). Durante la

microgravità quindi, si è notata una continua sequenza di dry-out e attivazioni, fino al ritorno alla condizione di ipergravità (Vedi figura 6.7).
Un altro risultato notevole durante i test nei voli parabolici, è stata l'osservazione di una progressiva miglior distribuzione del fluido tra i canali, a seguito di vari passaggi in microgravità (vedi figura 6.14). Grazie a ciò, durante la prima serie di parabole nel test a medio alta potenza, si è passati da una condizione di dry-out nei canali centrali e accumulo di liquido nei canali laterali, ad una distribuzione omogenea del fluido. Questo è stato dovuto al fatto che, a seguito della attivazione, la fase liquida veniva portata nei canali adiacenti, che precedentemente si trovavano in condizioni di dry out (Vedi figura 6.16).
Per confrontare le performance della PHP nei diversi test, è stata scelta la resistenza termica equivalente $Req = (Teva - Tcond)/(Q)\ [K/W]$ che indica la capacità del dispositivo di dissipare il calore fornito dal riscaldatore. Questo ha evidenziato un netto peggioramento tra il funzionamento in gravità normale rispetto a quello in microgravità a causa dell'alternanza tra le fasi di dry out e attivazione. La differenza di R_{eq} aumentava con l'aumentare della potenza termica fornita (vedi figura 7.2). Anche il confronto tra il funzionamento in verticale ed orizzontale ha mostrato un netto peggioramento delle prestazioni nel secondo caso. La causa di ciò è stata la formazione del dry out nell'evaporatore che, nel caso della massima potenza testata, faceva registrare un valore di R_{eq} simile a quello del test eseguito con la PHP vuota (vedi figura 7.1).
Questi test hanno portato ad ottenere i risultati desiderati, evidenziando una netta variazione nel funzionamento tra le condizioni di gravità normale e ipergravità e quelle di microgravità. A causa della grande sezione di canale, nelle prime due il funzionamento è stato governato dalle forze di gravità mentre nell'ultima dalla capillarità.

Extended Recap

In this study, it is described the design, the building process and the tests performed on a two phase passive device: a semi-transparent flat-plate Pulsating Heat Pipe (PHP).
The PHP is a heat exchanger, basically made up of a capillary diameter tube bent in an S-shape or sometimes made up of a squared channel engraved in a metal plate (as in this case), partially filled with a fluid.
Some instabilities are generated inside the channels during the evaporation and condensation, causing the oscillation of the working fluid (in case of closed loops also circulation) once a heat flux is supplied.
The objective was to visualize and record the different flow regimes of the working fluid (FC-72) in varied gravity forces.
In order to work out this project, we took part in the 62nd parabolic flight campaign promoted by the European Space Agency (ESA) and performed by Novespace in Bordeaux, where it was possible to perform tests in condition of microgravity, hyper gravity (1,8g) and normal gravity.
It was necessary to develop a special PHP made by a copper plate glued on a glass. . On the copper plate it was engraved a looped channel which had an S-shape forming 11 U-Turns on the evaporator zone. Between copper and glass, the channel presented a square cross-section of 2.5mm each side (see figure 3.4). An electrical heater (Thermocoax with a resistance of 3.81Ω) was fixed on the back of the copper plate by brazing (see figure 3.9).
The condenser was an aluminium heat sink (on which the PHP was fixed) with two fans of 132 m^3/h each, that blowed the heated air off the fin zone (see figure 3.7).
A high frequency recording system together with a mirror was used to record the functioning of the PHP.
The peculiarity of this PHP, beside the fully transparent side, was to have a much larger channel section than the one defined by the critical diameter.
This one was calculated according to a criterion based on the Bond number, which for the FC-72 is 1.66mm at a temperature of 20°C.
This choice was made in order to compare the different functioning between normal and hyper gravity conditions (in which the capillarity force was negligible) and the functioning in microgravity, where the effect of capillarity is prevalent.
Beside the PHP, it was necessary to adapt the experimental rack previously used during the parabolic flight campaign 58, 59, 60 and 61, modifying or replacing some components.

During the phase of design, strict safety rules imposed by Novespace (Rosier P., 2014) had to be observed in order to perform the experiments on the aircraft.
The gluing process of the glass on the copper plate was the most difficult building part. The placing of the glue on the copper plate was done with the help of a computer numerical control machine, in order to get the most homogeneous result possible (see figure 4.1).
During the project development, we chose to build two distinct PHP using two different types of glue.
The first one was glued by an epoxy resin (Loctite 3609), characterized by an excellent adhesiveness, a low outgassing but a poor elasticity once hardened. This caused, after four days curing at 70°C, a slight concavity on the copper side, due to its higher thermal expansion compared to the glass. Because of the colour of this glue, this PHP was called “Red” (see figure 4.10).
The other PHP was glued by a silicon (Nusil CV7-2289-1p). In this case, after the curing process (48 hours at 70°C), it was not noticed any deformation. This was because of the high elasticity of this glue, which balanced out the different thermal expansion between copper and glass. Because of the colour of this glue, this PHP was called “White” (see figure 4.13).
Both the PHP were tested on the capability to maintain the vacuum inside the channel and potential leakage. The red PHP revealed an excellent leakage proof ability. In the white one it was detected the presence of gasses inside the channels due to a small leakage or to some outgassing of the glue. Anyway, it was possible to perform tests without influencing the performances.
Some ground tests were performed before the 62nd parabolic flight campaign for a deeply characterization of the device.
During the tests with the PHP in a vertical position bottom heated, it behaved like an interconnected two-phase thermosiphon. It was possible to notice how the vapour generated in the evaporator moved to the condenser in the centre of the channel, while the condensed liquid returned on the evaporator zone along the channel walls thanks to the gravity force (annular flow) (see figure 5.3).
Inside the PHP the temperature was strongly irregular, with the central zone hotter than the sides (see figure 5.2). This was mainly caused by a strong fin effect on the side of the heat sink, which went on until the vertical support of the assembly. In order to reduce this undesirable effect, two long slots were machined in the aluminium of the heat sink, just at the sides of the copper plate (see figure 3.8).
This thermal non uniformity strongly influenced the fluid distribution inside the channels. On the sides, where the temperature was lower, it was noticed a higher presence of liquid with

some channels sometimes completely filled with it (liquid storage) or in a pool boiling condition. The amount of liquid decreased moving towards the centre where only a liquid film evaporation was detected (see figure 5.3). Due to the large channel section, the slug and plug flow never set up.

This kind of functioning was verified for different heat power levels and for both the PHP.

A test with the white PHP in horizontal position was also carried on.

With this configuration, the evaporator zone went immediately in dry-out, because of the gravity perpendicular to the PHP and for the dimension of the channels which did not allow the slug and plug motion. However, thanks to the difference of pressure inside the liquid due to the gravity, added to the small capillary pressure, some liquid was pushed to the evaporator zone, avoiding the unwanted thermal crisis.

Due to a problem occurred to the red PHP after a ground test, during the test in parabolic flight only the white PHP was used.

The tests in parabolic flight, were performed during three days divided in: test at mid-low power, test at medium-high power and test at maximum power allowed by the PHP before the action of the security system (see table 3).

During each test, 31 parabolas were performed. For each parabola, 22 seconds of microgravity were preceded and followed by 20 seconds of hyper gravity (1.8g) (see figure 2.7).

It was noticed that the functioning in hyper gravity was similar to the normal gravity one.

As soon as the microgravity condition was established, the fluid set up in slug and plug. The evaporator zone went in dry out more or less fast depending on the power level. The dry out condition persisted until some liquid went on the evaporator zone. Its evaporation caused a local increase of pressure which pushed the liquid of the adjacent channels into the evaporator (phase identified as activation of the PHP) and so on until the next dry out (see figure 6.8 and 6.10). The microgravity condition was characterized by this sequence of dry out and activations until the return in hyper gravity (see figure 6.7).

Another remarkable result during the parabolic flight, was the gradual better distribution of the fluid among the channels after some passages in microgravity (see figure 6.14). Thanks to this, during the first series of parabolas in the medium-high power test, the fluid distribution inside the PHP went from a dry out and liquid storage condition to a more homogeneous condition. After the activation, in fact, the liquid was pushed into the adjacent channels which were before in a dry out condition (see figure 6.16).

To compare the performance of the PHP in the different tests, it was chosen the equivalent thermal resistance $Req = (Teva - Tcond)/(Q)\ [K/W]$. It represents the capacity of the device to dissipate the heating flux transferred to the fluid on the evaporator zone. Req

highlighted a clear decrease of functioning in normal gravity compared to microgravity because of the succession of dry out and activation phases. The difference of Req increased with the increasing of the heat power (see fig 7.2).

The comparison between vertical and horizontal position showed a clear decrease of the performance in the second case. This was due to the dry out in the evaporator, which, at the maximum tested power, registered a Req value close to the one with the empty PHP.

These tests led to the desired results, highlighting a clear difference of functioning between normal and hyper gravity condition and the microgravity one. Due to the large channel section, in the first two conditions, the functioning was ruled by the body forces, while in microgravity by the capillarity.

Index

Sommario

In questo elaborato vengono descritti ed analizzati i risultati ottenuti a seguito di diversi test su di uno scambiatore di calore passivo a transizione di fase, una Pulsating Heat Pipe (PHP) semi trasparente a facce piane. Questo dispositivo viene testato simulando diversi carichi termici in diverse condizioni di gravità: gravità normale (1g), ipergravità (1,8g) e microgravità (0g).

Per poter eseguire questi test si è preso parte alla 62° campagna di volo parabolico promossa dalla European Space Agency (ESA) ed eseguita da Novespace, Bordeaux, Francia.

La PHP testata è formata da una piastra di rame incollata ad un vetro. Nella piastra di rame è stato ricavato un canale ad anello, con un percorso ad "S" che forma 11 curve a U nella zona dell'evaporatore, tra rame e vetro il canale presenta una sezione quadrata di lato 2.5mm.

La particolarità di avere una faccia di vetro permette di visionare e registrare per mezzo di una videocamera ad alta frequenza il comportamento del fluido (FC-72) all'interno dei canali durante i test.

I risultati ottenuti si sono rivelati di grande interesse, la possibilità di confrontare i dati numerici alle registrazioni video ottenute durante i test ha reso possibile una maggior comprensione del funzionamento della PHP durante il transitorio tra le condizioni di gravità normale e quelle di microgravità ed approfondire gli effetti che la gravità provoca sulle sue prestazioni.

Parole chiave: Pulsating heat pipe; Trasparente; Microgravità; Volo parabolico; Capillarità; Regime di flusso.

Abstract

This Thesis deals with the results of some tests performed on a two phase passive device: a semi-transparent flat-plate Pulsating Heat pipe (PHP). This PHP was tested by simulating different thermal loadings in different gravity conditions: normal gravity (1g), hyper gravity (1,8g) and microgravity (0g).
In order to perform these tests, we took part in the 62nd parabolic flight campaign promoted by the European Space Agency (ESA) and performed by Novespace, Bordeaux, France.
The tested PHP was made by a copper plate glued on a glass. On the copper plate was engraved a looped channel which had an S-shape forming 11 U-Turns on the evaporator zone. Between copper and glass, the channel presented a square cross-section of 2.5mm each side.
Thanks to the feature of this device, which presented a transparent side, it was possible to display and record with a high-speed camera the different types of fluid (FC-72) motion and distribution inside the channels during the tests.
The results obtained were very interesting. The opportunity to match the numerical data with the video recorded during the tests made possible a deeper knowledge of the behaviour during the transition from normal gravity condition to microgravity and the effect of microgravity on the PHP performances.

Keywords: Pulsating heat pipe; Transparent; Microgravity; Parabolic flight; Capillarity; Flow pattern.

1 Introduction

In order to perform a higher heat exchange with the most compact devices but increasing good reliability too, the interest for the two phase passive devices is becoming higher and higher.
The big advantages of these devices compared to the mono phase heat exchangers are: the possibility to take advantage of the latent heat of evaporation/condensation improving the heat transferred. With best performances thanks to the lower thermal resistance too.
They are passive devices, so the absence of a pump for the fluid circulation and low mass flow rate strongly increase the compactness and reduce the risk of failure.
Small temperature gradient between the cold and hot sources.
The Pulsating Heat Pipe (from now on, it will be called with the abbreviation PHP) is the last developed device (Akachi, 1990) in the family of the two-phase passive devices.
It is basically made up of a capillary diameter tube bent in a S-shape or sometimes it can be made up of a squared channel engraved in a metal plate. It could be close on itself to form a closed loop or with the two ends of the channel closed (open loop).
The functioning of this device is based on the instability of the fluid motion. The continue sequence of evaporation and condensation generates an oscillation inside the channel (in case of closed loop also circulation) thus increasing the heat exchange between the hot and cold sources.
Due to the large number of non equilibrium conditions and the absence of a single thermodynamic state which represents the system, the thermo-hydraulic analysis is hard to approach, so the experimental way is the most used.
The behaviour of the PHP strongly depends on the flow patterns (Charoensawan P., 2003), therefore some studies involved the visualisation of the fluid motion inside the PHP or in a single capillary tube, in order to have a best comprehension of the effect on its functioning according to the different flow patterns (Khandekar S., 2003; Ayel V., 2013; Mameli M., 2015).
It is also acknowledged that the gravity strongly affects the performances of the system (Gu J., 2004; Mameli M., 2014; Araneo L., 2014; Ayel V., 2015; Mameli M., 2015).
The numerical analysis by Gu J. (2004) based on Weber number, $We = \rho_l u_l^2 \, D/\sigma$ which is the ratio of the forces of inertia and surface tension, shows that the PHP could work with good results under microgravity, with a large channel diameter although it may not work on the ground.

1.1 Objectives

The main objective of this work is the development and study of the functioning of a semi-transparent flat-plate Pulsating Heat Pipe in different gravity conditions, in order to get a better comprehension of the fluid motion.
To do this, it was necessary to develop a totally new PHP. It was made by a copper plate, with an engraved channel and a glass plate glued on it instead of the previous version (Ayel V., 2015) which was made by two copper plates brazed together. The presence of the glass introduced some new difficulties on the building process, especially due to the gluing.
The idea was to construct a PHP with a hydraulic diameter of the channel much higher than the critical one (Akachi H., 1996) for the normal gravity condition and to see the different functioning between the fluid motion in normal gravity and microgravity at a wide range of heating power.
In order to perform the experiment in different gravity condition, we took part in the ESA 62nd parabolic flight campaign operated by Novespace.
The designing and building process had to follow strict rules (Rosier P., 2014) in order to have this experiment approved under the Novespace Aeronautic Standard.

1.2 Physics of a Pulsating Heat Pipe

The two phase heat exchangers are among the most performing solutions for the heat exchange, due to the latent heat exchanged during the phase transition (evaporation and condensation phenomena).
The most common two phase passive devices are basically three:

- Thermosiphons
- Heat pipes
- Pulsating heat pipes

All these devices are “passive”, or “thermally driven”, that is the circulation of the fluid is not regulated by a pump, but by the same fluid behaviour.
The thermosiphon is the simplest one; it consists of a tube with both extremities closed and partially filled with a working fluid.
The heat source is located on the bottom, the liquid adsorbs the heat and starts to evaporate; the vapour, due to the higher pressure, moves through the pipe up to the top. When it reaches the upper part, the cold source removes heat from vapour, which condenses on the internal

tube surface. Then due to the gravity force, the condensed phase moves down along the tube wall and reaches the bottom part where an identical cycle begins continuously (see figure 1.1a).

The main problem of the thermosiphon is that it can work only if the gravity field is oriented in a favourable way (bottom heated) because of its diameter being higher than the critical one in order to avoid the capillary pumping.

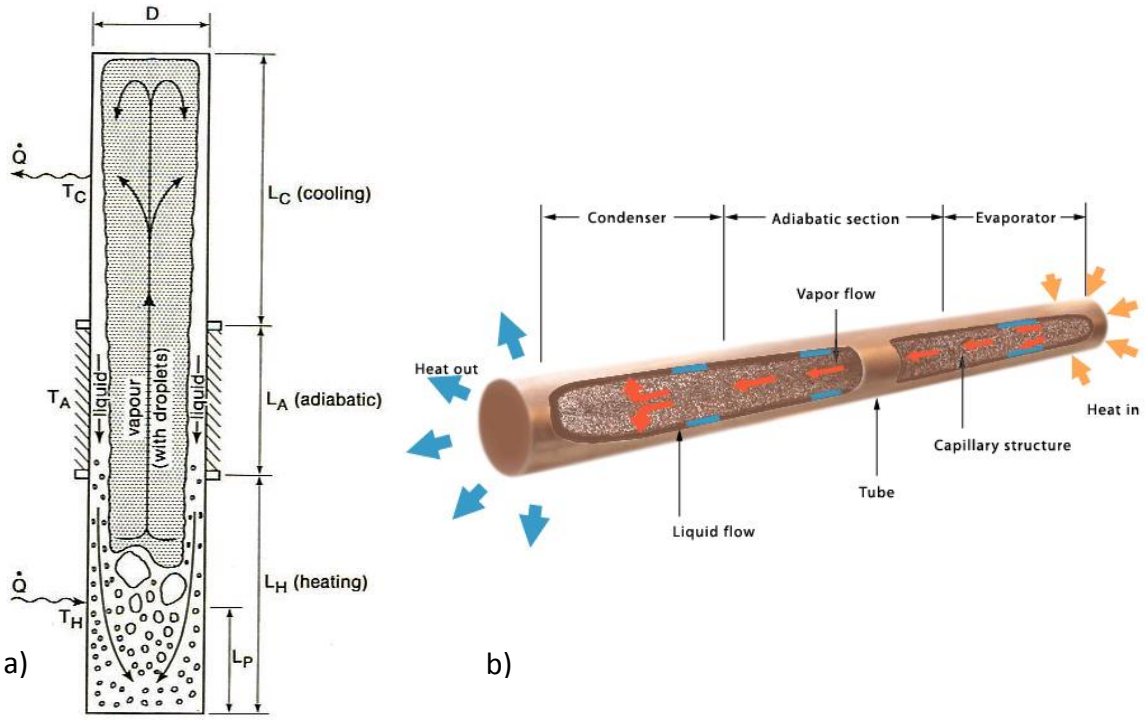

Figure 1.1: a) Scheme of a classic thermosiphon (Lock G.S.H., 1992). b) Scheme of a capillarity heat pipe (Aavid Thermalloy)

With the heat pipes it is possible to take advantage of capillarity by using tubes with a porous internal coating or with some small channels engraved on the internal wall. The bigger benefit of this is the possibility to transport the liquid phase in absence of gravity too or even in unfavourable gravity conditions (top heated).

In this case, the condensed liquid on the condenser zone, can come back to the evaporating zone thanks to capillarity (see figure 1.1b).

In both thermosiphons and heat pipes, the heat exchange is based on absorption and dissipation of latent heat due to the change of phase. Due to this fact, the difference of temperature between the evaporator and the condenser zone is normally limited.

The pulsating heat pipe is the latest developed technology concerning heat pipes and consists in a series of channels linked together in order to have a coil shape. They are generally made by a single bended tube (Araneo L., 2014) or with two metal plates brazed together (Ayel V., 2015) with a channel engraved in one of it. No liquid storage volume or wick structure are present in the PHP.

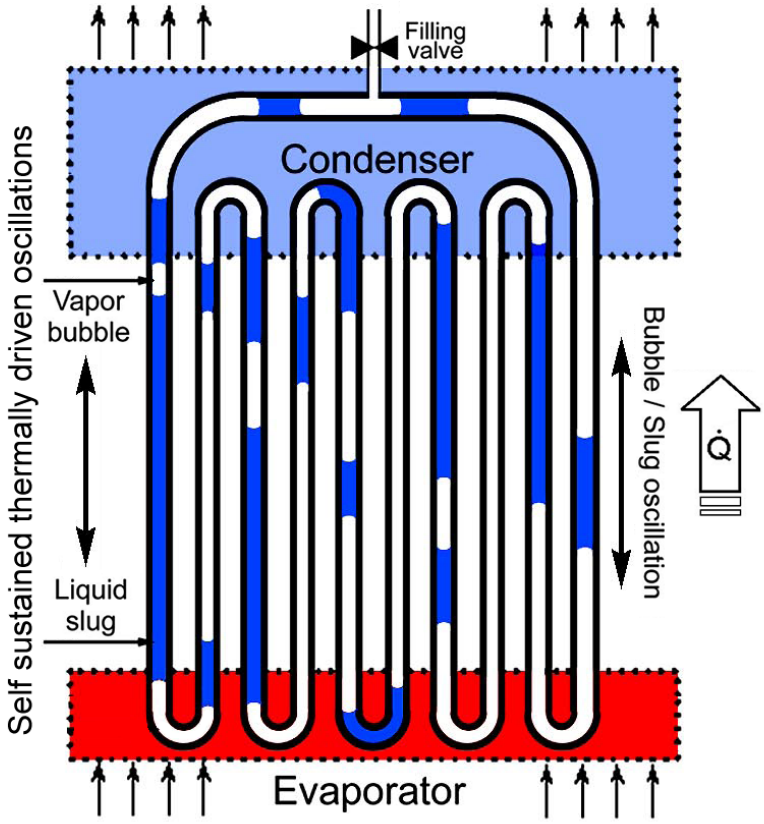

Figure 1.2: Scheme of a closed loop pulsating heat pipe (Khandekar S., 2003)

The device is partially filled with a working fluid which is distributed inside the channel. Depending on the channel diameter, the fluid can distribute forming liquid slugs and vapour bubbles (see figure 1.2), in case of small section, or it can stratify according to the different density between liquid and vapour for a diameter higher than the capillary critical one (see paragraph 1.3.1).

The PHP always works under unsteady conditions, instability is the basis of its passive functioning (Khandekar S., 2010). Instability is mainly generated by three physical phenomena:

- Phase transition (evaporation/condensation)
- Gravity force

- Capillarity force

The sum of these three factors, causes the circulation and oscillation of the fluid and creates an effective heat transport.

It is possible to find three main types of two phase flow patterns (Ayel V., 2013):

- Slug and plug regime
- Semi annular regime
- Annular regime.

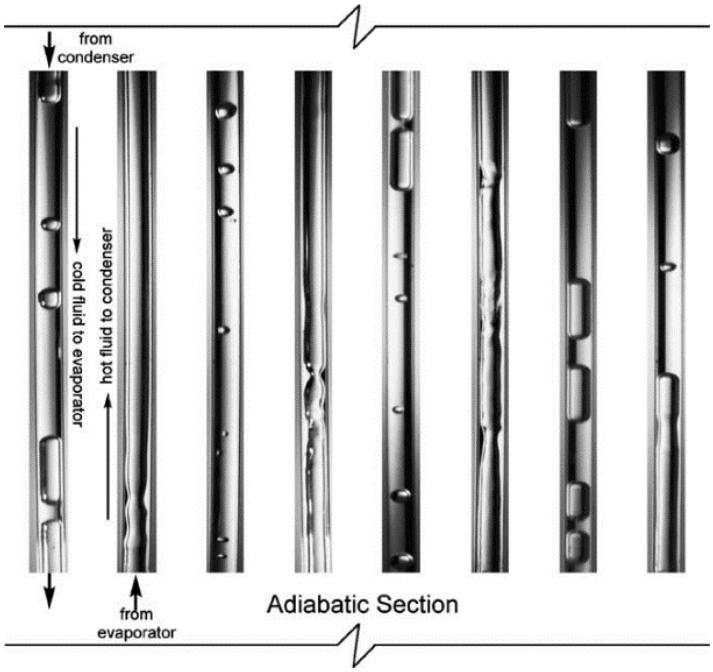

Figure 1.3: Typical PHP fluid distribution patterns, showing different flow regimes during the functioning of a PHP (Khandekar S., 2003).

On the Slug and plug regime, the fluid maintains a distribution of vapour plugs (bubbles) and liquid slugs. With this regime, the heat flux at the evaporator increases the temperature of the liquid up to evaporate it. This causes the expansion of the vapour plugs and consequently, the increase of the local pressure until the fluid starts moving. It moves along the channel until it reaches the condenser zone where it condenses, but also propagates the motion to the adjacent channel. The value of pressure gradient needed to start the bubble motion depends on the surface tension at the interface, friction forces and inertia of the fluid.

The pressure gradient is the driving force of the fluid and in order to have a bubble motion (Ayel V., 2013), it has to be higher or at least equal to the pressure losses plus the capillary pressure.

$$\Delta P_{vapour} \geq \Delta P_{losses} + \Delta P_{capillary}$$

The functioning of a PHP in slug and plug regime is well described in the following pressure-enthalpy diagram:

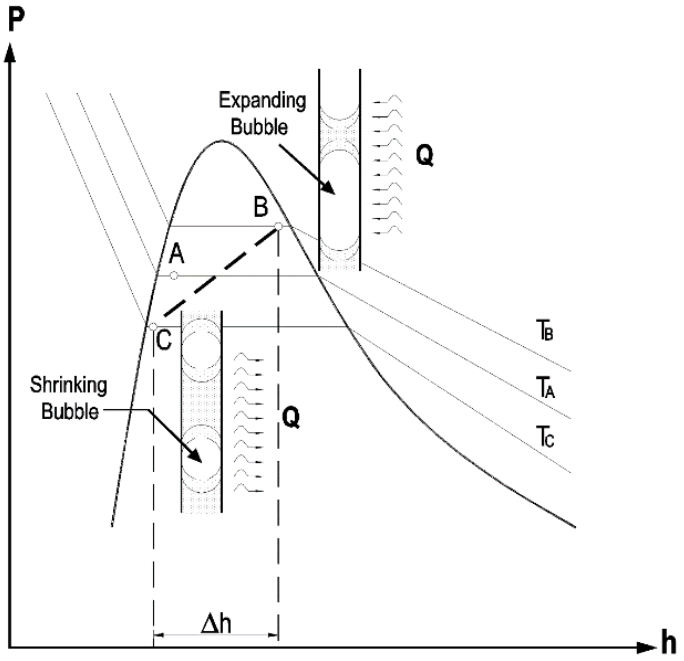

Figure 1.4: Generic P-h diagram of a typical PHP working condition (Karimi, 2004)

Let's consider the point A in the figure 1.4, which corresponds to an intermediate thermodynamic state for the system. By applying a thermal flux to the evaporator, the bubble size increases. This causes an increase of pressure and temperature moving the system to the point B. When the bubble reaches the condenser region, the implosion occurs, causing a reduction of pressure and temperature level and moving the system to the point C. The instabilities among these points cause the fluid motion and consequently the heat exchange (Karimi G., 2004).

As before asserted, the device is totally passive and the heat source is the only one which could generate the pressure instabilities and make the motion start.

The heat transfer phenomenon is due to the sensible heat caused by the mass transfer, latent heat due to the fluid changing phase, heat conduction and convection along the axial and transversal direction.

During the annular regime, the system works in a pretty similar way compared to a conventional thermosiphon. This means that the vapour phase moves along the centre of the

channel in direction of the condenser and the liquid film moves in the opposite way on the internal surface.

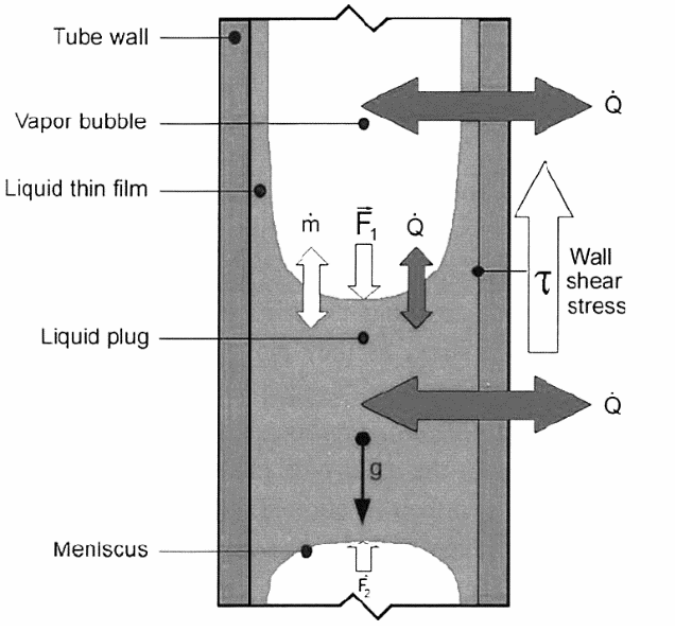

Figure 1.5: Fundamental transport operation in a PHP (Khandekar S., 2010)

1.3 Design Parameters of a PHP

During the design of the PHP, there were several parameter to consider and optimize to perform the better results according to the objective.
The numerous studies about the PHP show an influence of such geometrical and operational parameter for a correct PHP functioning, the most important aspects are analysed here below:

- The internal channel section size
- The internal channel shape
- The filling ratio (liquid to volume ratio)
- The kind of working fluid
- The number of U-Turns

Here below a short analysis of the functioning of the PHP varying these parameters.

1.3.1 Internal channel section size

The internal channel section is the most important parameter for the PHP dimensioning. Depending on its value, it is possible to have a negligible effect of the capillarity inside the channel in order not to establish a slug and plug flow regime inside it. In that case, the functioning of the PHP can be attributed to a thermosiphon, which only works thanks to the gravity force.

Some criteria have been developed in order to establish the critical diameter for a slug and plug regime. The most common is the criterion based on the Bond number. The Bond number relates the effect of gravity force to the surface tension forces.

This criterion is useful to find the maximum hydraulic diameter above which the capillarity has a negligible effect. (Akachi H., 1996)

It's important to notice that this criterion is not related to the PHP functioning but it is a good index only for the possible presence of bubbles inside a channel filled with liquid in static condition. Above the limit imposed by critical Bond number, the meniscus breaks because of the gravity force and inside the channel the fluid organized depending on the different density of the different phase.

The Bond number is defined as:

$$Bo = \frac{Dh\,(\rho l - \rho v)g}{\sigma}$$

Where:

- Dh: Hydraulic Diameter [m], defined as:

$$Dh = \frac{4A}{P}$$

  A: Cross-section area of the channel [m^2]

  P: Wetted perimeter[m]

- ρl: Volumetric mass density of the working fluid in liquid phase[kg/m^3]
- ρv: Volumetric mass density of the working fluid in vapour phase[kg/m^3]
- σ: Surface tension [N/m]
- g: gravity or any other acceleration [m/s^2]

A critical value for the Bond number around 4 was experimentally found, below which the surface tension forces dominate on the gravity ones. Due to this it is possible to define the critical diameter:

$$Dc = 2\sqrt{\frac{\sigma}{g(\rho l - \rho v)}}$$

It is possible to notice how the diameter is strictly linked to the gravitational field and so in absence of gravity the critical diameter goes to infinite. On the Figure 1.6 is drawn the value of critical diameter as a function of the fluid temperature and a comparison between the value in normal gravity condition and in microgravity (considering a value of 0.01 m/s^2 due to the possible presence of vibration).

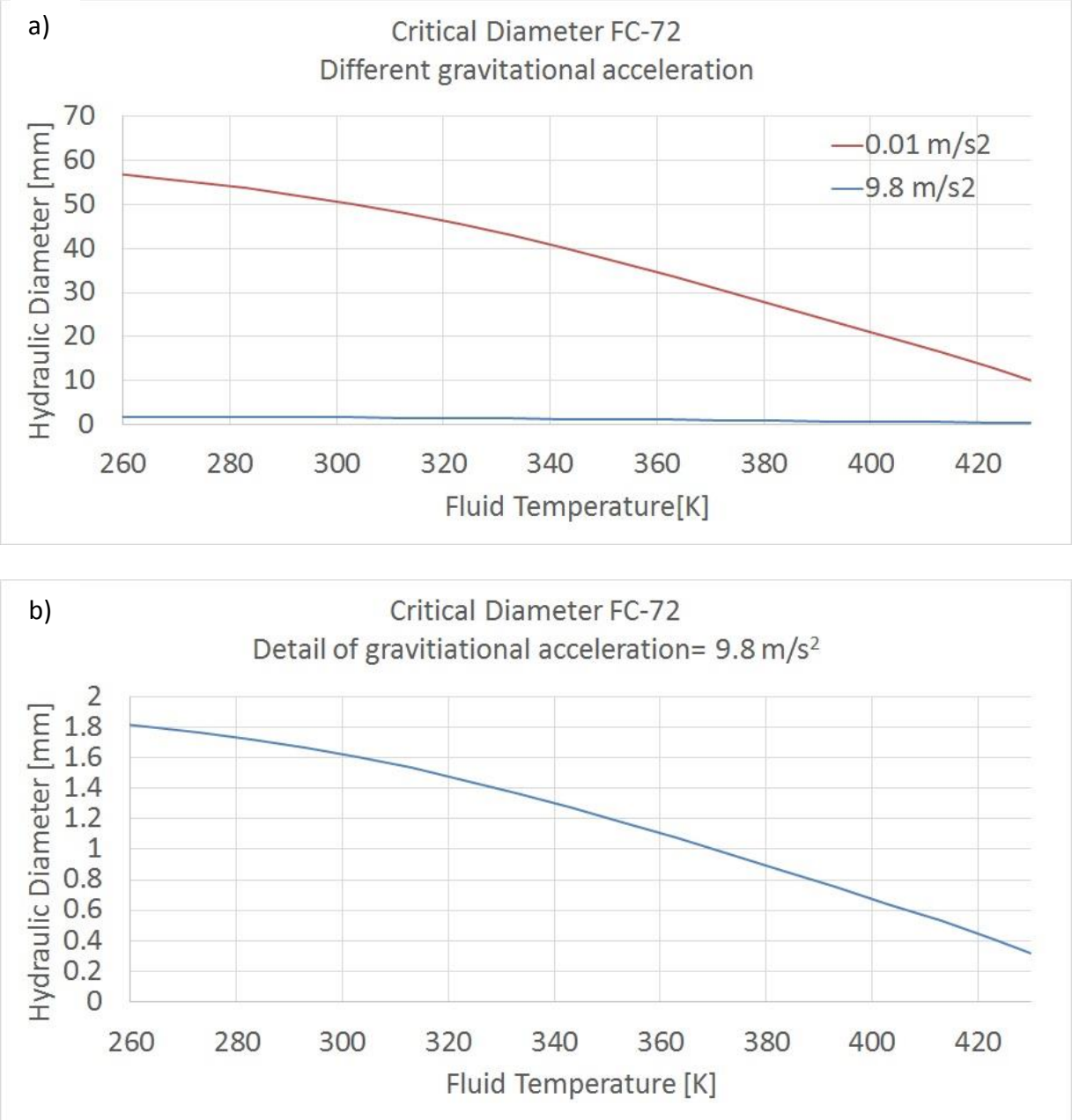

Figure 1.6: Diagrams of the critical diameter for the FC-72 at: a) comparison between normal gravity condition and microgravity b) Detail at normal gravity condition

For our experiment, it was decided to adopt a hydraulic diameter above the critical one in order to see the difference of functioning between normal gravity condition and microgravity. At ambient temperature (20°C) for the working fluid FC-72, the critical diameter calculated with the criterion based on the Bond number was 1.66mm, while at higher temperature, the surface tension decreases and the critical diameter is smaller. For this reason an internal squared channel section of 2.5mm x 2,5mm (hydraulic diameter of 2,5mm) was chosen.

1.3.2 Channel shape

Another feature which influences the motion of the fluid inside the PHP, is the shape of the channel. The most common used channel shapes are squared or circular, depending on the PHP being a single bended tube or, like in this case, if it has been obtained by a channel engraved in a metal plate.
The circular section performs lower pressure losses compared to the squared one but, in some types of flow regimes like in the annular, the corners could help the liquid return on the evaporator zone thanks to capillarity.

1.3.3 Filling Ratio

The filling ratio (FR) is the ratio between the liquid volume at ambient temperature of the working fluid inside the PHP and the total volume of the channels. The filling ratio is defined as:

$$FR = \frac{V_{liquid}}{V_{PHP}}$$

Due to this, a filling ratio of 100% corresponds to a PHP fully filled of liquid, on the other hand a filling ratio of 0% corresponds to an empty condition.
As analysed by Yang H. (2008) the filling ratio affects the thermal resistance and the heat power exchange. It has been registered that a low filling ratio provides a lower resistance for low heat transfer power, thanks to the lower hydraulic resistance, but the situation is opposite for higher powers, with the maximum value of heat transfer around a filling ratio of 60%, when low filling ration would show premature dry-out (see figure 1.8).
A good compromise between thermal resistance and heat power exchange is a value of filling ratio of about 50%.

It was observed that for a filling ratio above 70% the formation of bubbles is strongly reduced and the thermal behaviour is comparable to a mono phase thermosiphon. With a filling ratio lower than 30% the vapour occupy most of the PHP and the dry-out is dominant. Down to the limit with a filling ratio of 0% where it works in a pure conductive condition.
In the Figure 1.7, it is highlighted the interaction between filling ratio, heating power and channel diameter.

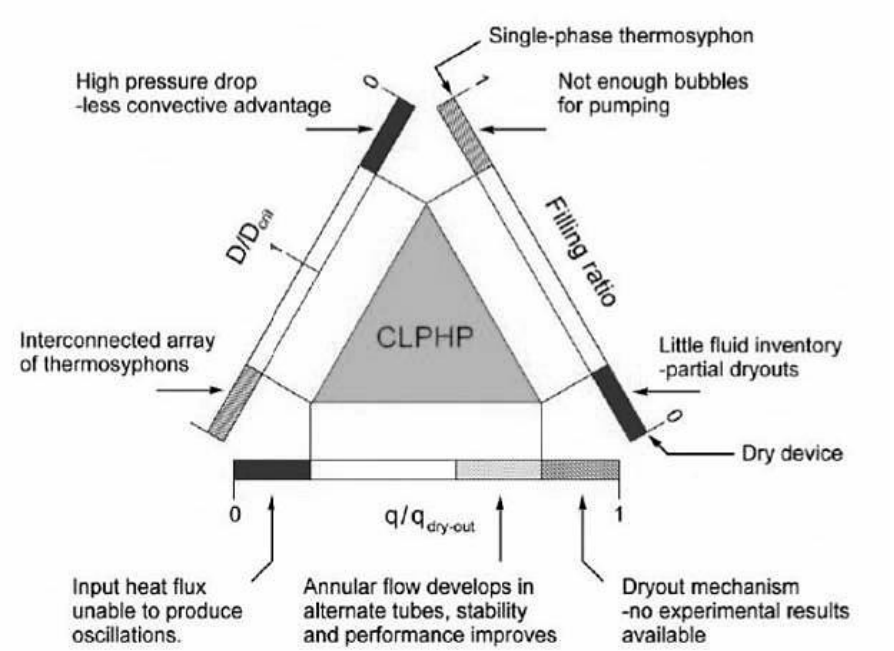

Figure 1.7: Functioning of a PHP varying the boundary condition (Khandekar 2004)

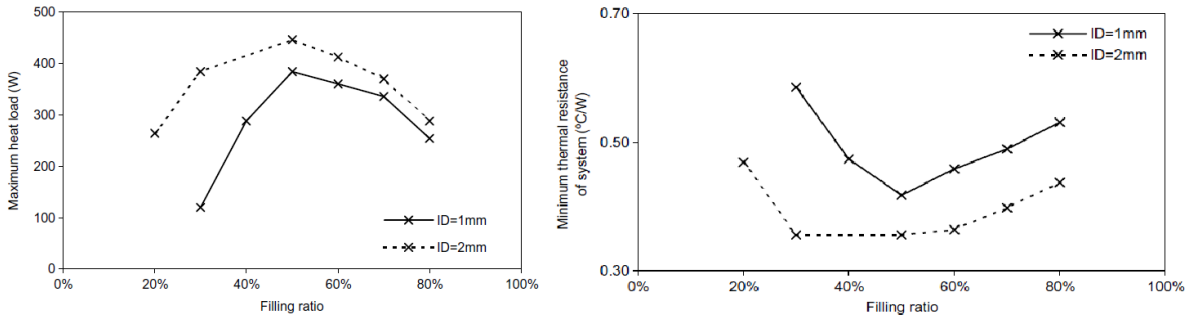

Figure 1.8: Minimum thermal resistance of system versus filling ratio (horizontal heat mode, air cooling with 5 m/s) (Yang, 2008)

1.3.4 Working fluid

There are several working fluids which can have good performances in the PHP. The choice is strictly related to the specific PHP applications where it is important the range of working temperature.
Generally speaking, the performance of a working fluid is linked to the liquid dynamic viscosity, surface tension, latent heat and specific heat (Mameli M., 2012).
The liquid dynamic viscosity has to be low, in order to reduce the pressure losses inside the channel.
Concerning the surface tension, a higher value of it guarantees a higher value of critical diameter but on the other hand, it causes bigger pressure losses inside the channel. A liquid with a low value of surface tension would be a good choice.
It is also better to have a low latent heat in order to get a faster generation and collapse of the vapour bubble. In case of excessive low value of latent heat, a very fast evaporation can happen with the possibility of a dry-out phenomenon.
The specific heat has to be high in order to increase the amount of sensible heat which the liquid is able to transport from the evaporator to the condenser.
In this case, it was chosen to use the Perfluorohexane (C_6F_{14}), also known with the commercial name of FC-72, mainly because of its nontoxic and non inflammable proprieties, in view of the parabolic flight campaign which required a non dangerous fluid.

Molecular composition	C_6F_{14}
Average Molecular Weight	338
Boiling point (1atm)	56 °C
Pour point	-90 °C
Vapor pressure at 25°C	30.9 kPa
Liquid Density	1680 kg/m3
Density	1.68 g/cm3
Liquid specific heat	1100 J/kgK
Liquid thermal conductivity	0.057 W/mK
Latent Heat of Vaporization (at normal boiling point)	88 J/g
Surface tension σ	10 dynes/cm

Table 1: Physical properties of FC-72. All values determined at 25°C unless otherwise specified (M3, technical data sheet)

1.3.5 Number of U-turns

Another important parameter for the functioning of the PHP is the number of U-turns on the evaporator side. There are some studies in literature about the minimum number of U-turn which permits the activation of the PHP.
For example, in the study of Charoensawan P. (2008), the functioning of the PHP is analysed, varying the number of U-turns with two different internal channels diameter and varying the PHP inclination too.
As shown in the figure 1.9, a minimum number of 16 U-turns is required to enable the PHP to work with all the inclinations. With a lower number of U-turns the performance starts to became worse and worse, starting from the inclination close to the horizontal until the limit value of 5 U-turns with no activation in horizontal configuration.
The activation begins at lower temperature for a higher number of turns. It was also noticed that for a higher channel section, fewer turns were required for the activation.
In the case in object it was chosen a number of U-turns equal to 11, also considering the high hydraulic diameter of the channel.

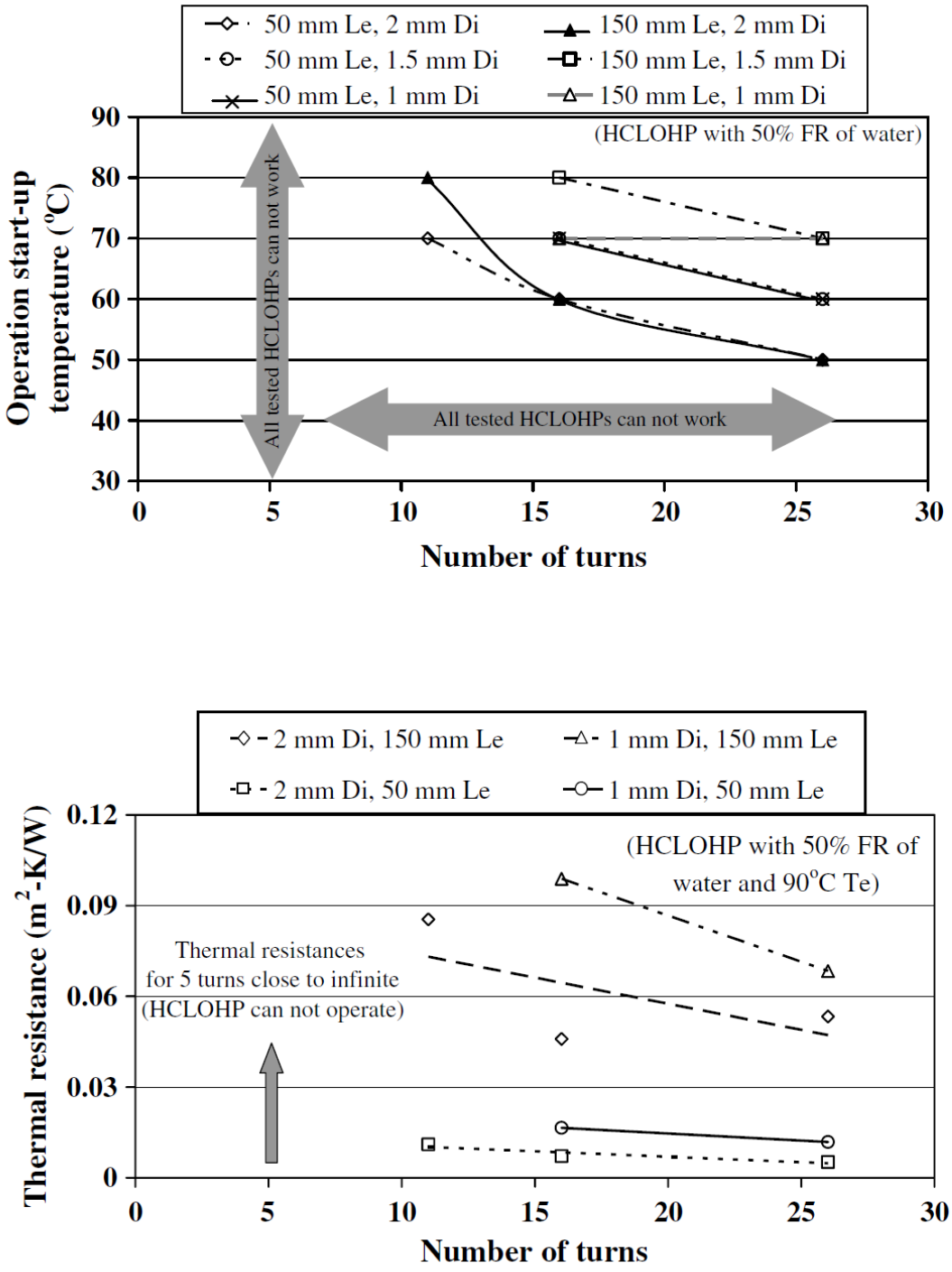

Figure 1.9: Influence of number of U-Turns to the PHP behaviour (Charoensawan P., 2008)

2 Parabolic flight description

The Parabolic flight is a particular kind of flight where several parabolic manoeuvres occur, in order to perform tests in condition of weightlessness.
It is a condition where an object is only submitted to the gravity, all other forces are balanced out or null. Whereas the gravity cannot be cancelled, the microgravity condition can be simulated by putting the object in weightlessness condition.
This kind of parabolic flight campaign is performed by Novespace, with the support of ESA (European Space Agency), in their facilities at the airport of Bordeaux.
During each flight on the Airbus A310 (62nd ESA parabolic flight campaign was the first with this new aircraft after the Airbus A300), 31 parabolas were performed.
The Parabolic flight campaign was carried out during two weeks, in which the main steps were:

- Arrival at the Novespace facilities and preparation of the experiment set-up.
- Reviewing the experiment by the Novespace engineer.
- Loading the experiment on the aircraft.
- Fine-tuning and some ground tests in the aircraft.
- Safety in-depth training for all the participants at the parabolic flight.
- Parabolic flight.
- Briefing after each parabolic flight and tune-up of the experiment for the next day.

Figure 2.1: Novespace aircraft, Airbus A310

In order to get permission to board on the Novespace aircraft for the parabolic flight, each crew member had to undergo a medical check-up.
To reduce the unwanted seasickness caused by the numerous parabolas, a facultative injection of scopolamine is highly recommended. (Gai F., 2013)

2.1 The ZERO-G Aircraft

The aircraft used by Novespace for the parabolic flight campaign is an Airbus A310 (see figure 2.1) with some modifications on the cabin.
On the cockpit, some indicators were inserted showing to the pilot the vertical and longitudinal acceleration of the aircraft. In order to perform perfectly the parabolic manoeuvre, an additional removable control stick was installed. (Gai F., 2013)
The cabin was divided into five sections as shown in the picture.

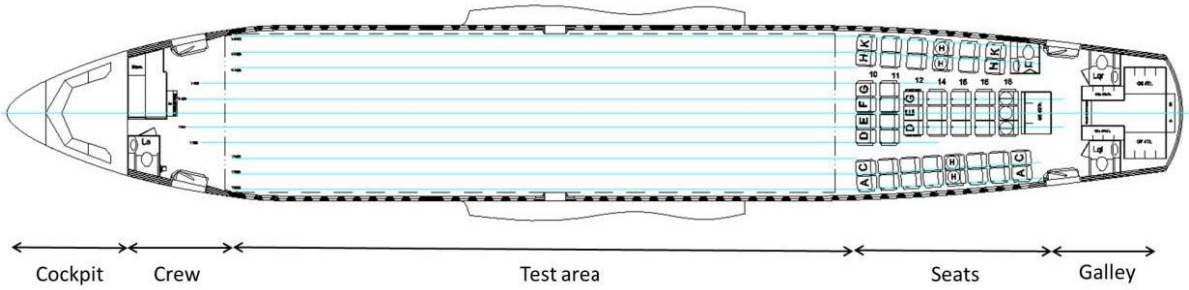

Figure 2.2: Map of the Novespace aircraft. (Verthier B., 2014)

The test area includes the zone where all the experiments are performed. In this zone, floor, ceiling and walls are cushioned with soft white panels in order to avoid any accidental injury in case of collision during the micro o hyper gravity. Safety nets are installed at the beginning and at the end of this zone to limit the experiment area.
The test area have a length of 20m and is 5m wide. The cross-section is detailed on the figure 2.4.

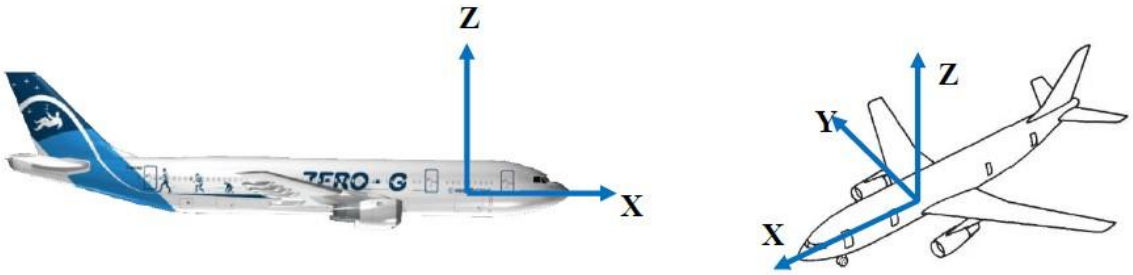

Figure 2.3: Reference axes of the aircraft. (Verthier B., 2014)

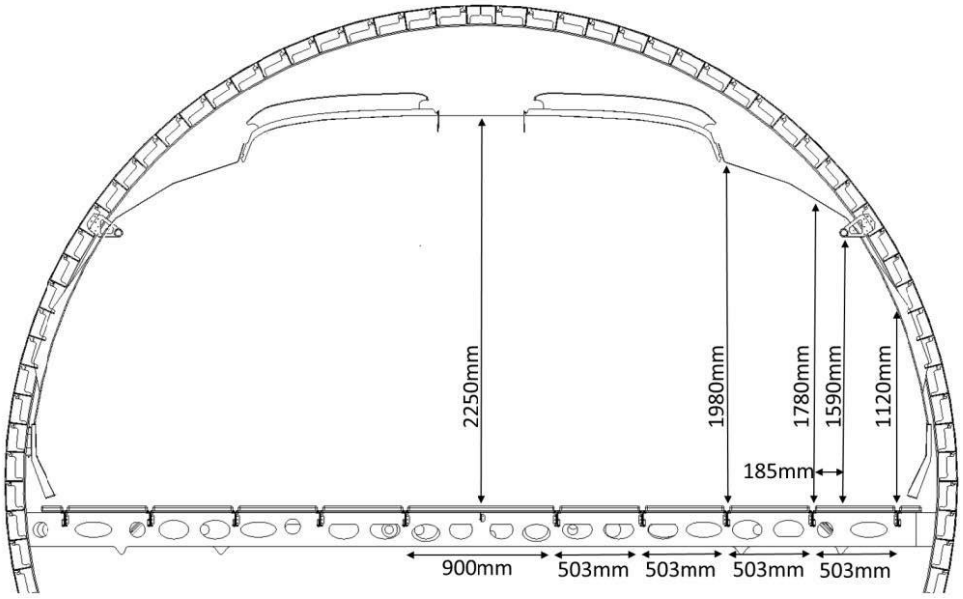

Figure 2.4: Cross-section of the test area. (Verthier B., 2014)

The experimental rack had to be fixed onto the tracks normally used on airliners to attach passengers' seats. These tracks are 503mm distant one from the other along the Y axis and have attaching points spaced 1 inch (25.4mm) along the X axis.

During the flight the pressure and thermal condition are quite constant. Novespace referred a pressure of 850hPa (+/- 5hPa) during all the parabolas, i.e. since 10-20 minutes after the take off. Also the temperature is controlled between 17°C and 20°C (these values are only indicative and it can be a little higher or lower). It is important to notice that the temperature is not guaranteed during the night or on the ground where, depending on the external conditions, it can be less than 0°C during the winter or higher than 35°C in the summer. *(Verthier B., 2014)*

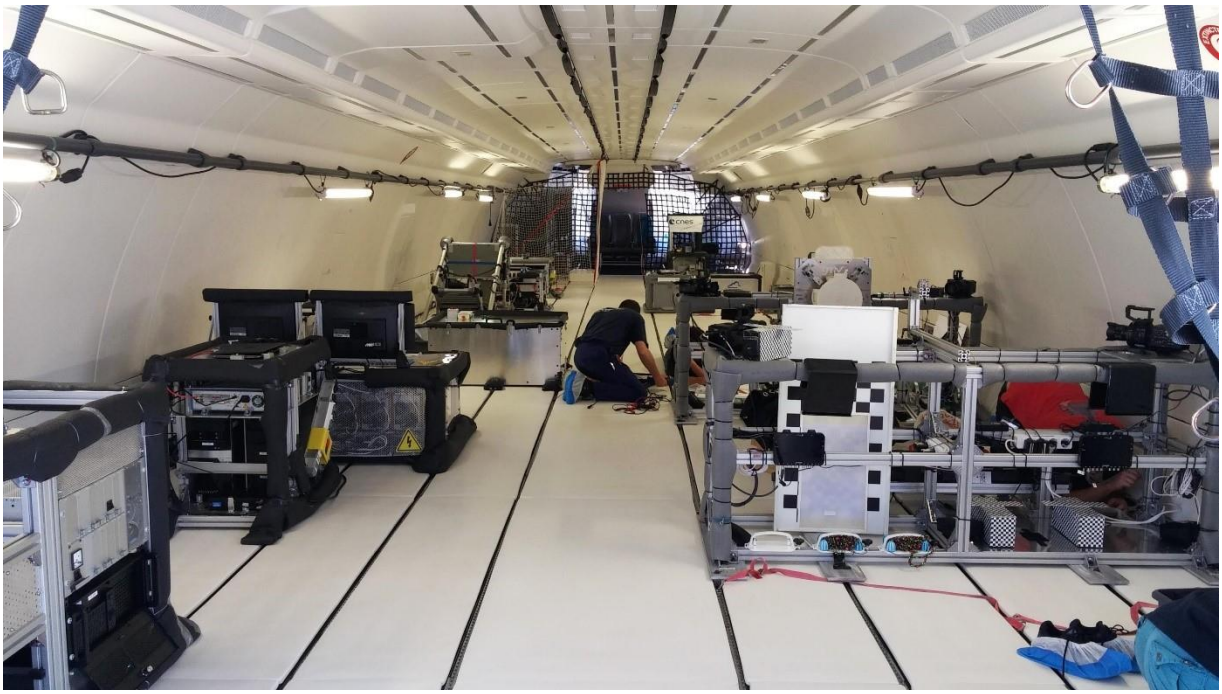

Figure 2.5: Photo of the test area before the first day of flight

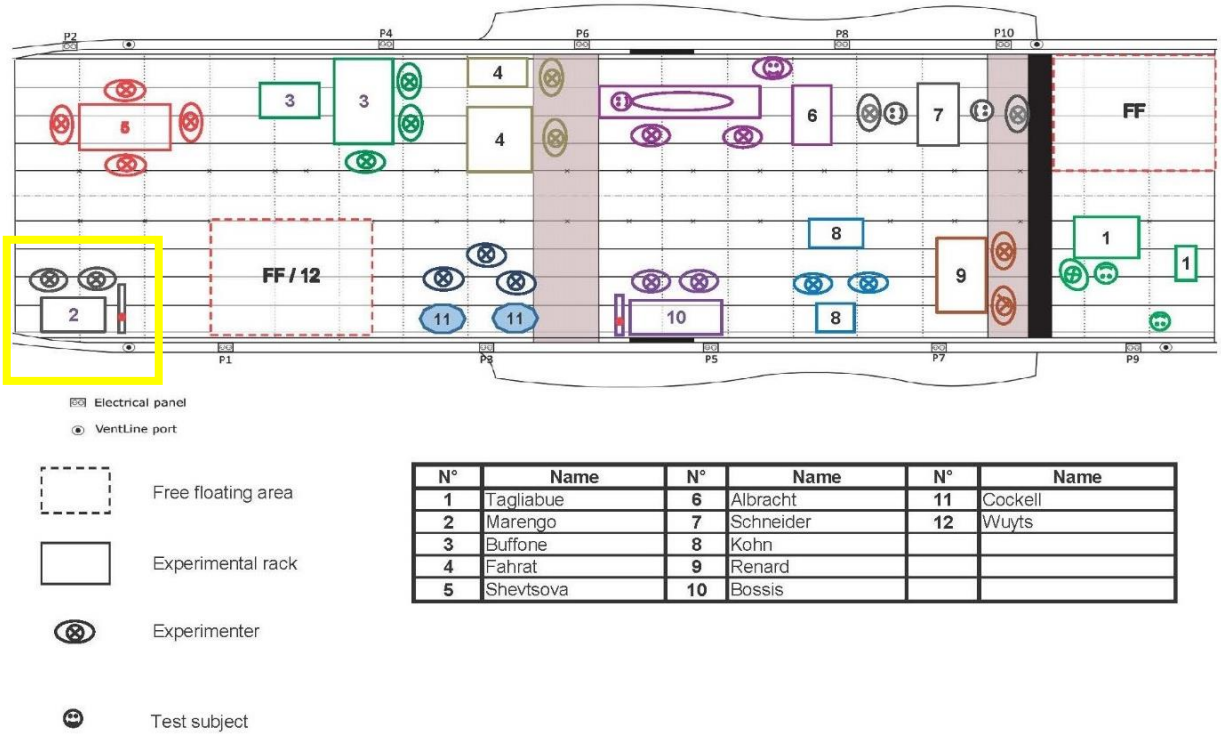

N°	Name	N°	Name	N°	Name
1	Tagliabue	6	Albracht	11	Cockell
2	Marengo	7	Schneider	12	Wuyts
3	Buffone	8	Kohn		
4	Fahrat	9	Renard		
5	Shevtsova	10	Bossis		

Figure 2.6: Diagram of the disposition of the experiments inside the cabin, the experiment of this study was the number two (yellow box)

2.2 Parabolic manoeuvre

The parabolic manoeuvre or parabola (the real trajectory is an arc of ellipse) is the manoeuvre which allows to have a weightlessness condition for up to 22 seconds. The weightlessness condition is obtained cancelling the drag and lift load and let the aircraft be subjected only to the earth gravity force.
The lift load is the aerodynamic load along the Z axis and it is possible to cancel it by tilting the aircraft.
The drag load is the aerodynamic load along the X axis, this is not possible to cancel but could be compensated by varying the engine thrust.
This manoeuvre required four hard-trained persons, two pilots and two flight engineers, in order to have the best and most stable microgravity condition.
The two pilots controlled the pitch and roll axis (independently, that is one axis for each pilot, by the two cloches), one flight engineer managed the power thrust throttle and the other checked the system of instruments.
The manoeuvre is divided in 3 main part: entry phase, injection phase, exit phase.

- **Entry phase**: it is the first part of the manoeuvre. From an altitude of 6000m circa, the speed is increased to the maximum value of about 810km/h. When the speed is reached the pilot starts the pull-up phase increasing gradually the aircraft attitude (angle to the horizontal) to about 47° at about 7500m of altitude and a speed of 650km/h. During this phase, due to the centrifugal force, a vertical load factor (referring to the aircraft Z axis) of 1.8g is applied and the aircraft and persons inside it weigh 1.8 more than on the earth. This is the condition of hyper gravity.
  This phase lasts for 20 seconds circa.
- **Injection phase**: Once the angle of 47° is reached, the crew starts the manoeuvre so called “injection”. During this manoeuvre, the power thrust is reduced and the aircraft is driven to perform a trajectory of an arc of ellipse. In less than 5 seconds the vertical load collapses from 1.8 to 0 and the microgravity phase begins with the aircraft in a free fall condition.
  At the top of the parabola, the aircraft is at an altitude around 8500m with a speed of 390km/h circa. The microgravity is maintained for at least 22 seconds.
- **Exit phase**: When the aircraft reaches an attitude of 45° downwards during the descent in free fall, the pull-out phase starts. This manoeuvre is the symmetrical of the pull-up phase. The full throttle is reestablished and the aircraft is driven to reach a horizontal steady flight.

During this phase aircraft and passengers inside it find themselves in a condition of hyper gravity once again for at least 20 second.

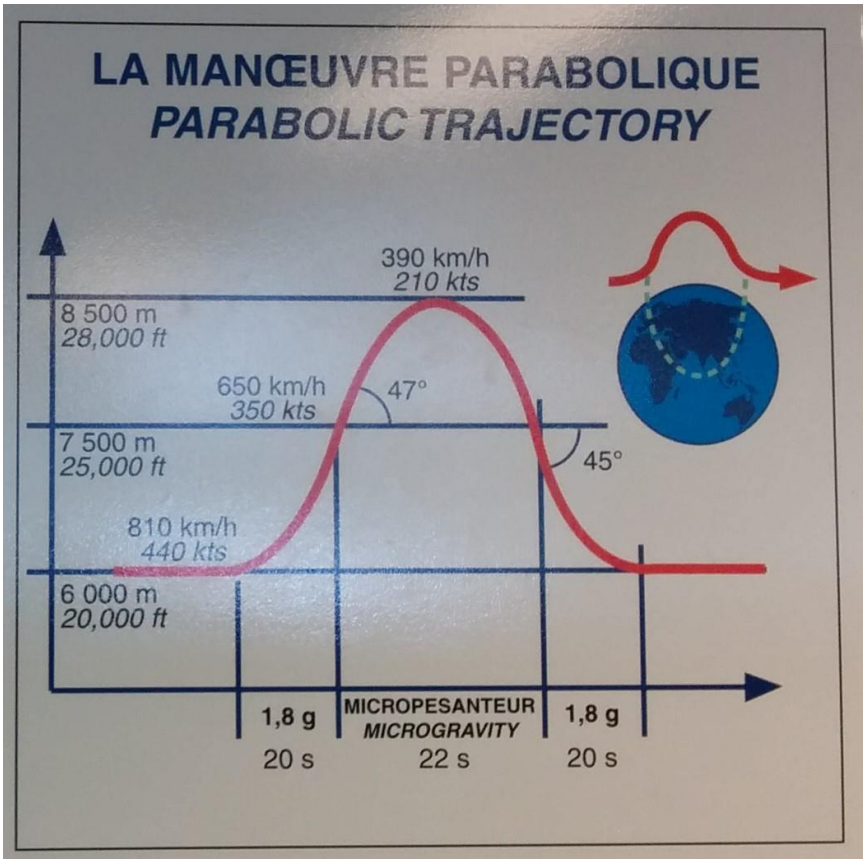

Figure 2.7: Diagram of one parabolic manoeuvre

In order to help the passengers to manage their experiments during the different phases of the manoeuvres, some audio warnings are given by the crew. Before each parabola the residual time before the pull-up is announced. When the manoeuvre begins, the crew announces the grade of the aircraft too. It is possible to find the details of the audio crew announcements in the figure 2.8.

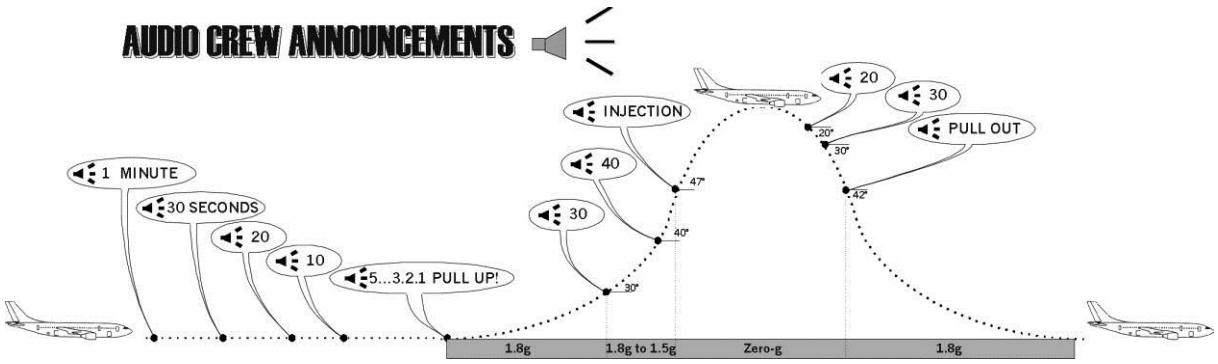

Figure 2.8: Diagram of the audio crew announcements. (Gai, 2013)

For our experiment, these announcements were very important to manage the start and the stop of the video acquisition.

In each parabolic flight the plane performed 31 parabolas organized in 6 series. Each series composed by five parabolas, except for the first series which had the parabola number 0 too, with the purpose to check if every experiment worked well.

Each series is followed by an interval time of 5 minutes of horizontal flight, except between the series three and four, where the interval was of 8 minutes.

Between every two parabolas the minimum lapse of time was 100 seconds. (Gai, 2013)

3 Description of the Experimental Rack

To take part to the 62nd ESA parabolic flight campaign, the experiment had to be installed on a rack, which had to follow the “Novespace experiment design guidelines in parabolic flight” (Rosier, 2014) and had to be approved by a Novespace engineer before loading it on the aircraft.

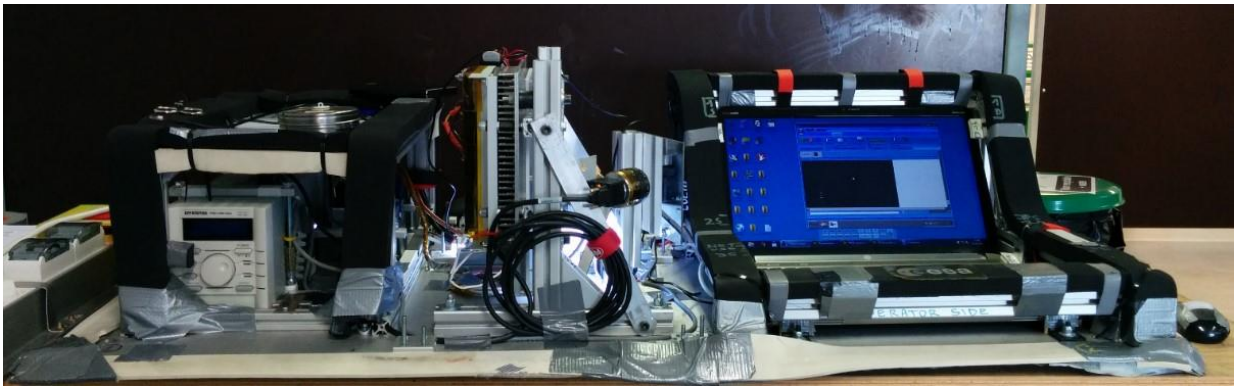

Figure 3.1: Frontal view of the experimental rack

Our rack was divided into three main sections (see figure 3.2), the first one on the right with PCs, multiplugs and small power supplies, the central one with the PHP assembly and the last one on the left with the power supply for the heater, the data logger and g-sensor. Each component had to be well fixed to the rack to prevent any free fluctuation during the microgravity phase and also was dimensioned to stand at possible acceleration up to 9g .
A fireproof foam was stuck to cover all the supports, sharp angles or exposed parts, to reduce the consequences of any accidental hit between the operator and the experimental rack during all the parabolas
The rack was the same used during the 61st ESA parabolic flight campaign except for the PHP and its support which was totally new and specially developed for this experiment.

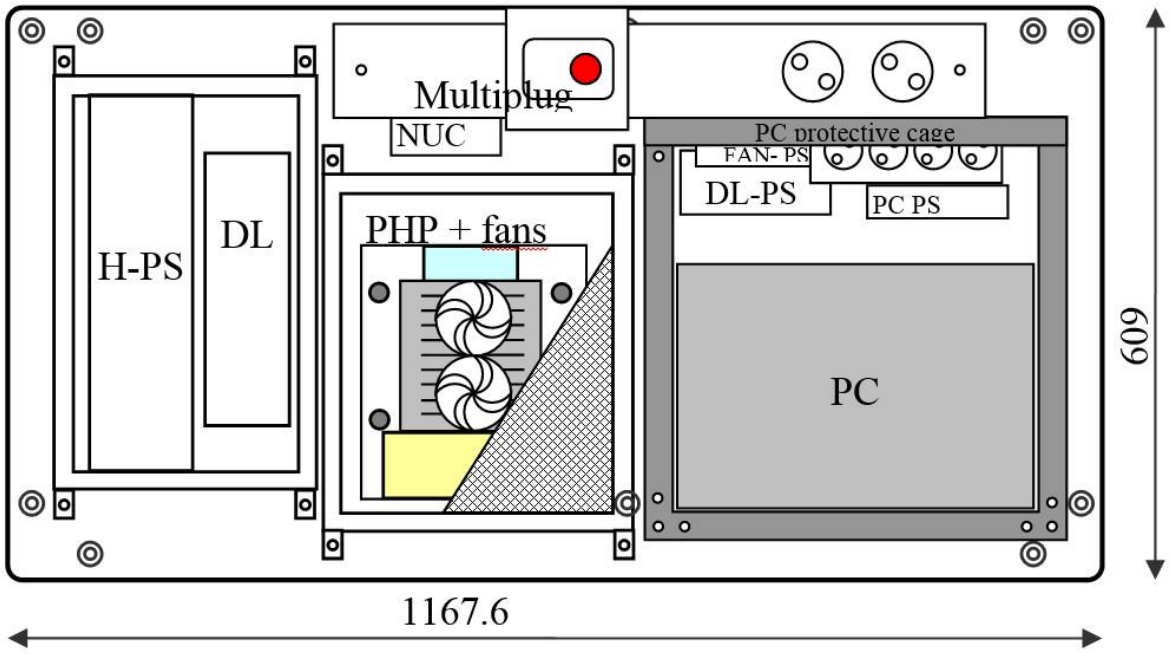

Figure 3.2: General layout of the experiment: the rack plate with the PHP cage covering the PHP assembly, PS=Heater power supply DL=data logger, notebook PC with its protective cage, PS and multiplug (Araneo, 2015)

3.1 PC and power supply zone

On the right part of the rack there was one laptop, one mini PC, three power supplies, one for fans and light, one for the data logger and one for the laptop and two multiplugs.
The Laptop (HP Pavilion DV6), which managed the acquisition software, the Heating power and the mini PC, was fixed to the rack with some aluminium profile (ITEM) to maintain both the base and the monitor in position. The mini PC (Intel NUC D34010WYK) is linked with the camera and has the only task to manage the video acquisition. It works with the monitor of the laptop.
Behind the laptop there were the three power supplies and the two multiplugs. One multiplug was linked to the power supply of the aircraft and gave power to the mini PC and the second multiplug which fed the fan and light, data logger, laptop and the power supply for the heater with separated switches one for each plug.

3.2 PHP Assembly

It was constituted by the studied PHP and the components which made it work. It was built in order to be easily disassembled from the rack to simplify the ground tests and the maintenance work.
During the parabolic flight, it had to be covered by an external protective cage (not shown in the figures) for safety reasons.

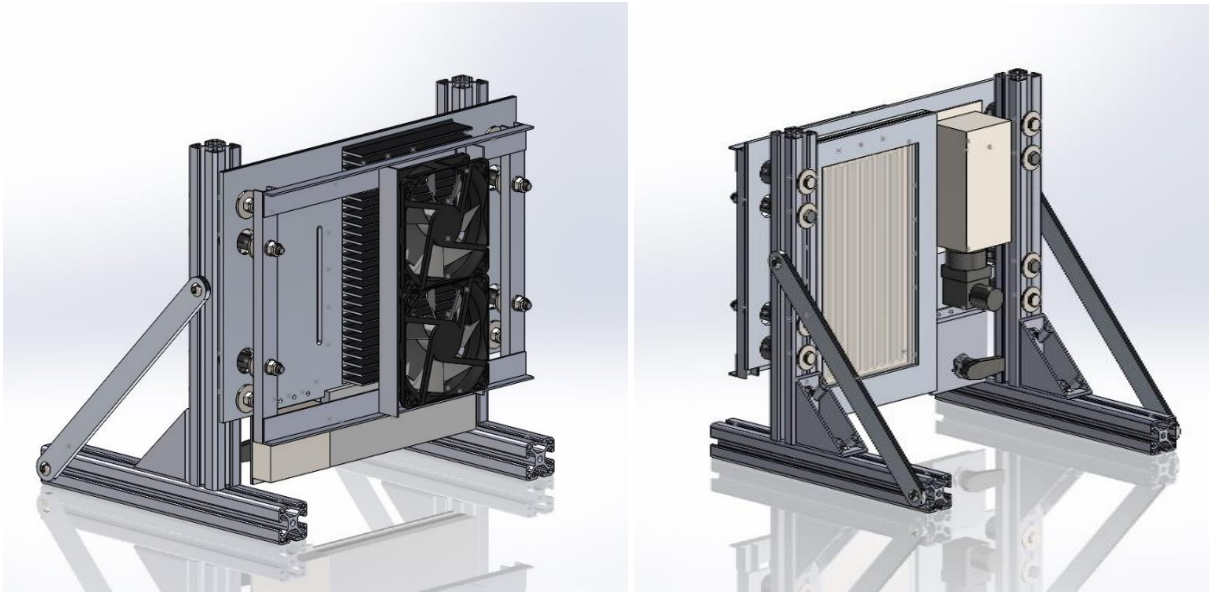

Figure 3.3: CAD Drawings of the PHP assembly

3.2.1 PHP

It was the core of the experiment, it is composed by a machined copper plate with a glass glued on it to allow the visualization of all the phenomena. The heater was brazed on the copper plate and is a smaller copper plate with an electric heater (Thermocoax) inside it; the condenser is made by an aluminium heat sink with an air flow forced by two fans. All parts which could present a leakage of fluid must be included inside a second containment to prevent the dispersion of the fluid inside the airplane in case of failure of the PHP.

3.2.1.1 Copper Plate

It had the overall dimension of 204mm X 124mm X 2,5mm. A rectangular channel, 2,5mm wide and 2mm deep, was engraved by a CNC machine to form a close loop. It presented 11 U-Turns on the evaporator zone (see figure 3.4).
Two copper pipes of 1/16" were inserted and brazed into two of the sides of the copper plate in order to link the filling valve and the pressure transducer: the one on the right top for the pressure transducer and the other one in the middle of the 6th U-Turn on the evaporator zone for the filling valve.
The pressure transducer is the General Electric, PTX5076-TA-A3-CA-H0-PS, 5 bar absolute. The valve is a Swagelok, SS-41S2.
On the external side of the copper plate, six square channels, side 1mm, were machined for hosting the connections of 12 "T" thermocouples. (bead diameter 0.3 mm, tolerance Class 1) Six thermocouples were positioned on the evaporator zone and six on the condenser, two on the top of the condenser, two on the middle (7cm from the top) and two on the bottom part (13cm from the top) (see figure 3.5). Other 4 thermocouples were positioned, one for the ambient temperature, one for the air temperature near the heater (inside the second containment), one for the inlet air temperature of the condenser fins and one for the outlet air temperature of the condenser fins.
The PHP was fixed to the heat sink with three clamps of Ertalon screwed directly on the heat sink.
To perform a better heat transfer a conductive pad of 0,5mm thick was placed between the copper plate and the heat sink.

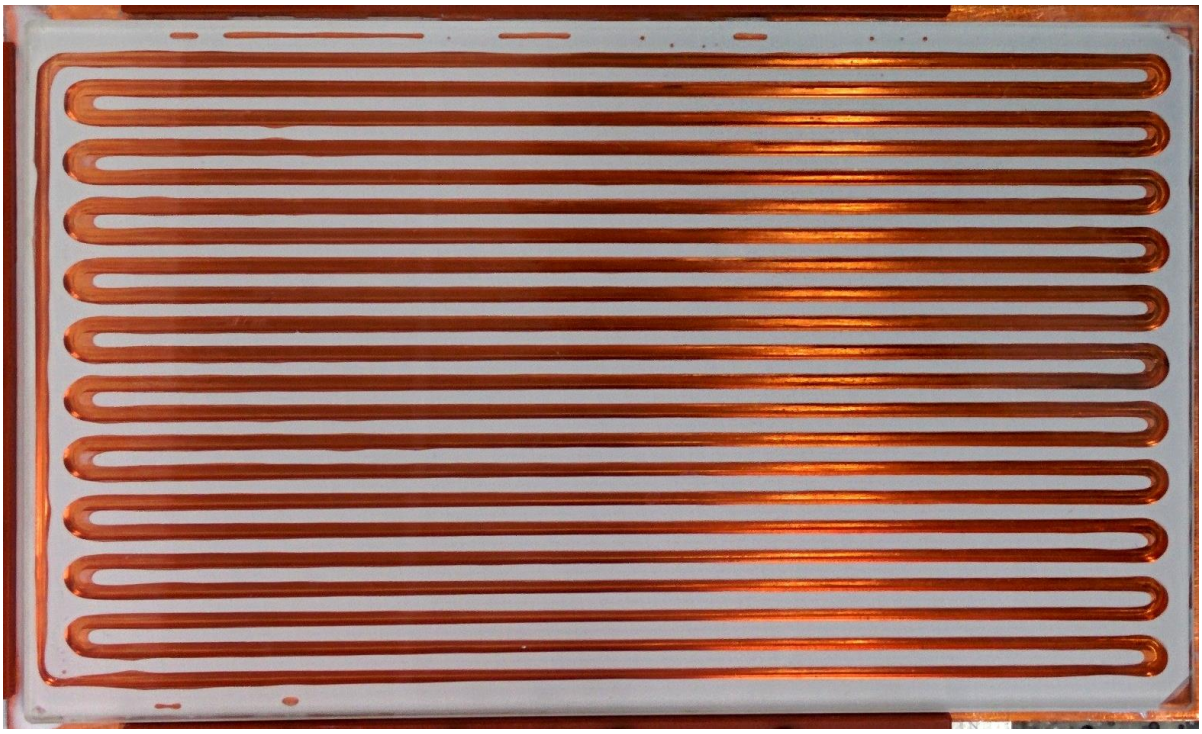

Figure 3.4: Front view of the "white" PHP with the NUSIL glue

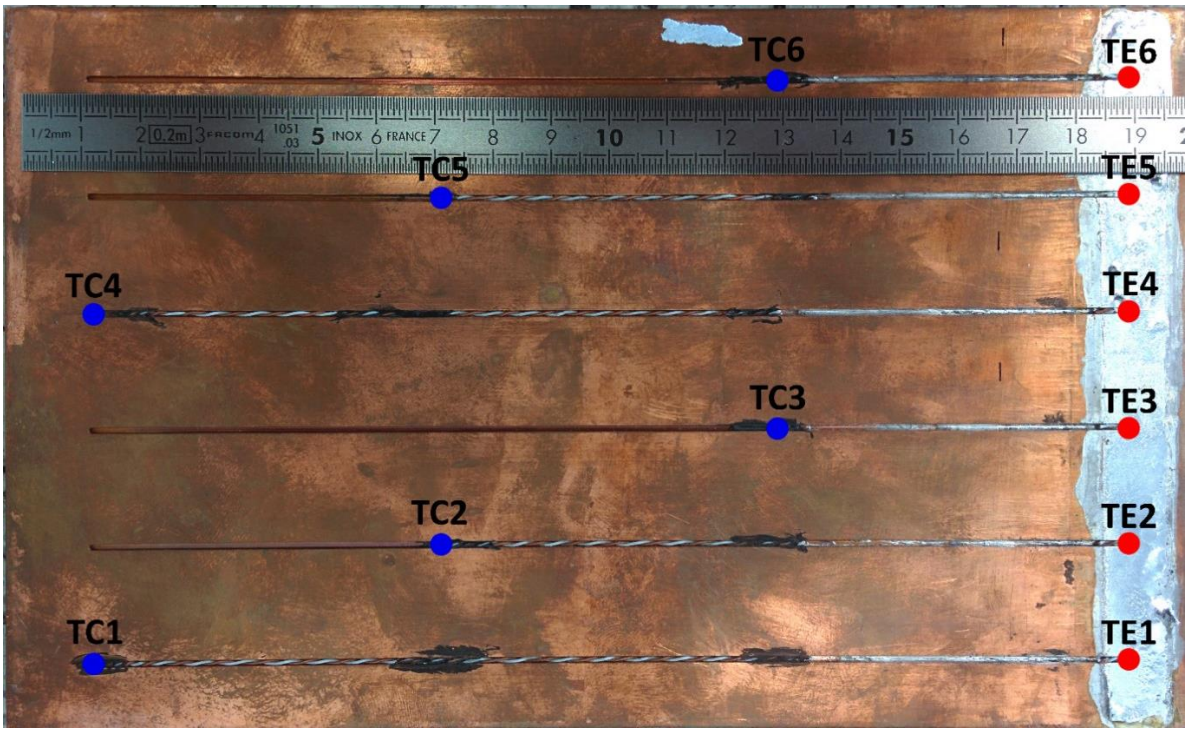

Figure 3.5: Rear view of the PHP with the position of the thermocouples (TCx= condenser, TEx= evaporator)

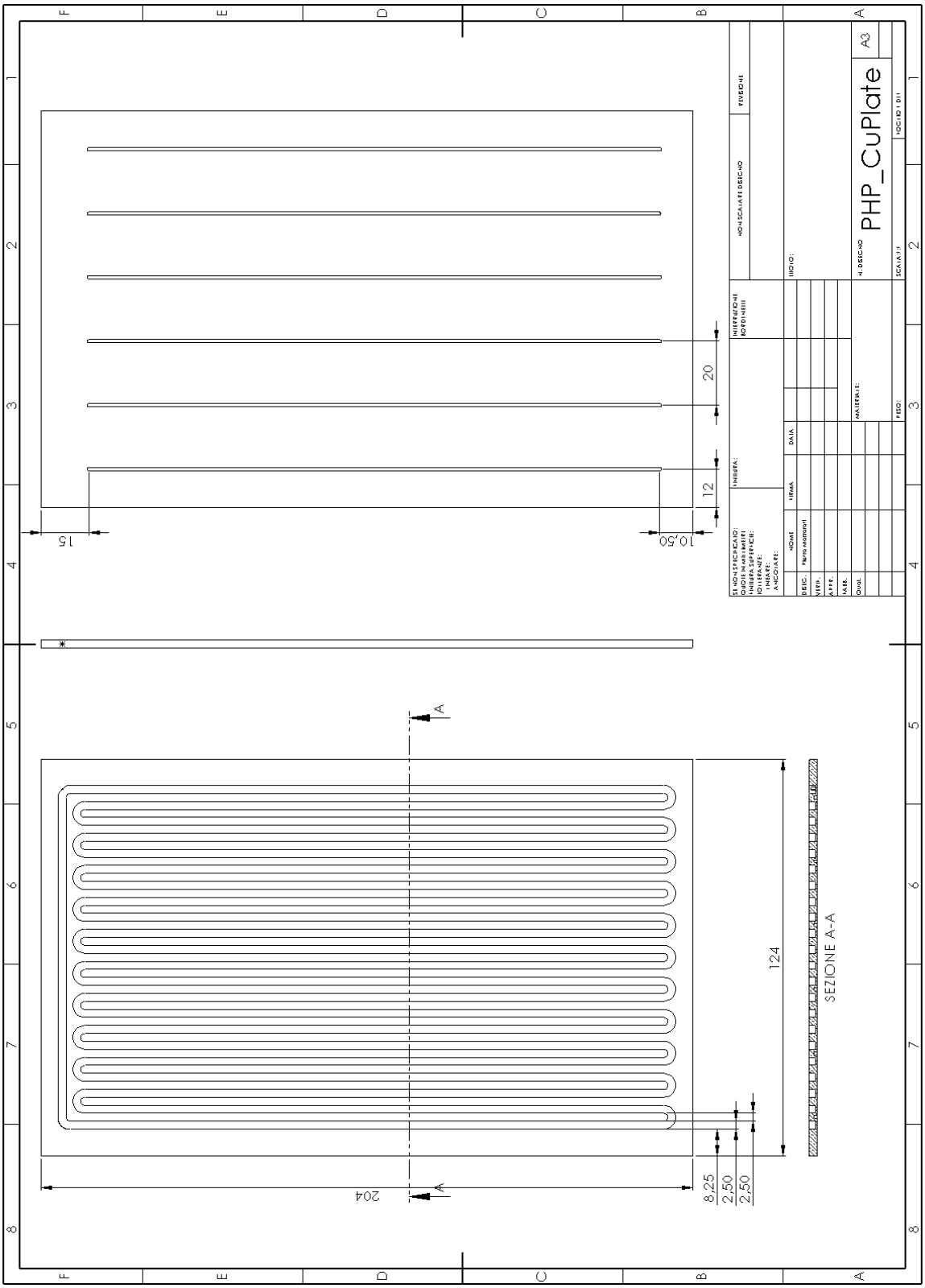

Figure 3.6: Technical drawing of the copper plate

3.2.1.2 Glue

The glue must have some specific properties:

- Good adhesiveness on copper and glass;
- Good elasticity in order to compensate the different thermal dilatation between copper and glass;
- Outgassing as low as possible in order to have a negligible release of non condensable gasses inside the PHP;
- Good ability to stand high temperature (minimum 150°C).

It is very hard to find a glue that matches all this properties because if it has good elasticity, generally silicon glue, it also presents considerable outgassing. To avoid outgassing a good choice is to use epoxy resin but, in this case, the elasticity is very low.
It was decided to test two different PHPs: one using silicon glue (Nusil CV-2566P) with its primer (Nusil SP-120) to increase the adhesiveness on the copper plate (from now on, it will be called “White” because of the colour) and one using epoxy resin (Loctite 3609, called “Red” because of the colour).
The thickness of the glue was 0,5mm with the aim to create together with the engraved copper plate and the glass a square section of the channel of 2,5mm.

3.2.1.3 Glass

We chose a Borosilicate glass with the overall dimension of 200x120mm and a thickness of 3mm. This kind of glass has a very good resistance to temperature fluctuations and a very high transparency but it has a very low coefficient of thermal dilatation compared with the one of the copper plate. This caused some problems due to the high curing temperature with the epoxy resin.

Borosilicate Physical Properties	
Density [kg/m2]	$2.23*10^{3}$
Hardness [HK]	480
Coefficent of thermal expansion [m/K]	$3.25*10^{-6}$
Thermal Conductivity [W/mK]	1.14
Index of refraction [-]	1.472
Poisson's ratio [-]	0.2
Young's modulus [KN/mm2]	64
Softening point [°C]	820 ±10

Table 2: Proprieties of the borosilicate glass

3.2.2 Condenser heat sink

The Condenser zone of the PHP copper plate was connected to a heat sink, cooled by an air flow forced by two fans (see figure 3.7).
The heat sink, machined from a commercial extruded profile, is an aluminium plate of 320x200mm and 4mm thick with a finned part of 172mm X 120mm in correspondence of the condenser.
In order to reduce the thermal bridge along the side of the heat sink and have a more homogeneous cooling on the condenser zone, two slots were machined just next to the PHP (see figure 3.8).
The heat sink is also the support for all PHP Assembly except for the fans which are fixed to the vertical support with some L and U aluminium profiles.
The two Fans (Sunon PMD1209PTB1-A) are 92mm of diameter each and blow off $132m^3/h$ from the fins to outside the cage in order to have a more homogeneous distribution of fresh air. To avoid air recirculation an air shield was stuck along the whole perimeter of the fans outlet to better direct their flow.

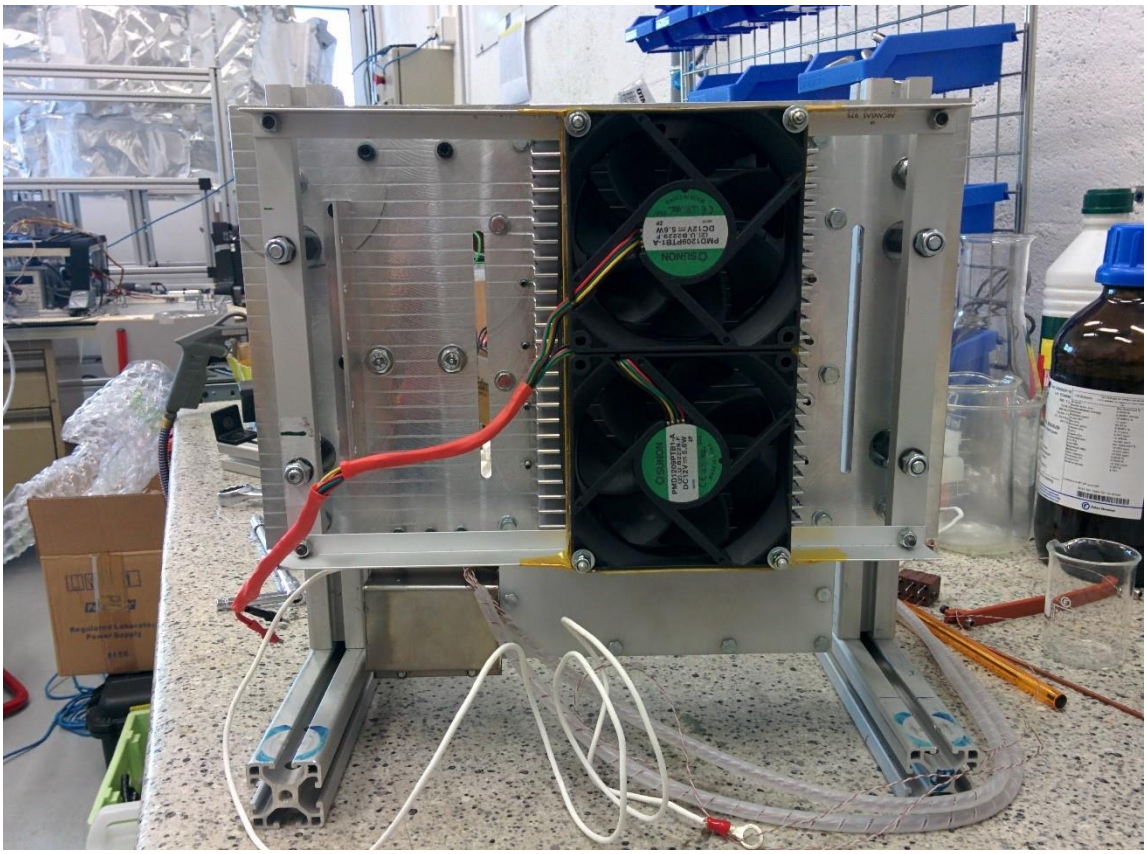

Figure 3.7: Rear view of the PHP assembly showing the heat sink and the fans

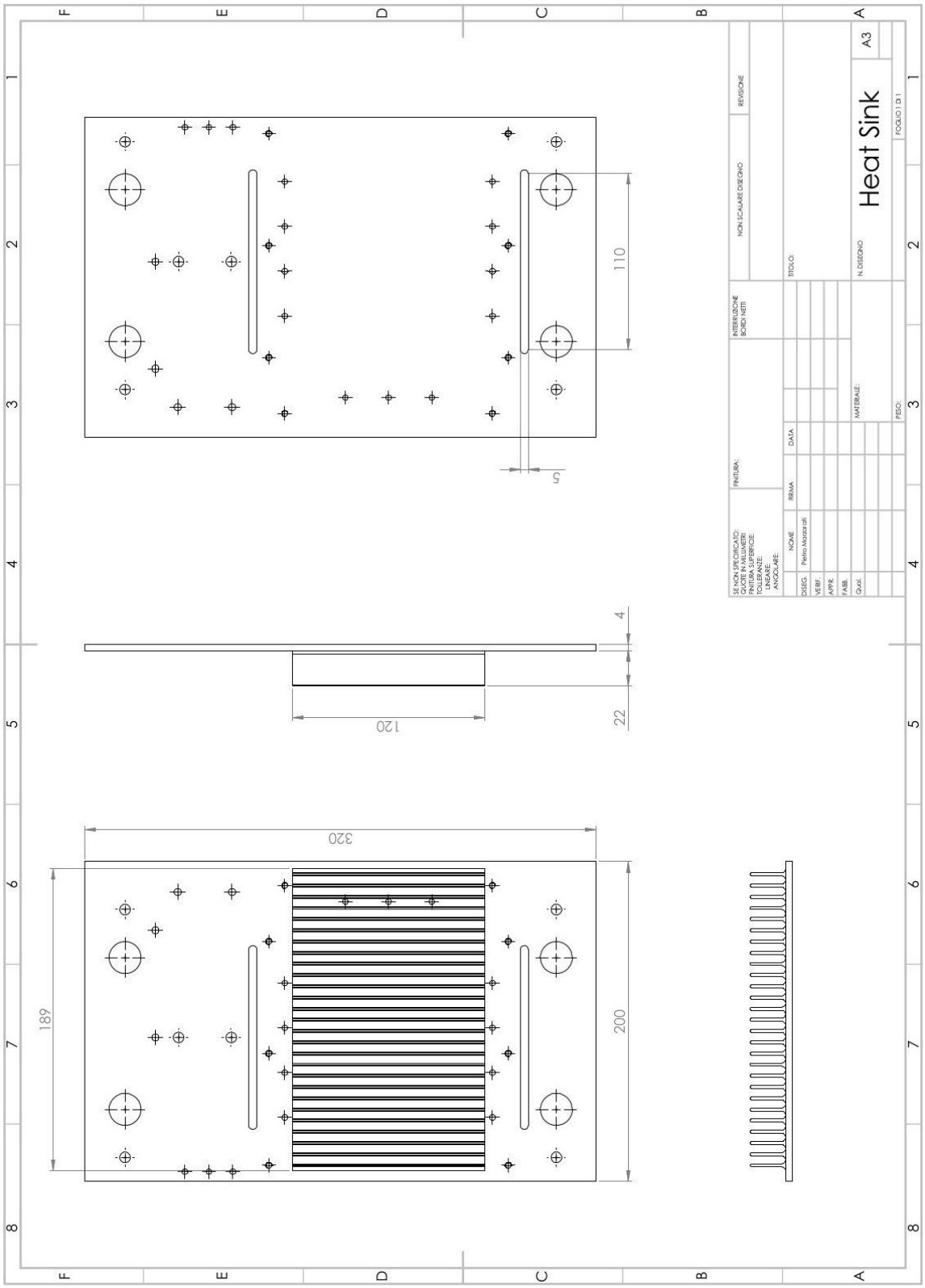

Figure 3.8: Technical drawing of the Heat sink

3.2.3 Heater

The heater (see figure 3.9) is an externally isolated electric resistor of 30cm (Thermocoax Type ZEZAc10) bent in a S shape, with a resistance of 3,81Ω with a maximum used power of 150W. The Thermocoax was inserted in a small copper plate of 120 x 10 x 2mm , which was directly brazed on the copper plate of the PHP. In order to prevent the evaporator overheating, two thermal switches (DMP 11MP 150H 046E) with a cut-out temperature of 150°C were positioned on the Thermocoax. They were clamped to the heater by an Ertalon 4.6 clamp (see figure 3.10).

Figure 3.9: Heater brazed onto the copper plate with the Thermocoax bended in a S shape

Figure 3.10: View of the heater with the two thermal switch hold by the Ertalon 4.6 clamp

3.2.4 Recording devices

The high speed camera we used (Ximea MQ013MG-ON), was directly linked with the mini PC by an USB3.0. It had a lens with a focal length of 8,5mm which allowed to fit all the PHP on the recording area with the help of a mirror (see figure 3.11).
The camera was mounted on the left vertical support of the heat sink at half height of the PHP, an angulated polycarbonate mirror mounted on a vertical aluminium profile support reflected the image of the PHP towards the camera. In order to have a better image quality two led stripes of 4W, 160mm length each, were needed. One was stuck on the base plate of the rack in front of the PHP and the other on the top of the protective cage on the internal side. We recorded with a frame rate of 50 Hertz.
We had to cover all the parts near the mirror and the internal side of the protective cage opposite the PHP with a black cardboard to avoid unwanted reflection on the recording area.

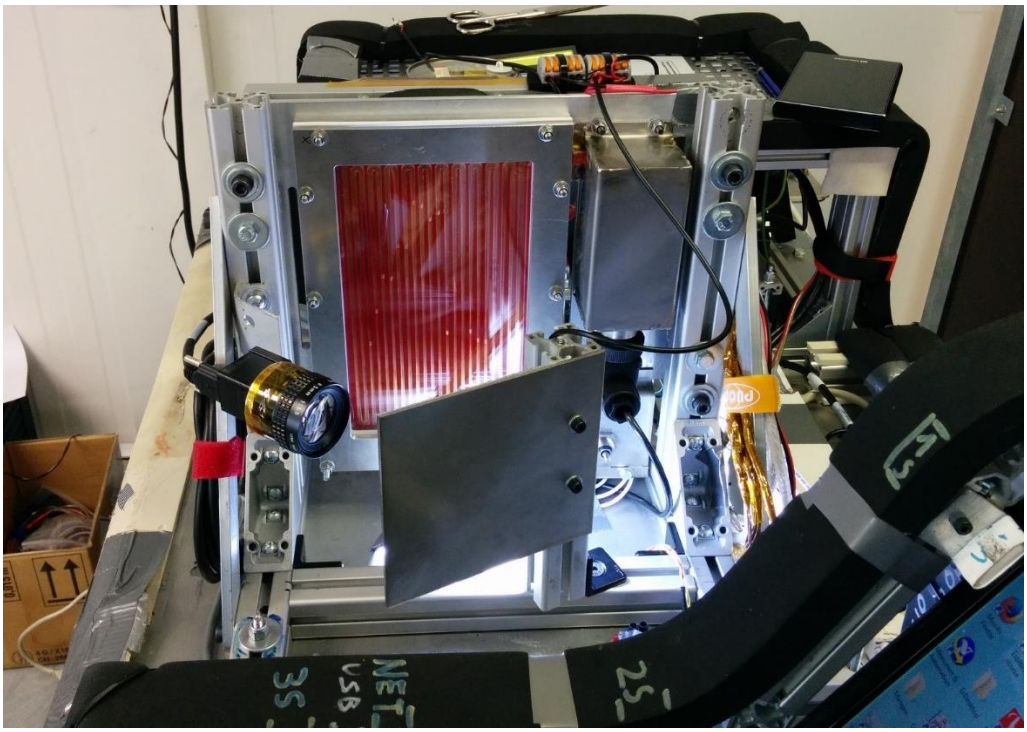

Figure 3.11: The PHP assembly, with the small Camera on the left, the mirror and one LED light. The second LED stripe stuck on the protective cage is not present on the picture.

3.2.5 PHP holding support

The structural part was made of four 30mm aluminium profiles (ITEM) positioned in order to form two reversed Ts. The support should be able to support, in case of emergency landing, an acceleration of 9g along the aircraft X axis, that is on the direction perpendicular to the PHP. To increase the rigidity of the support two transversal rods links the vertical and the horizontal structural profiles (not shown in the figure 3.12).
The heat sink, which acts also as the support of the PHP, pressure transducer, valve and thermocouples, was fixed to the vertical support by four silent block (Wagner D20mm h15mm M6) in order to reduce the vibration generated by the aircraft and by the fans, and to insulate electrically the PHP assembly.

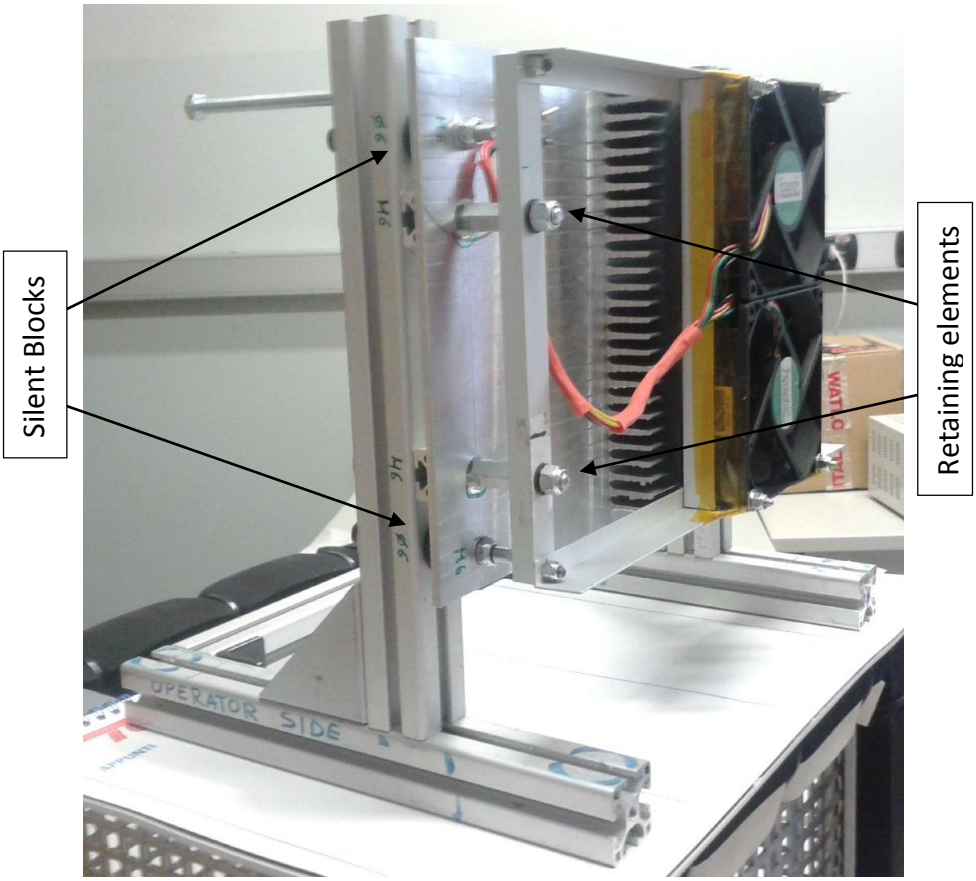

Figure 3.12: Side view of support and heat sink. On the picture are indicated the silent block and the retaining elements. (Araneo, 2015)

In case of high acceleration, 4 screws M6 were inserted to avoid the break of the silent blocks and the detachment of the heat sink from the support. The frame to support the two fans was attached to these screws too (see figure 3.13).

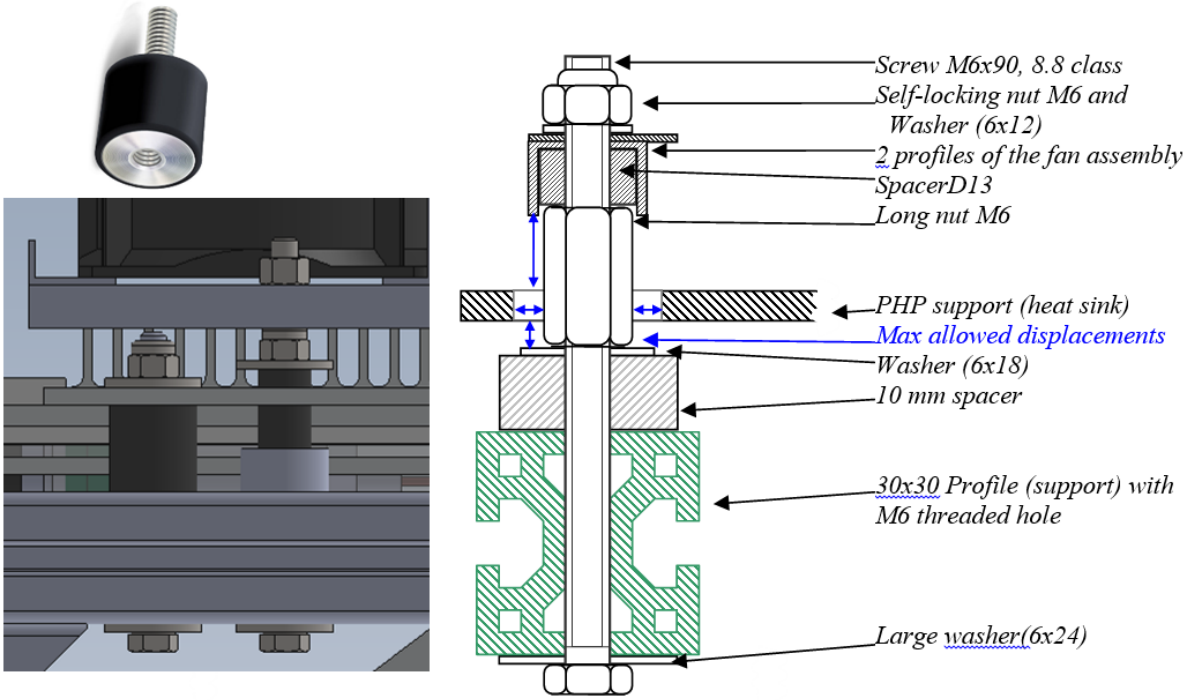

Figure 3.13: Anti-vibrating support and retaining elements. (Araneo, 2015)

3.3 Data Logger Zone

Under the protective cage it was positioned the Heater Power Supply (GWinstek PSH-3610), which is a programmable power supply controlled by the Labview software on the laptop. Next to the Power supply there was the gravity sensor (Dimension Engineering ACCM3D) and the data logger.

The data logger was the NI CompactRIO 9073 with the module NI 9214 for the 16 thermocouples and the two modules NI 9205 and NI 9264 to collect the signal from the g sensor and the pressure transducer and give power to both sensors too.

3.4 Safety Devices

3.4.1 Overheating protection

Some preventative measures, both software and hardware, had to be taken to avoid overheating on the evaporator. (Rosier, 2014)
First of all it was inserted a cut out temperature on the Labview software. When the temperature in at least one thermocouple on the evaporator zone (included the air near the heater thermocouple) exceeded 130°C, the software immediately cut the power to the heater. The same procedure was applied to the condenser thermocouple, but in this case the cut out temperature was of 80°C.
The Hardware protection was made of two thermal switches linked in series between the power supply and the electric resistor which, in case the temperature exceeded 150°C, immediately opened the electric circuit. The two thermal switches were in direct contact with the hottest part of the heater (see figure 3.14).
All the hot parts of the PHP were intended to support temperatures higher than 150°C.
To avoid the direct contact with the hottest part, which can be dangerous for the operator, a second containment was used. It was made of Ertalon 66SA which is able to resist to high temperature (180°C for short periods), it is very easy to machine and offers a good electric and thermal insulation.

Figure 3.14: Thermal Switches (in blue) hold by the Ertalon 4.6 clamp

During the ground test, the maximum temperature read by the thermocouple in the worst condition (horizontal and 130W at the evaporator) was 120°C, so we expected that during the

parabolas with the PHP in an operative favourable way i.e. vertical with the evaporator under the condenser or in microgravity, we shouldn't pass over the safety value.
Thanks to the Ertalon 66SA containment (see figure 3.15), it was possible to touch the evaporator zone without burning. During the parabolic flight, the external protective cage covered all the PHP assembly.

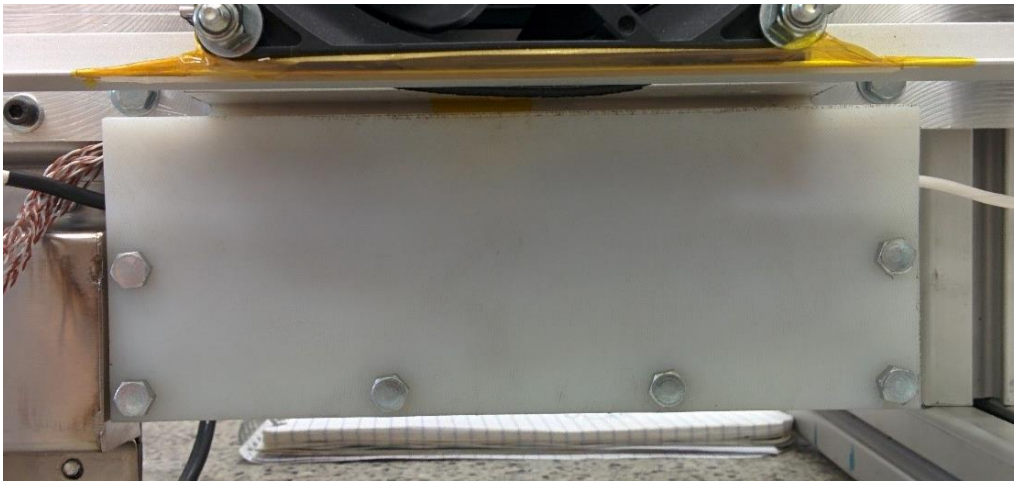

Figure 3.15: The Ertalon 66SA cover of the heater

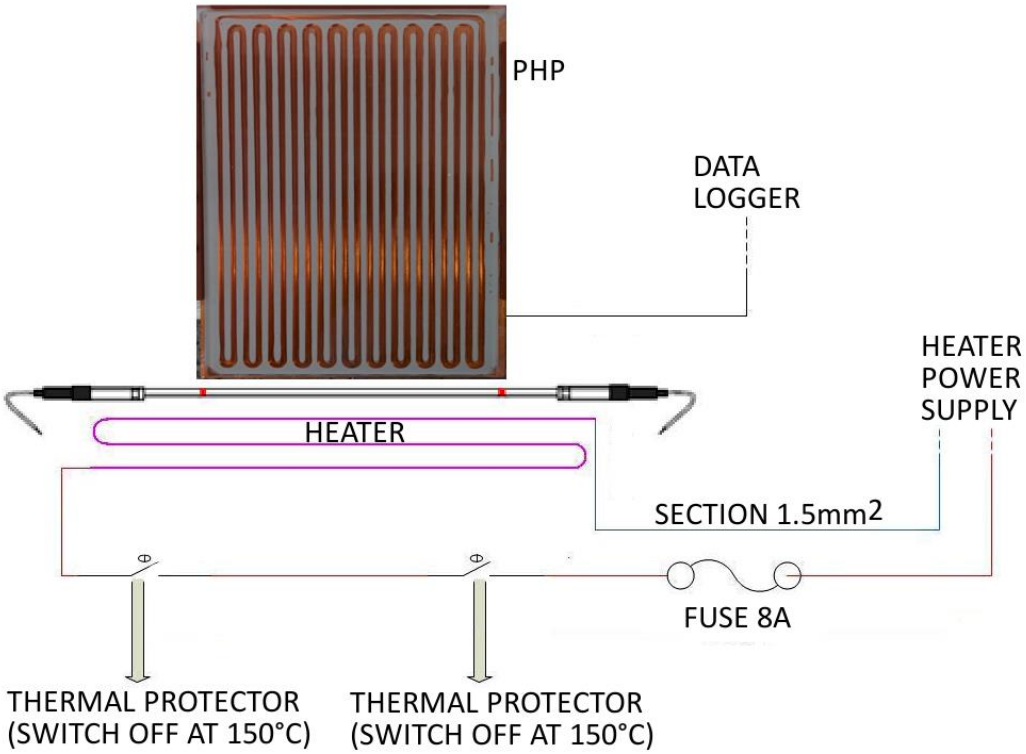

Figure 3.16: Details of the electrical heater schematic. (Araneo, 2015)

3.4.2 Electrical Protection

Due to the large use of the electric current, it is important to introduce a safety system to prevent any injury on the side of the operator. (Rosier, 2014)
All the cables are at low voltage except for those which give power to the heater. Due to the resistance of 3,81Ω of the Thermocoax, with the maximum power at the evaporator, we have an electric tension of 23,9V from the power supply with a current of 6,3A, so we are in any case inside a safety level (25V is a limit for a not so dangerous consequence on humans).
The entire safety system is well described by Rosier P. (2014).
For any separately-purchased converter, which wasn't supplied together with off-the-shelf electric equipment, a fast fuse had to be added at the converter output in order to open the electric circuit in case of short circuit. Due to this, three fast fuses were inserted after the power supply of the heater with a broken limit of 8A (6,3A of maximum current in normal functioning at 150W), fans, lights and data logger with a 2A fast fuse, one for each power supply.
The experiment had to be linked to the aircraft ground connection, in this case the multiplug provided for this. All the metal structures of the rack had to grant an electrical continuity to the ground too.
The electric cables shall be sized according to the intensity of the current in it. In order to have a low resistance, a cable with a section of 1,5mm^2 to link the power supply to the heater (Novespace suggests a minimum section of 0,93mm^2 for a current of 10A) and 0,75mm^2 for all the others was chosen. In case of strand wire, it is compulsory to use crimp type terminal on the electric connections.

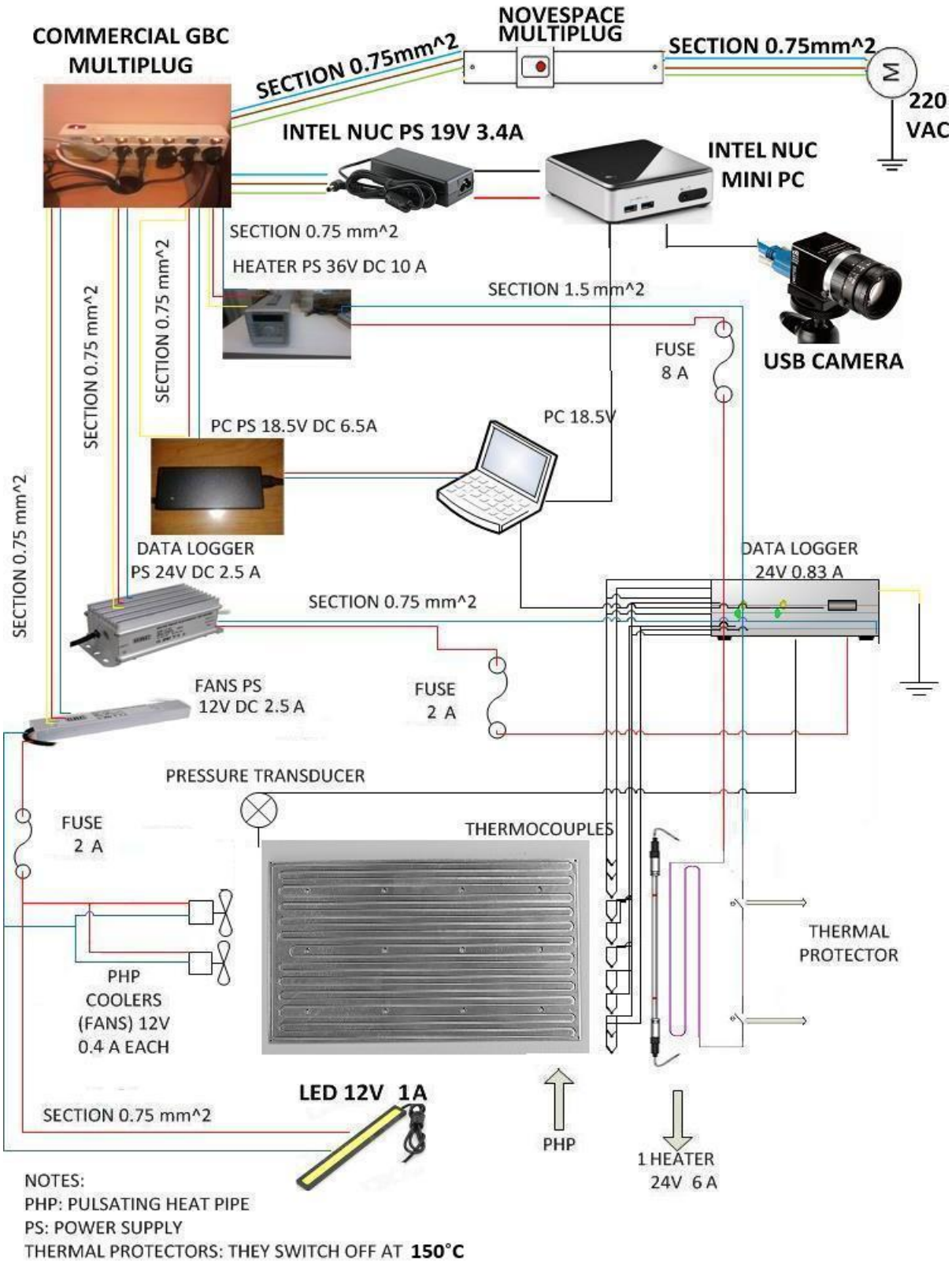

Figure 3.17: Details of the general electrical schematic. (Araneo, 2015)

3.4.3 Fluid Leakage Protection

If a fluid is used on the experiment, you must take in consideration the risk of contamination of the cabin. Due to this fact, it is compulsory to have a second containment to avoid fluid leakage into the cabin. (Rosier, 2014)
The fluid which was used, FC-72, is not inflammable and only slightly irritant.
In our case, the first containment was guaranteed by the copper plate, the glue and the glass. In case of failure, a second containment was positioned in conformity with Novespace guidelines.
One part of the second containment was the heat sink itself, where the PHP was attached. An aluminium frame surrounded the PHP. A PTFE frame, which pressed a little bit on the glass and helped to maintain the PHP on position, was added. Next to this a polycarbonate sheet was added to close the second containment and allow to see inside and finally an external aluminium frame to distribute the pressure of the bolts (see figure 3.18 and 3.20).

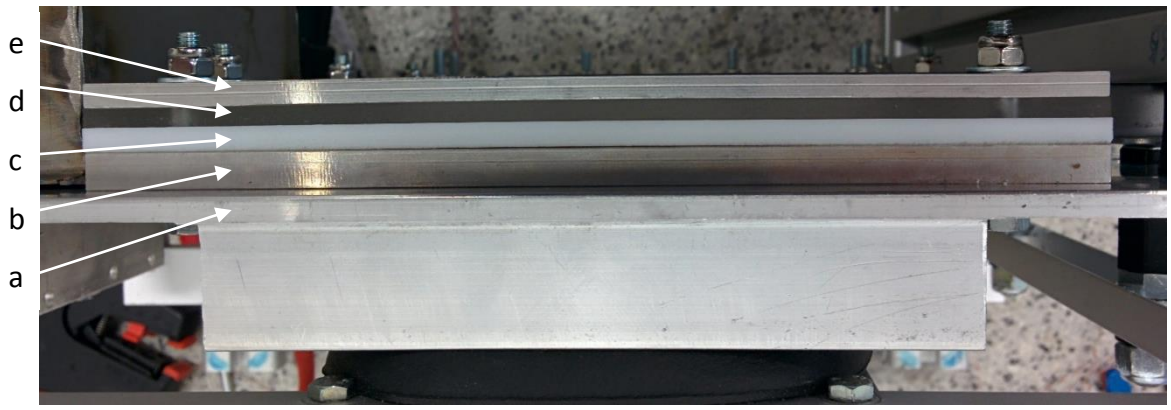

Figure 3.18: Top view of the PHP second containment. a)Heat Sink, b)aluminium frame, c)PTFE frame, d)polycarbonate window, e)aluminium frame

In normal operating condition, that is when the minimum temperature of the vapour of FC72 is less than 50°C, the pressure inside the channel is below the ambient pressure inside the aircraft. Therefore, in case of leakage, due to the difference of pressure, the result will be the coming in of the air inside the channel and not the dispersion of the fluid in the second containment.

In case of quickly release of the fluid it will evaporate immediately, producing less then one litre of vapour. A second containment was also placed for the filling valve and the pressure transducer, made by a sheet of stainless steel, appositely bended to form a box (see figure 3.19).

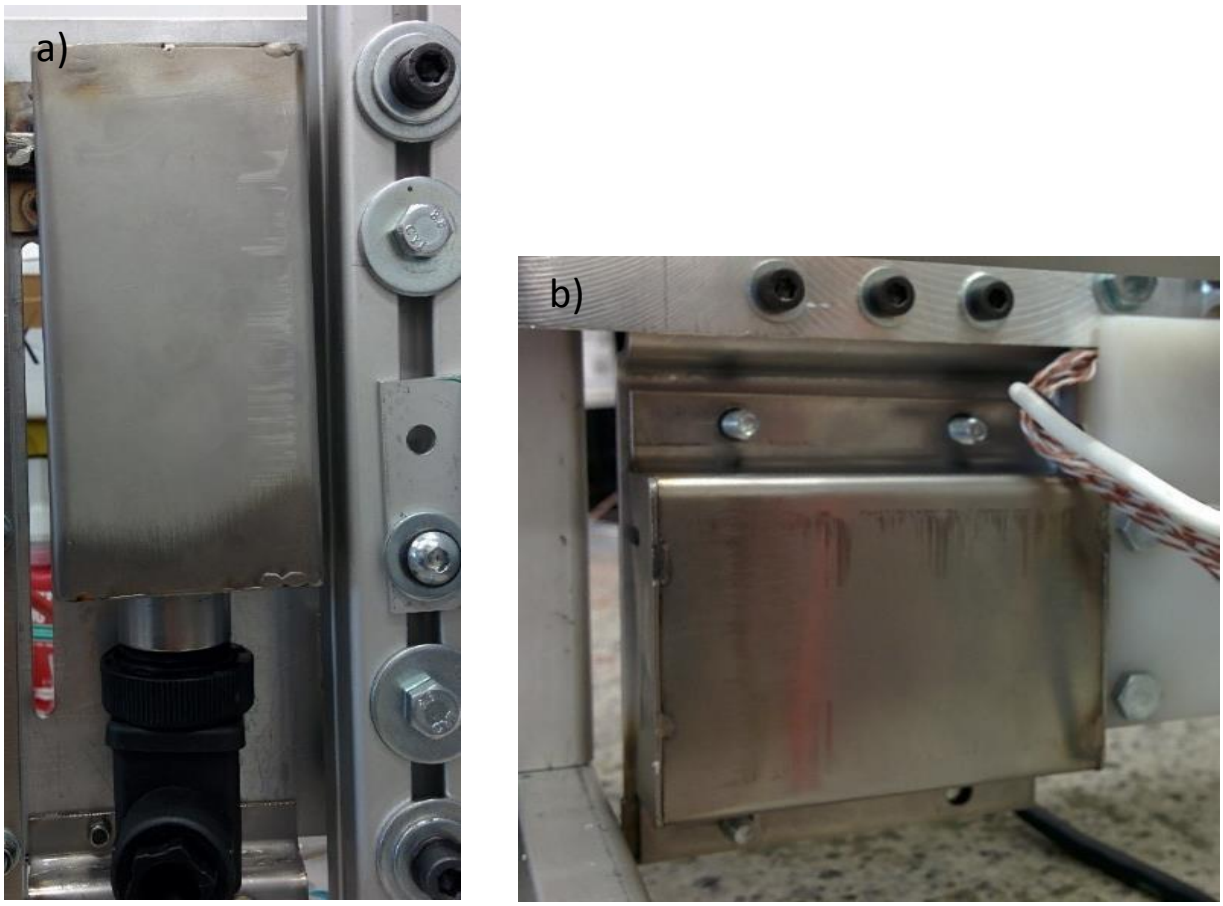

Figure 3.19: a) Second containment for the pressure transducer. b) Second containment for the filling valve

On the evaporator, the Ertalon protection also worked like a second containment for the fluid. In our case, the second containments were not perfectly sealed to avoid any problem of over-pressure and let the gas go out in case of depressurization of the cabin or failure of the security control on the temperature.

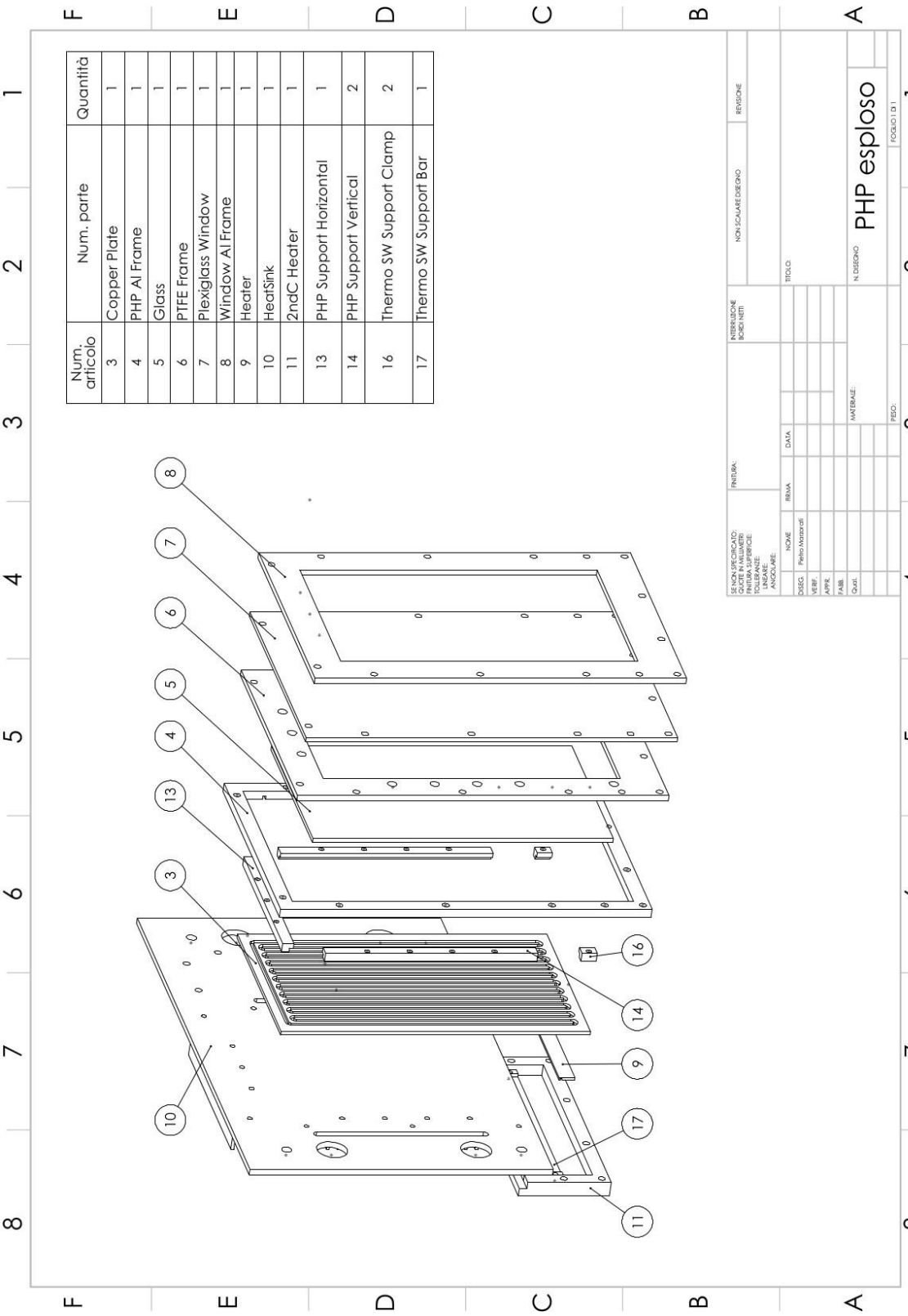

Figure 3.20: Exploded view diagram of the PHP second containment

4 PHP construction and assembly

The gluing of the glass on the copper plate was one of the most difficult parts of the building process. Here below are described some steps up to the building of the final version.
Another essential part of the assembly was the filling of the PHP with the working fluid. During this procedure it is important to follow all the required steps to reduce as much as possible the introduction of non condensable gasses inside the PHP.

4.1 Gluing process

The main difference between this PHP and those built for the parabolic flight campaign number 60, is that one side was now made of glass instead of Copper.
The gluing process soon introduced some difficulties in the building process. It was important to choose the correct glue, which must have some specific proprieties, and to spread it in the correct way to obtain the most homogeneous distribution not to hide the channels and to have a good grip on glass and copper in order to avoid leakage.
For the gluing process, it was decided to use the machine LPKF ProtoMat 92s to place the glue evenly.
The LPKF ProtoMat 92s is a circuit board plotter governed by a PC. For our purpose, the mill was removed and an appositely created syringe holder was positioned in its place.

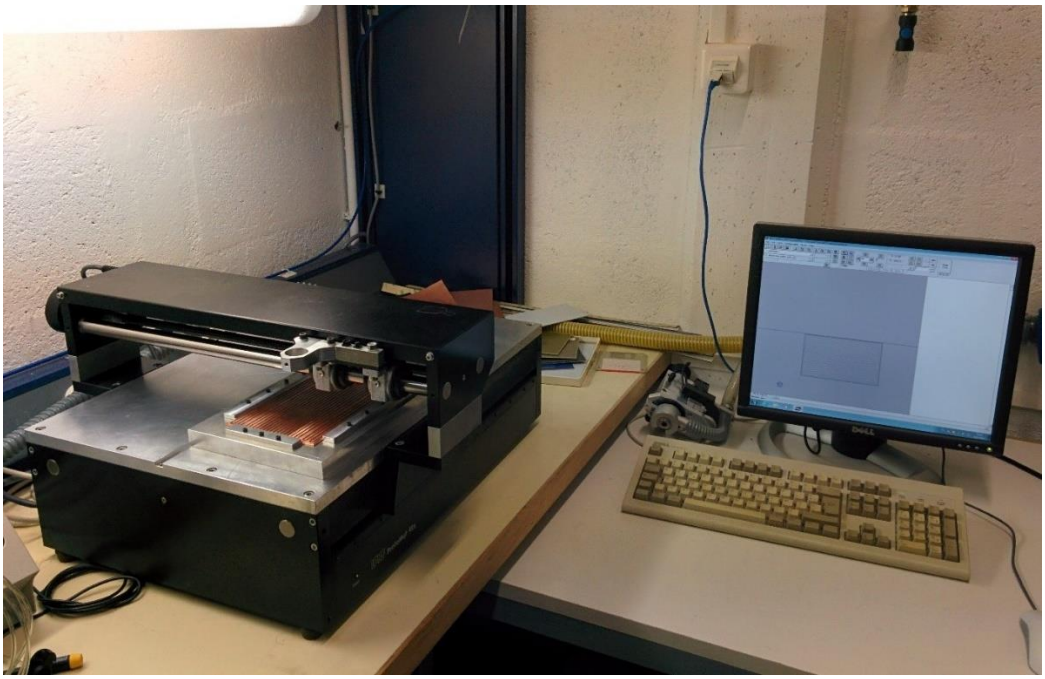

Figure 4.1: Gluing desk with the gluing machine controlled by the computer (the syringe is not present)

The glue was spread out from the syringe with a pneumatic command, which used compressed air at 0,5MPa, a constant pressure on the syringe plunger was applied and it was possible to change the extrusion speed by changing the needle of the syringe.
The routing for the machine was drown on the machine software and thanks to this it was possible to spread the glue with a quite good precision (see figure 4.2).
The first series of tests was performed with the epoxy resin Loctite 3609. Due to its colour, the PHP built with this glue was called “Red” PHP.
A second type of glue was used, the silicon CV-2566P. Due to its colour, the PHP built with this glue was called “White” PHP.

Figure 4.2: Routing for the gluing machine software

4.1.1 Gluing Test #1: Speed check

The aim of this test is to find the correct movement speed of the syringe in order to have the good amount of glue.
Since at the time of this test, the final geometry of the PHP to be used during PFC 62 had not yet been defined, The copper plate used for this test has the same geometry of the one which had been used during the previous parabolic flight campaign number 60, which had slightly different geometry (Ayel V., 2015; Scalambra A., 2014). The copper plate has the overall dimension of 200 x 120mm, the channel is 1,6mm wide and 1,7mm deep with a spacing between two adjacent channels of 3mm except for the two couples of channels which are separated by 5mm.
The copper plate is positioned on an aluminium support and held by four profiles screwed on the support. After the gluing, the glass, a 3mm thick borosilicate glass, was positioned on it and was maintained 0,3mm distant from the surface of the copper plate by the four profiles. After that an aluminium foil, 10mm thick and larger than the glass, was positioned to distribute the pressure and spread the glue correctly.
During the first test, two lines of glue were placed for each speed, in this case it was chosen a movement speed of 4mm/s, 3mm/s, 2mm/s and only one line for 1mm/s . It was expected a much bigger line for the 1mm/s and a thinner one for the 4mm/s maintaining the same extrusion speed.

It is possible to notice on the figure 4.3b how the spread of the glue is not uniform and not congruent with the different movement speed.

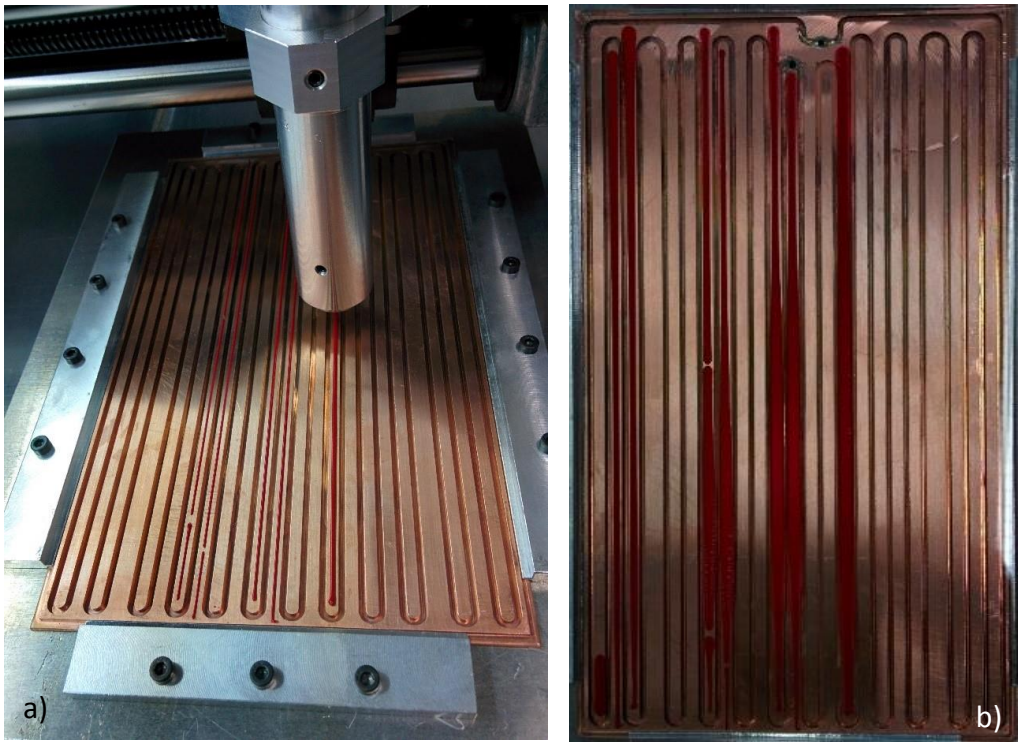

Figure 4.3: a) Gluing process. b) Result of the first gluing test. Loctit "red"e glue.

This may be due to the fact that the surface of the copper plate, the support and the profile where the glass was placed were not perfectly level or to an eventual raise at the centre of the copper plate due to the squeeze by the profile which holds the copper plate.
Another basic parameter for the correct distribution of the glue is the centering of the PHP with the reference point of the gluing machine, which has to be done manually. A preliminary positioning was done with the help of a ruler and moving the PHP trying to set it as parallel as possible with the reference point of the machine. After that, the syringe was moved to the four corners and in the middle of some channels to check the correct position. In case it wasn't parallel with the machine reference point it was adjusted by rotating the PHP. If the PHP was only shifted compared to the machine reference, it was adjusted by changing the machine reference within the software.
Another problem occurred in this test was the presence of a short interruption of glue in the middle of the lines. It is possible to notice how in the two lines at 3mm/s there are three little gaps, this was probably caused by some bubbles inside the syringe which randomly went out

causing the interruption of the glue extrusion. If it happened during the final gluing the operator had to put some glue in the gaps manually.
The copper plate, the support and the four profiles were processed manually in order to have a better planarity, after this, it was checked with a comparator and the result was an average deviation of +/- 0,05mm.
The gluing test was repeated with four lines at 3mm/s, two lines at 2mm/s, two lines at 4mm/s and two lines at 5mm/s.

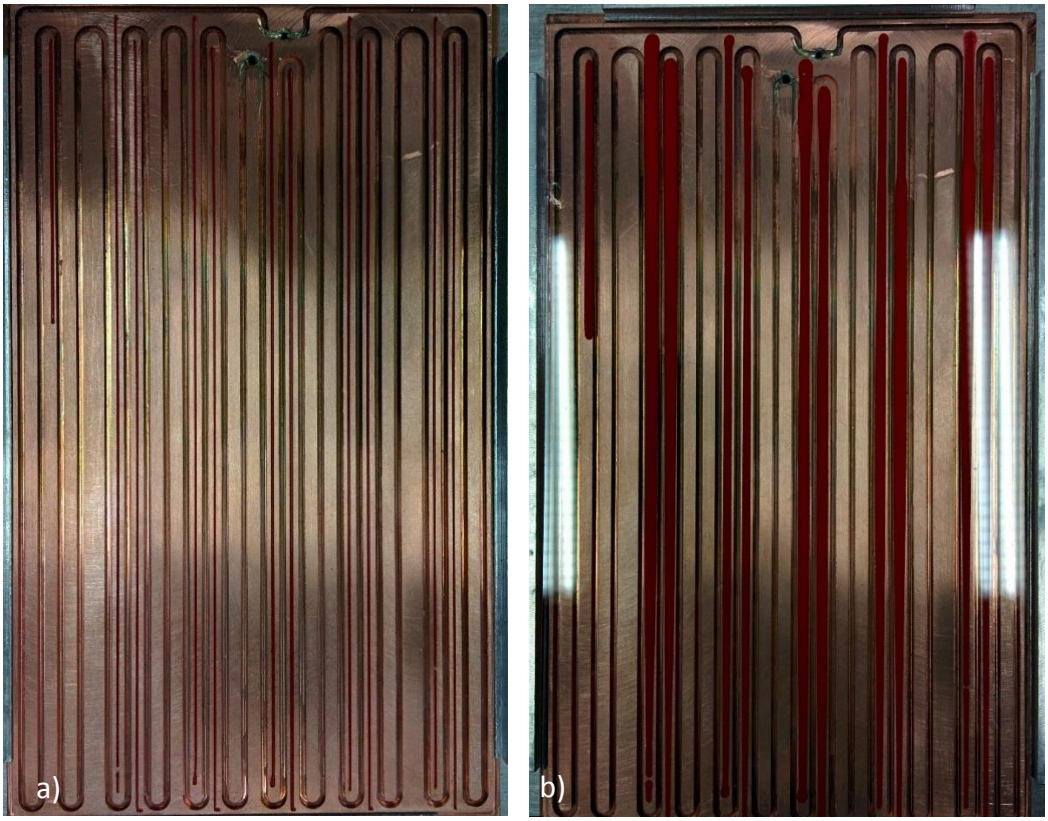

Figure 4.4: Gluing test. a) Deposition of the Loctite "red" glue, from left to right: four lines at 3mm/s, two at 2mm/s, two at 4mm/s and two at 5mm/s. b) Spreading when the glass is applied.

It is possible to notice on the figure 4.4b how the distribution now is a little better, but not enough to be considered a good result.
There are still evident some gaps due to the presence of air bubbles in the syringe. During this preliminary tests the gaps weren't filled because the main objective was to find the correct movement speed.

In order to have a more homogeneous spread of the glue, it was decided to place four calibrated spacers on the corners between the copper plate and the glass and to rub off a part of the profiles for the support also used for the spacing, so that they didn't touch the glass.
For the last speed check it was tested the same speed still with two lines each speed. In this case it was tested: 4mm/s, 3mm/s, 2mm/s, 1mm/s, 2mm/s, 3mm/s.
It is evident (see figure 4.5) that the result with the new way of spacing glass and copper was much better than the previous one, with a nearly perfect spread of the glue.

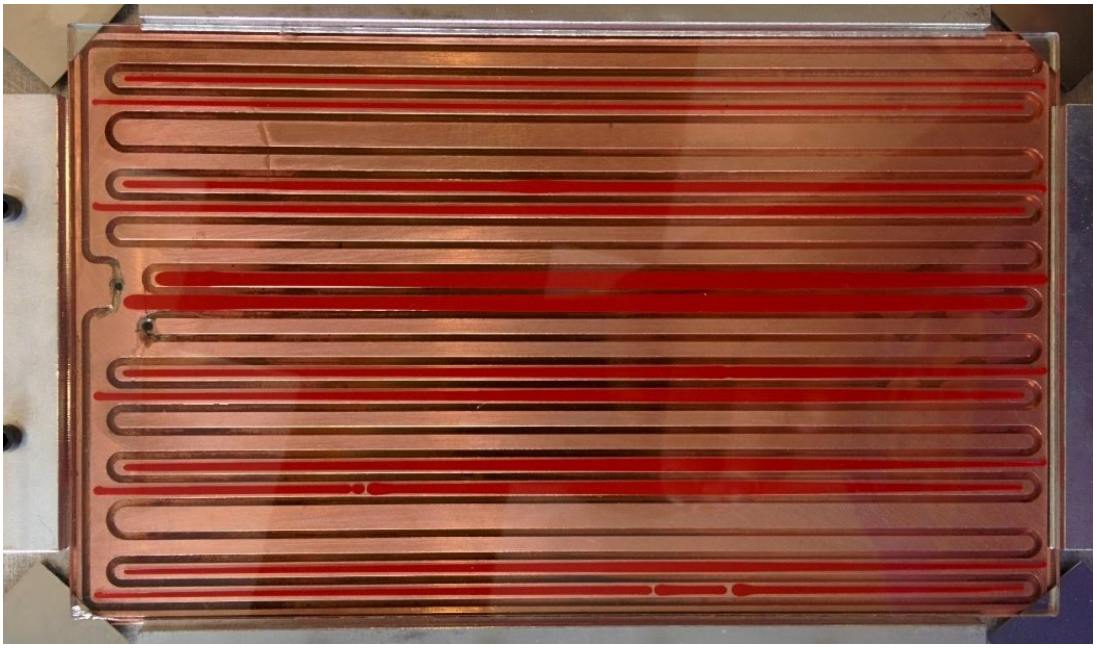

Figure 4.5: New gluing test. From the bottom: two lines at 4mm/s, two at 3mm/s, two at 2mm/s, two at 1mm/s, two line at 2mm/s and two at 3mm/s. Glass applied with four spacer on the corners. Loctite "red" glue.

After these three tests, it was decided to use a movement speed of 2mm/s. We took this decision considering the fact that this test was performed on a copper plate with 3mm of space between two channels instead of 2,5mm which we will effectively have on the copper plate during the experiment.

4.1.2 Gluing Test #2: Stress Test

The first real gluing test was carried out with a movement speed of 2mm/s except for the two bigger spaces, which was of 1mm /s, and the perimeter which was of 5mm/s. The external perimeter was not built like a complete ring but the corner was let free of glue to leave room for the 0,3mm spacer.
After the gluing, the PHP with the support and the weight on the glass, was put in the pre-heated oven at 120°C and, because of the high inertia of the system, was let there for 60', while the producer recommended a minimum time of 4' with a temperature of 120°C for the curing.
After the curing, the spacer was removed and the glue was manually put on the corner. An additional cordon on the perimeter was needed because the amount of glue already present was not enough.
The PHP was put in the oven once again for a second curing.

Figure 4.6: PHP after the cure of the glue. Loctite glue.

The gluing showed nearly perfect except for two points where it revealed a little more spread. The starting position of the syringe needle near the curves had to be adjusted because, due to the considerable distance between the needle and the copper plate, the starting point of the glue was not close enough to the U-Turns (see figure 4.6).

After the curing, the PHP turned out to be a bit bent, concave on the copper side and convex on the glass side. It was more or less 2mm deep at the point of maximum concavity.
This was due to the different thermal dilatation between copper and glass. The thermal dilatation coefficient is much higher for the copper then the glass so after the glue solidification at 120°C, once back to the ambient temperature, the higher contraction of the copper compared with the glass caused the concavity .
With this PHP we wanted to test the capability to maintain vacuum inside the channel and potential leakage, the capability to resist to thermal cycles with a maximum temperature of 150°C in vacuum condition, a second leakage test after the thermal stress and finally the maximum pressure which the PHP was able to support before fail.
The empty test took place in two stages. At the beginning the PHP was linked to a rotary pump Alcatel Pascal 2010 C2 in order to create a preliminary vacuum inside the channel.
After some minutes, the PHP was linked to the leak detector ASM Graph 142 which is able to verify the presence of leakage thanks to a helium detector. If the leak-rate is under 10^{-8} mbar*l/s the system is considered leakage proof. After one hour of pumping the leak-rate was around 10^{-10} mbar*l/s so the vacuum was verified.
After that, the PHP was put into the oven for some thermal cycles. It consisted in 5 thermal cycles between 150°C and ambient temperature (around 20°C) using only natural convection in order to check the capability of the PHP to stand this kind of stress.
At the end of the test the structure of the PHP seemed to be inaltered.
After the second leak test the PHP resulted no more leakage proof. This can be due to the continue dilatation and compression of the material and to the very low elasticity of the glue which may have created some micro fractures inside, which allowed some air to pass through.
The last test was to check the maximum pressure which the PHP is able to stand. Some nitrogen was introduced inside the PHP until it was checked a fast decrease of pressure.
The glass broke at 3.4 bar.

Figure 4.7: Glass broken after the maximum pressure resistance test. The limit value was 3.4 bar.

4.1.2.1 Glue strength at maximum pressure

Being the maximum pressure at the breaking point of 3.4bar, it corresponds to a strain of 0.24 N/mm^2 on the glass.

The surface of the glass where this force was applied was composed by the surface of the channels facing the glass and the space between the channels not covered by the glue, which was evaluated of 0,5mm each side (1mm per channel).

The surface of the top face of the channels was $7988mm^2$ and, adding the space free of glue, the total area where the pressure was applied corresponded to $12687mm^2$.

Due to this, the total force applied to the glass was 3045N.

Considering the total surface of the glass of $24000mm^2$ (120mm x 100mm), the surface of the glue where the force was applied was of $11313mm^2$. This corresponds to a strength on the glue of $0.27N/mm^2$.

The Loctite glue technical data sheet (Henkel, 2014) does not report the ultimate tensile strength of the glue. Examining the breakage (Figure 4.9), it was possible to suppose that it had been caused by a glass failure or a detachment of the glue in one of the corners of the PHP which caused a bending of the glass and the resulting breakage.

The Nusil technical data sheet (Nusil, 2014) reports the ultimate tensile strength of the glue which is 4.8 N/mm^2. This is much higher than the one recorded at the breakage point.
The definitive PHP was geometrically different from the tested one (channel width 2.5mm, space between channels 2.5mm), the surface of the glue was 15472mm^2 considering a better gluing and the space between two channels was fully filled with glue. As a consequence a pressure of 3.4bar inside the channels corresponds to a tensile strength on the glue of 0.13N/mm^2.
In case of aircraft cabin depressurization, the pressure inside the cabin drops at least to 0.3bar. In order to have the same strain on the glass, the pressure inside the channel should be 2.7 bar.
In order to avoid any risk of failure due to overpressure inside the channels, a risk factor of 2.5 was chosen setting the pressure limit at 1.1bar.

4.1.3 Gluing the Red PHP

After a few tests with the old copper plate it was decided to test the gluing process with the definitive copper plate and produce the first final version PHP which had to be used on the parabolic flight campaign 62.
The definitive copper plate had a thickness of 2,5mm in which was engraved a channel loop 2,5mm wide and 2mm deep. It was decided to increase the thickness of the glue from 0,3mm to 0,5mm in order to have a better tolerance to dilatation. The final section of the channel, in theory, was 2,5mm X 2,5mm. The channel had 11 U-Turns on the evaporator side, so the total volume inside the channel was 26648 mm^3.
For this experiment it was chosen to adopt a filling ratio of 50% so the volume of FC72 inside the PHP should be 13324mm^3. It was also necessary to insert the volume of fluid to fill the tubes which link the valve and the pressure transducer (both full of liquid). With a copper tube of 1/16" the volume to fill each tube is 116,4mm^3 for the valve and 102,5mm^3 for the pressure transducer. The total amount of FC72 inside the system is 13542,9mm^3 which is around 23g at ambient temperature.
This volume was calculated for a perfect gluing, where the glue filled the entire gap between two channels. On the real condition, the glue occupied only the central part of the gap and the volume of fluid inside the pressure transducer and the valve were not considered so the effective filling ratio could be a little less than 50%.
For example, if the theoretical section of the channel was 6,25mm^2 and assuming that the glue leaved 0,5mm of free space on each side, there is 0,5mm^2 to add to the theoretical section. This corresponds to an increase of 8% to the original section. Due to this fact, if we put inside the PHP the amount of fluid chosen before, the real filling ratio is not 50% but equal to 50/(100+8)*100=46.3%.
One possible solution is to fill the PHP twice; on the first the PHP is completely filled to check the real volume and on the second it is filled with a filling ratio of 50% based on the previous volume. Between the two fillings it is important to empty the PHP perfectly, in order to avoid any possible error.
In our case it was decided to put the quantity we previously calculated (around 23g) because the difference between the real filling ration and the desired 50% is irrelevant for the purpose of the experiment.
During this gluing phase, it was not possible to use the same parameter found during the previous test due to the bigger distance between copper and glass (0,5mm instead of 0,3mm).

To maintain a good speed of movement, it was chosen to change the needle of the glue syringe with one with a bigger hole, maintaining the same pressure on the syringe piston.
After some testing, it was found a good movement speed of 5,3mm/s.
Before proceeding with the gluing of the glass, heater and tubes were placed by brazing. In the brazing process, a metal paste (basically silver) with a lower melting temperature was inserted between the two copper pieces and everything was put into the oven for 30' of preheating at 150°C and 15' at 200° for the brazing (Figure 4.8). Between the heater and the copper plate 6 evaporator thermocouples were inserted, which were useful during the brazing process to check the temperature for a perfect joint.

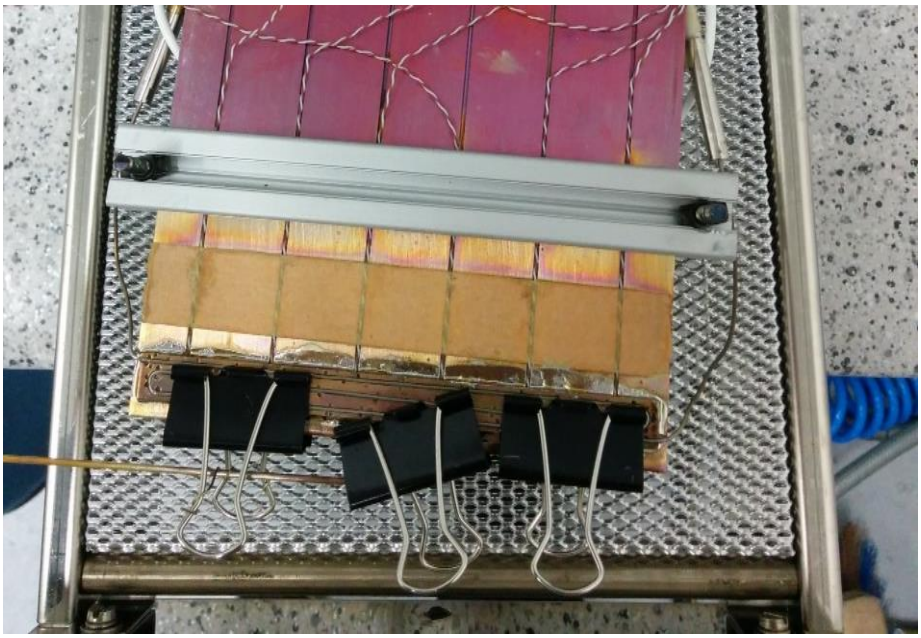

Figure 4.8: PHP just after the brazing process for the heater and the two tubes

To reduce the problem of the PHP bending after the cure of the glue, it was decided to put it into the oven for four days at a temperature of 70°C (a preliminary test was carried on by gluing two little pieces of copper with this curing temperature and 24h of permanence in the oven).
Even in this case the PHP resulted a little bent, much less than the previous one, for a value on the deepest point less than half millimeter (see figure 4.9).
This decreased a lot the thermal exchange on the condenser due to the not perfect contact between copper and heat sink.

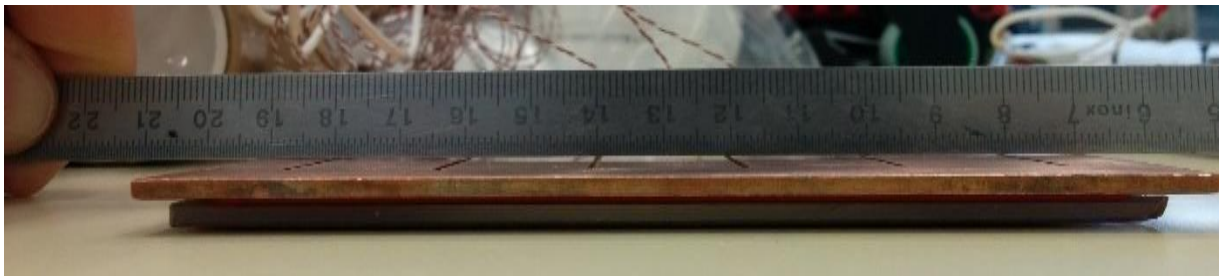

Figure 4.9: Bending of the PHP at ambient temperature due to the different dilatation between copper and glass during the glue curing

A possible solution in order to improve the thermal exchange could be to insert a thermally conductive paste or a pad between copper and aluminium (in this case, it performs much better than the air between the two materials, but much worse than a direct contact between the two metals). Another solution is trying to bend the PHP manually in order to make it as flat as possible or a final solution, using low power at the heater due to the low ability of thermal dissipation on the condenser.
Out of convenience, we chose the first solution and put a thermal pad of 0,5mm.
Another problem was the tube which linked the PHP to the pressure transducer. It is a copper tube of 1/16” with a stainless steel tube of 1/8” soldered at the end. This was done because the hole of the pressure transducer fit only with a tube of 1/8” or 1/4" and stainless steel was chosen to prevent the risk of deforming it when the pressure transducer clamped the tube because of the high ductility of copper. The tube happened to be sealed after the soldering.
The copper tube had to be substituted with another one and to prevent any risk of obstructing, a stainless steel cylinder was inserted at the very point where the pressure transducer goes to clamp and soldered (see figure 4.10).
When the PHP was mounted on the heat sink, it was checked the capability to maintain vacuum in the system. An important leakage on the upper part was soon noticed, maybe caused by the upper clamp that bent the copper plate little bit. The problem was solved by putting some Nusil glue into all the top interspaces. It was chosen the Nusil glue for its higher elasticity.

Figure 4.10: Final PHP with the Loctite glue. The Nusil Glue on the upper part of the PHP (Left on the picture) was not already placed

4.1.4 Gluing the White PHP

In order to eliminate the problem of PHP bending, the gluing process was tried with a different type of glue but maintaining all the other components unchanged.
It was chosen the silicon glue Nusil CV7-2289-1P, which compared to the epoxy resin used till now showed an elongation coefficient of 375%. This could help to follow much more the different thermal dilatation between copper and glass and prevent the undesirable concavity on the copper plate.

Figure 4.11: gluing process with the Nusil glue

Compared to the other, this glue is much more difficult to manage. First of all it is a bi-component glue with a mix ratio of 1:1 so before starting with the gluing, it was necessary to transfer the glue from a double syringe to a syringe which fitted the gluing machine with the appropriate mixing needle. Is important to be careful not to leave air bubbles trapped in the syringe to avoid the problem seen in the previous tests.
With this new glue it was necessary to test the movement speed again together with the dimension of the needle, due to the much lower viscosity of this glue compared to the Loctite.

Because of this lower viscosity, the glue positioned on the copper plate in few minutes spread to occupy all the space between the two channels decreasing the thickness a lot, with the risk not to reach the glass.
Due to the higher wettability, when the glass was positioned, it could occur that the glue, if in excess, could hide the channel.
Due to the length of the gluing process, this bi-component glue presents a considerable time dependence, because the viscosity increases from the time of mixing to the end of its use (working time declared approximately 3 hours). Due to this fact, the movement speed of the syringe cannot be constant: varying from 5,5mm/s at the beginning of the gluing process to 3mm/s at the end.
For the curing, the producer suggested a time of 15 minutes at 150°. In our case, in order to use a temperature as low as possible, we tried with 48 hours at 50°C (at this temperature the producer recommended a minimum curing time of 1 hour and 30 minutes).
Thanks to the low temperature and the high elasticity, the PHP was perfectly flat after the curing.

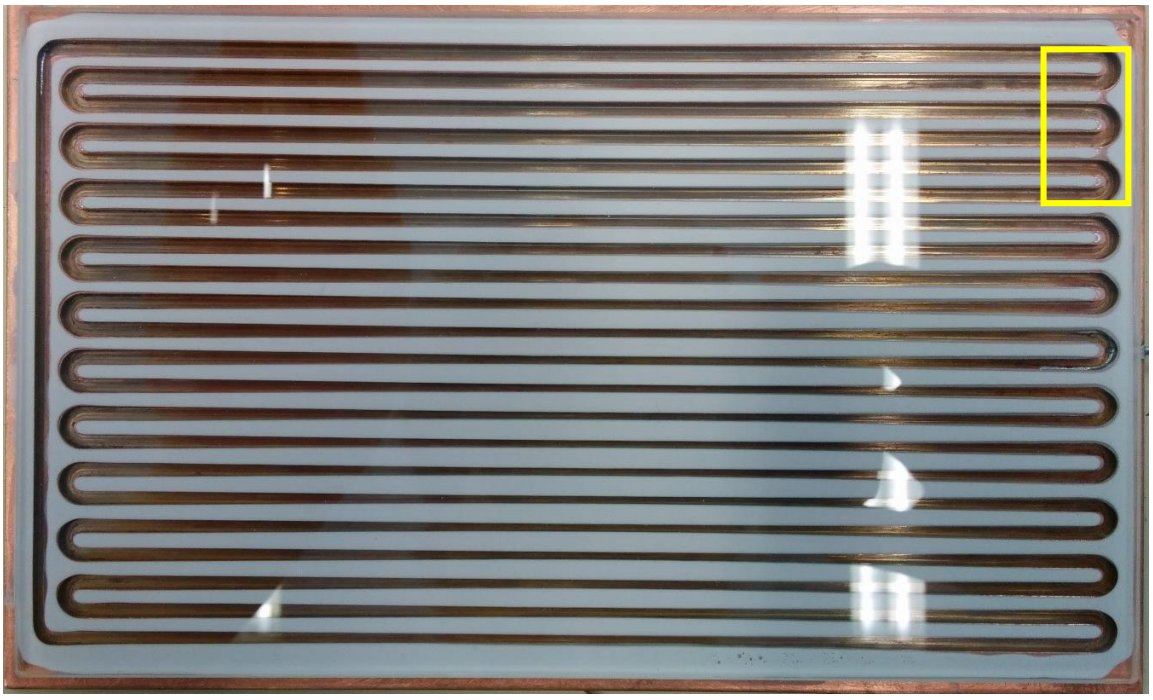

Figure 4.12: First PHP made with the Nusil glue. On the box the two little bridges on the glue

After the glue solidification, it was possible to notice two thin lacks of glue forming two bridges between the cannels in the evaporator zone, which let the fluid pass through three channels,

but due to the very small amount of this passage, it should not change the functioning (see figure 4.12).
The leakage test highlighted the non-perfect leakage proof of the PHP, with a leak-rate around 10^{-9} mbar*l/s. The result was however sufficent, after each hour it was noticed an increase of 250Pa, which can be a mix of a very little leakage and some outgassing tipical of silicon glue.
The same glue was later used in another PHP but, to increase the adhesivity on the copper plate, the primer Nusil SP-120 was spread before gluing. After the first PHP with nusil glue, we noticed that the adhesivity on the copper plate was not so strong as expected and the not perfect leakage proof result maybe due to this fact.
The primer was placed with a small brush on the copper plate before the gluing process.
To have a better result, after the machine gluing,some extra glue was put manually in the zone which needed it.
Due to the good results with the curing temperature of 50°C, it was decided to put the PHP into the oven for 48 hours at a temperature of 70°C (minimum time suggested for this temperature was 60 minutes). Even with this temperature the copper plate resulted perfectly flat.
The leakage test for this PHP scored a leak-rate of 10^{-10} mbar*l/s and the pressure increase of 200Pa/h, which can be a mix of a very little leakage and some outgassing tipical of silicon glue.

Figure 4.13: The second and definitive "white" PHP made with the Nusil glue and the primer on the copper plate.

4.2 Empting and filling operations

When the PHP had been fixed on its support, it was possible to proceed with the filling operation. In our case it was chosen FC72 as operative fluid and a filling ratio of 50%.
The first thing to do was to empty the PHP completely by connecting the filling valve (all the valves used are swagelok SS-41S2) to a vacuum pump. The PHP was let pumping by a rotary vane pump Pascal 2010 C2, which permits to reach at least 1mbar, for all the night.
After this preliminary empting operation the PHP was connected to another pump, it is important to close the valve during this operation to maintain the vacuum inside the channel. This second pump, ASM Graph 142, permits to reach a reduced pressure level and in addition, it has a Helium leak detector system, that could verify the presence of leakage in all hydraulics connections (figure 4.14). After a few hours of pumping, a very small amount of helium was released with a small gun to check the eventual presence of leakage. It is very important to release a very small amount of helium because of its fast distribution in the air because with a big amount it would be difficult to find the exact point of leakage.

Figure 4.14: Emptying process of the PHP made with the Nusil glue

After checking the absence of leakage,it was possible to close the valve and remove the connections with the pump.
If necessary, it is possible to procede with the empty test to evaluate the pure conduction performance.

Before proceeding with the filling task, it was necessary to fill the tank with the working fluid. First of all, the tank was linked to the pump in order to empty it and the pump worked until the leak-rate was stable at 10^{-10} mbar*l/s.
Once the tank was empty, with the valve closed, it was unlinked and put on an electronic scale to evaluate the initial weight of the empty tank.
After that, the tank was filled with a quantity of working fluid higher than the requested and the amount of fluid inside the tank was checked on the scale.
After filling the tank, it is very important to remove completely the eventual non condensable gasses which had been trapped inside the tank or inside the fluid during the filling procedure.
With a heat gun, the tank was heated at a temperature of minimum 70°C circa in order to have a pressure inside the tank higher than the ambient pressure (FC72 saturation pressure at 70°C is 153025Pa). When the temperature was reached the valve was opened for a couple of seconds and closed again, during this operation it was possible to see the vapour coming out from the tank. Now the tank was cooled in a bucket with cold water and once it was dry, it was weighed again in order to maintain the fluid mass inside it under control.
In order to reduce substantially the quantity of non condensable gasses, the cycle was repeated at least five times and than the process was repeated until the mass of the fluid inside reached a value a bit higher compared to the target.
Once the tank was ready, with the correct amount of fluid and a negligible quantity of non condensable gasses, it was linked together with the pump and the PHP with a T junction.
When, after some minutes, the vacuum condition had been recreated inside the connections and PHP, it was possible to proceed with the filling (figure 4.15).

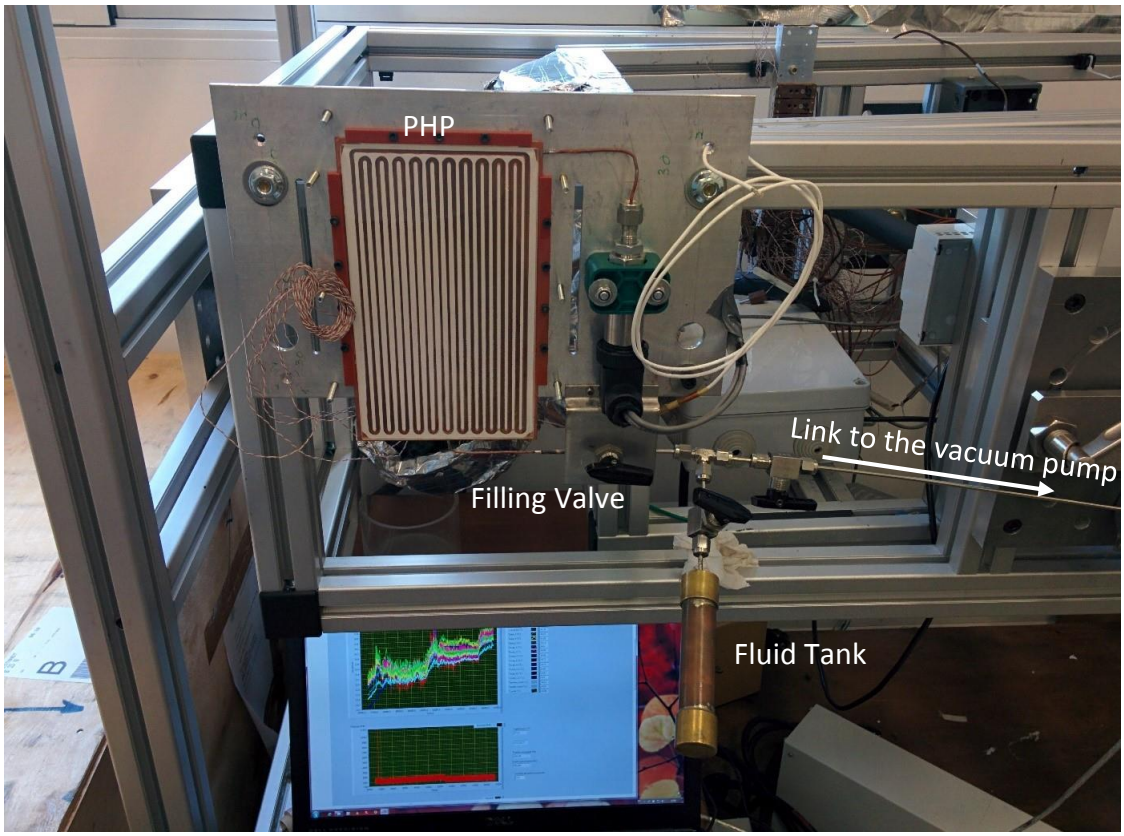

Figure 4.15: Filling proces of the PHP made with the Nusil glue. On the PC was checked the pressure in order to notice an eventually presence of non condensable gasses

First of all it si important to close the pump valve! After that,it is possible to open the valve of the PHP and the tank valve and with the heating gun start to heat the tank and the connections. After some minutes of heating,it is possible to close all the valves. In order to check the real quantity of fluid injected in the PHP, the tank was weighed and the result was compared with the mass before the filling. The difference is the amount of fluid inside the PHP.
The final check in order to evaluate the presence of non condensable gasses, is to compare the pressure inside the PHP with the saturation pressure at the temperature inside the PHP.
The emptying procedure is quite a simple operation. A tube is linked to the filling valve and let evacuate in a baker. The valve si opened and a power of 30W circa is given to the evaporator in order to increase the pressure inside the PHP and force the fluid outside the channel. To speed up the process, it is possible to move the PHP and distribute manually the fluid near the exhaust pipe of the PHP (the same of the filling) or create a light depressurization to force the fluid outside.

5 Laboratory ground testing

Before the tests during the parabolic flight campaign, some preparatory tests were carried out in a laboratory, in order to deeply characterize the thermal and hydraulic behaviour of the PHP.
Due to the larger hydraulic diameter of this PHP compared to the critical one, the fluid inside the channel stratified according to the different density between liquid and vapour with the liquid on the bottom (evaporator zone).
These tests, however, showed some interesting aspects of the PHP functioning in normal gravity condition.
Two types of ground tests were performed:

- Vertical test
- Horizontal test

The first one was realized with the PHP in vertical position in a favourable way (bottom heated) and the second one in horizontal position.
All these tests were performed with the white PHP (Nusil glue).

5.1 Tests in vertical position

The first series of ground tests was made with the PHP in vertical position.
With this configuration, a long time test was performed, which means testing the PHP at the same power level for different lapses of time, 2 hours and 30 minutes for the test at 100W, 3 hours and 30 minutes at 60W and 6 hours at 20W. Before each power changing, the power to the heater was cut out for some time, in order to bring the fluid back to the ambient temperature. These tests were performed only in bottom heated vertical position because, due to the large channel diameter, this position allows a non fully dry out configuration at the evaporator.
These tests were useful to understand the functioning of the PHP in normal gravity condition and to see possible changes of the temperature or of the fluid motion in a period of time.
With a heating power of 100W, the temperature at the evaporator and condenser increased rapidly. Figure 5.4 reports the time evolution of such tests.
It is possible to notice two rapid decreases of temperature (activations) very close to the beginning of the test, the first after only 20 seconds circa from the start of the experiment and

the second after circa 145 seconds in correspondence of the two peaks of temperature on the evaporator. In correspondence of the activation, the temperature decreases rapidly due to the starting motion of the fluid inside the channel.

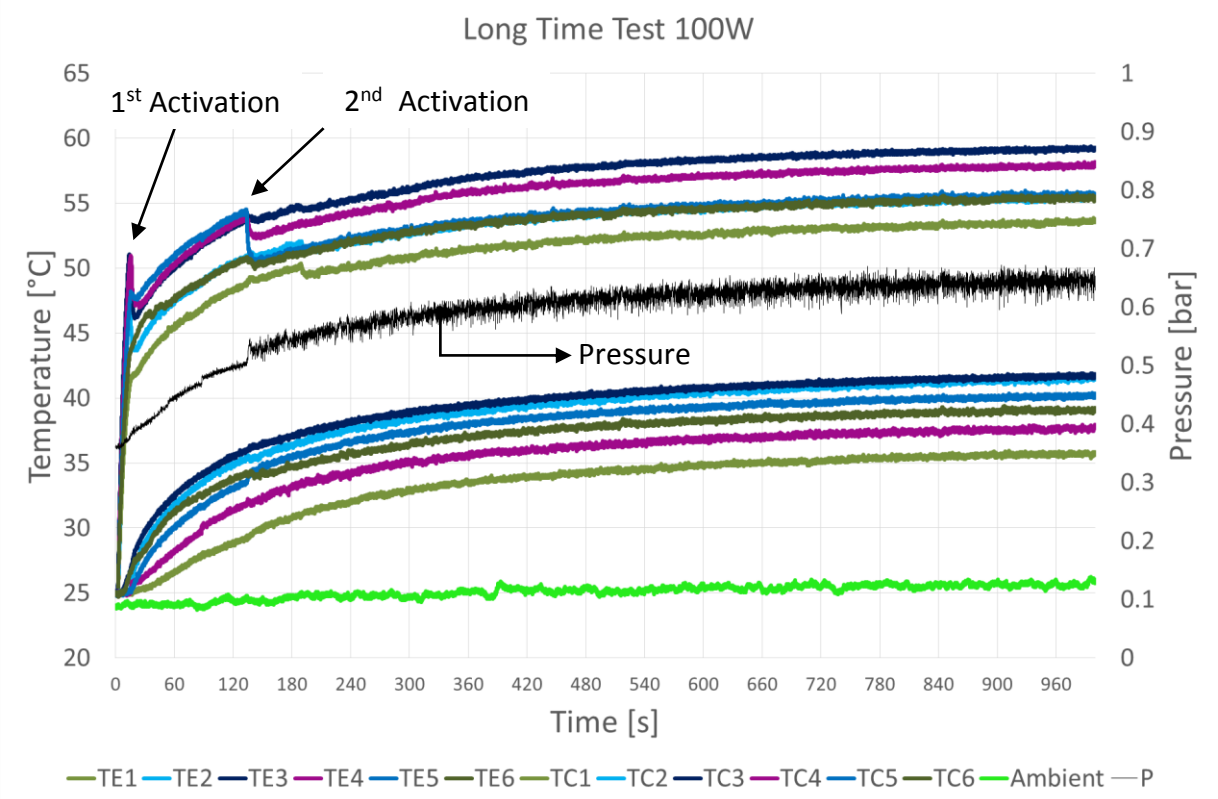

Figure 5.1: Diagram of the first 1000 seconds of the long time test at 100W (Vertical, bottom heated), TEx= Evaporator temperature, TCx= Condenser temperature, Ambient= Ambient temperature, P=fluid pressure.

After the second activation, the flow pattern inside the PHP was highly different between the centre and the side channels according to the temperature level.

As it is possible to see from the figure 5.1 and also 5.2, the temperature decreases from the centre of the evaporator to the sides. This is mainly caused by a strong fin effect on the side of the heat sink, which goes on until the vertical support of the assembly. In order to reduce this undesirable effect, two long slots were machined in the aluminium of the heat sink just at the sides of the copper plate (for further details see paragraph 3.2.2).

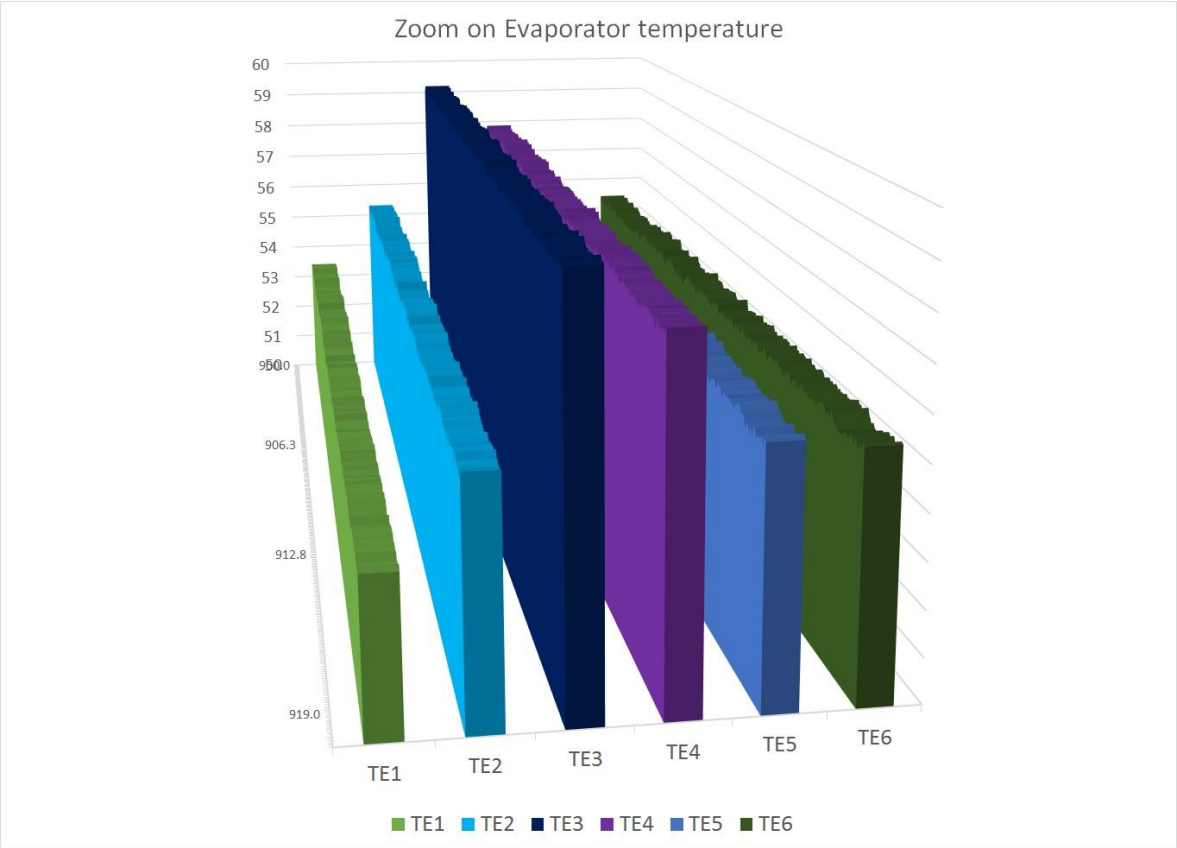

Figure 5.2: Diagram of the evaporator temperatures between 900 and 920 seconds from the test start

In correspondence of the thermocouples TE1, TE2, TE5 and TE6 (first three and last three U-turns in the blue box of the Figure 5.3) the channels presented a pool boiling condition. In this flow regime, small bubbles were generated in the evaporator zone and distributed homogeneously within the liquid.

In the central channels (red box in the Figure 5.3), due to the higher temperature, the flow regime was annular, with a functioning very similar to the classic thermosiphon but without the liquid storage on the evaporator.

The central U-Turn was nearly in a complete dry-out condition, only the evaporation of a very tiny liquid film avoided the thermal crisis of that zone (yellow box in the Figure 5.3).

The functioning of the PHP was the same for all the time of the test. Since the end of the rump-up phase, there was only a slight increase of temperature of circa 1°C for all the thermocouples without any changing in the fluid motion. This test was 2 hour and 30 minutes long.

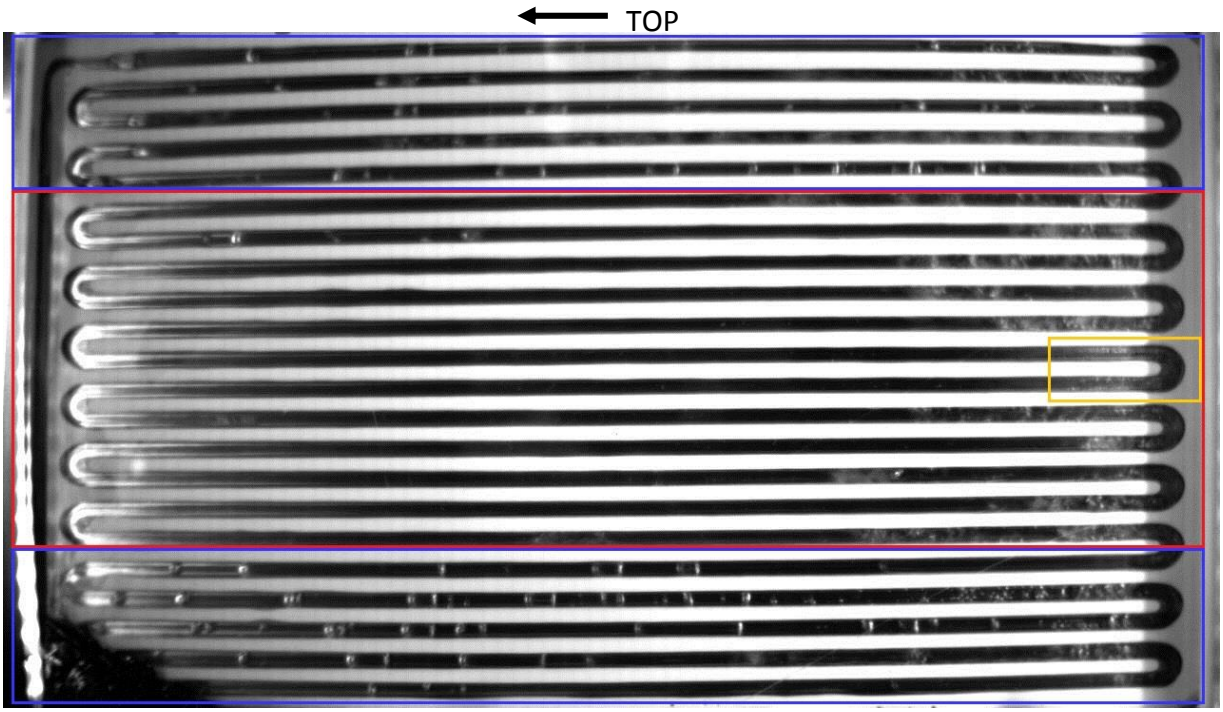

Figure 5.3: Frame of the functioning of the PHP after 1 hour at 100W (Vertical test, bottom heated), in the blue box the pool boiling, in the red one the annular flow, in the yellow one the evaporation of the liquid film.

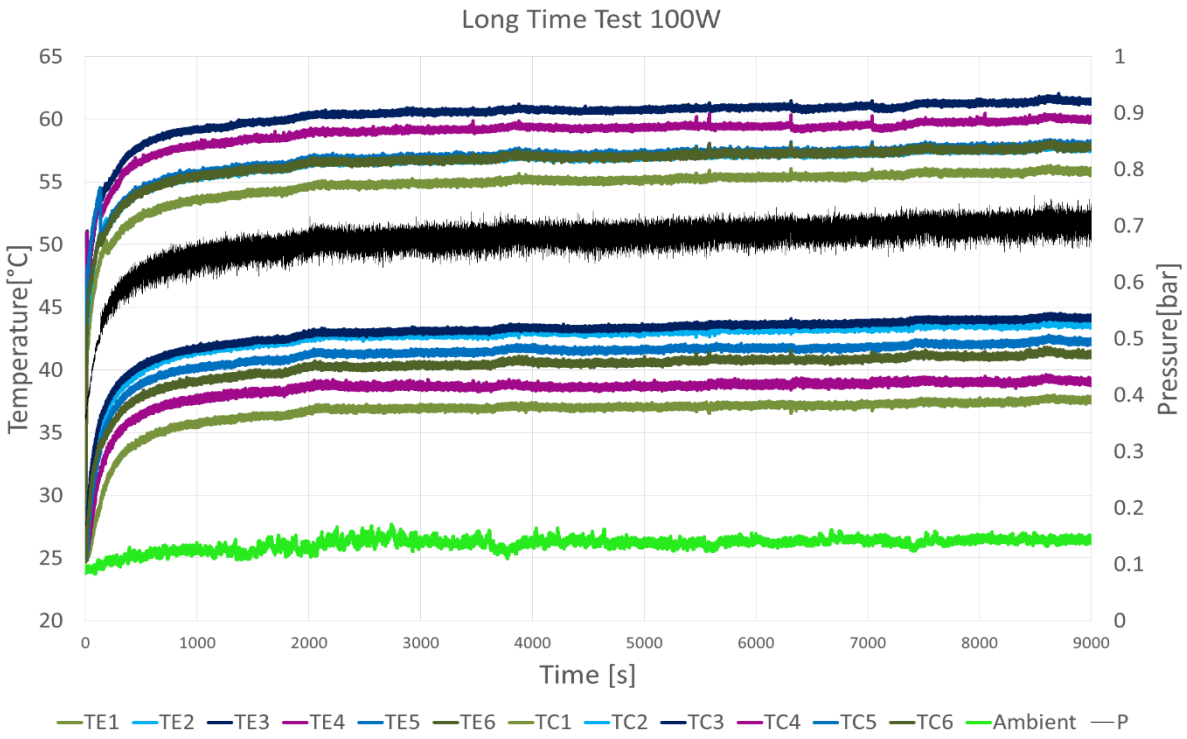

Figure 5.4: Diagram of the entire test (9000s = 2h30') at 100W (Vertical, bottom heated).

At 60W the situation was approximately the same, with some differences in the flow regimes. Looking at the figure 5.5, it is possible to notice the first activation after 30 seconds, after that another activation which involved only few channels happen at 560s. Another strong decrease of temperature appeared at 610s involving all the PHP except for the first three U-Turns on the right side (blue box in the Figure 5.6) monitored by the TE5 and TE6.
These channels were in a liquid storage condition. They had a thermal behaviour comparable to a mono phase thermosiphon. This highlighted the huge amount of heat removed from the evaporator by the evaporation of the liquid. In fact, the temperature recorded by the TE5 and TE6 was the highest in all the evaporator zone.
The other channels were all in an annular flow regime, except for the second U-Turn from the left, which was in a liquid storage condition.
Similarly to the test at 100W, the central channel showed a tiny film evaporation hardly evident in the figure 5.6.

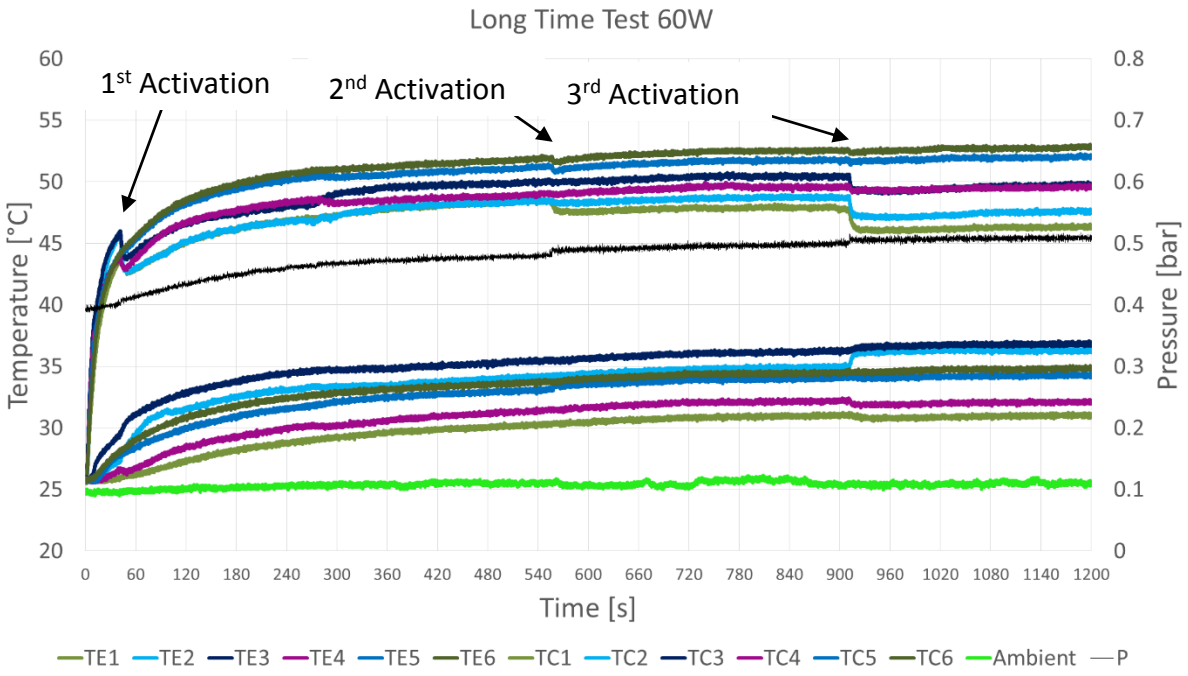

Figure 5.5: Diagram of the first 1200 seconds of the long time test at 60W (Vertical, bottom heated).

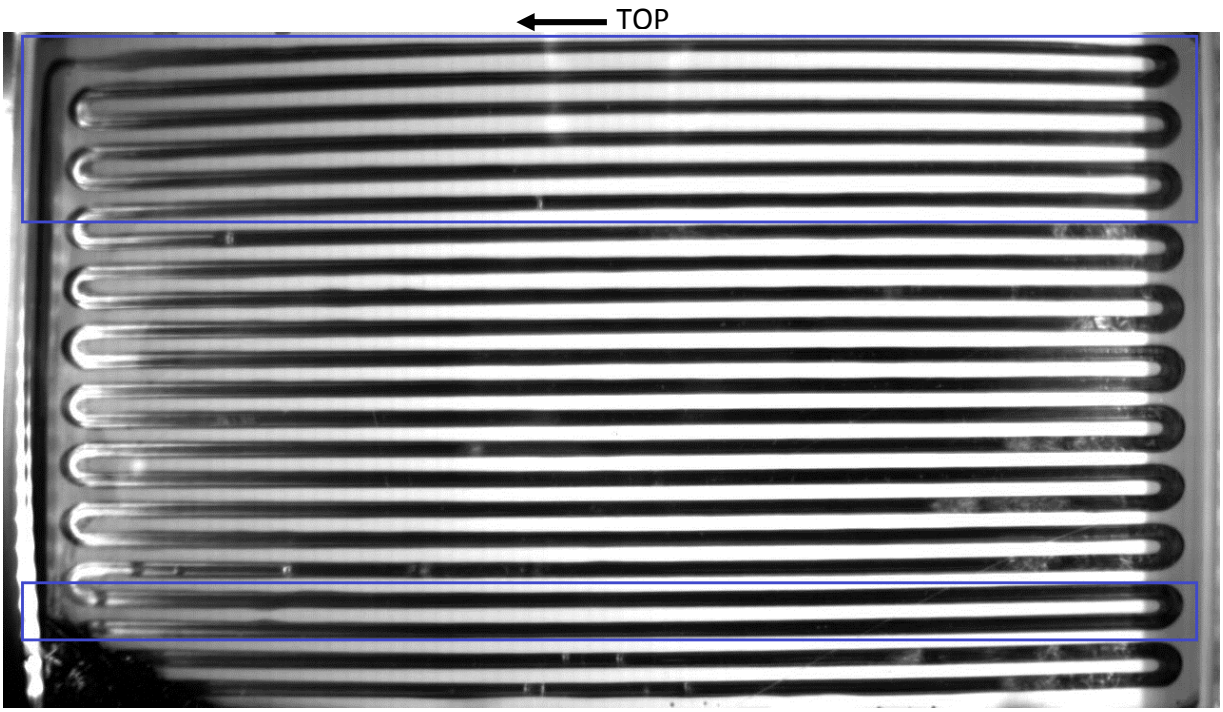

Figure 5.6: Frame of the functioning of the PHP after 30 minutes at 60W. On the blue box the channel in a liquid storage condition. (Vertical, bottom heated).

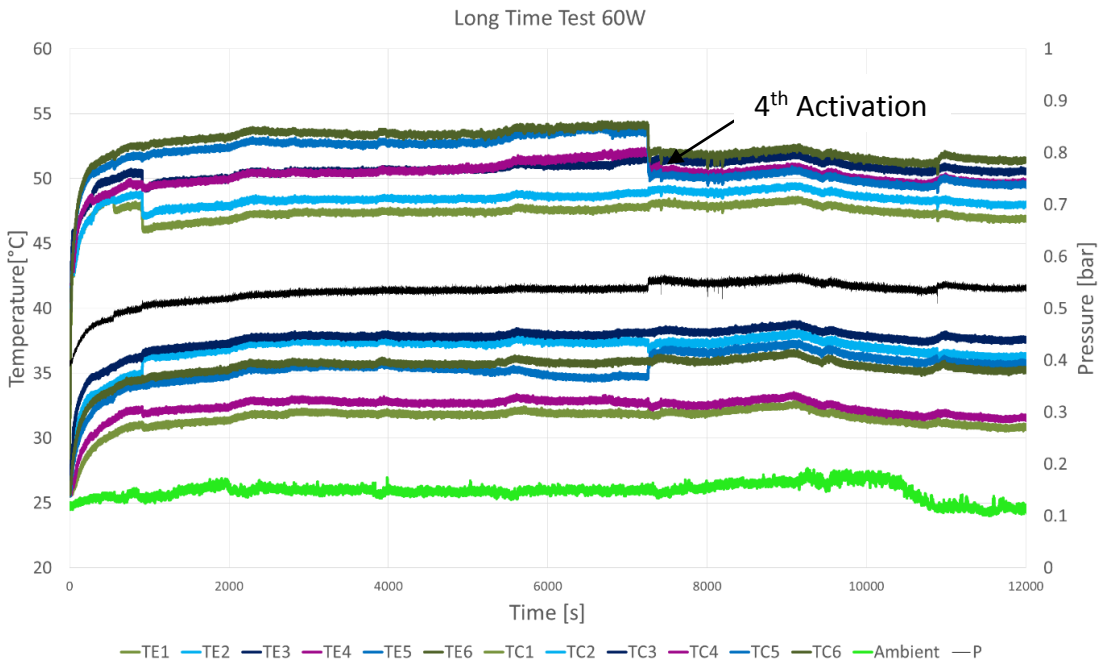

Figure 5.7: Diagram of the entire test at 60W. (Vertical, bottom heated).

After the third activation, the temperatures and the flow regimes maintained stable until the fourth activation, after circa 2 hours. This last activation involved the channels, which were in

a liquid storage condition causing a strong reduction of temperature on that side. Since that the flow regime was pool boiling instead of liquid storage, while on the other channel it remained unchanged (Figure 5.8).

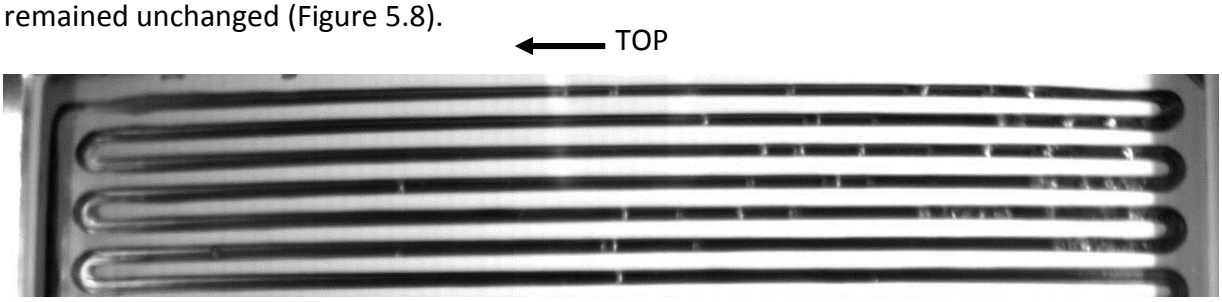

Figure 5.8: Detail of the pool boiling flow regime of the three external right channels. (Vertical, bottom heated).

At 20 W, due to the very low heat power, the flow pattern inside the PHP was pool boiling for the whole length of the test.

The pool boiling was concentrated in the central channels because of the higher temperature while on the side the fluid was mainly in a stop motion condition.

The temperature was stable from the end of the ramp-up up to the end of the test.

In this case was not possible to notice any relevant activation, there were only some temperature fluctuations of about 0.5°C.

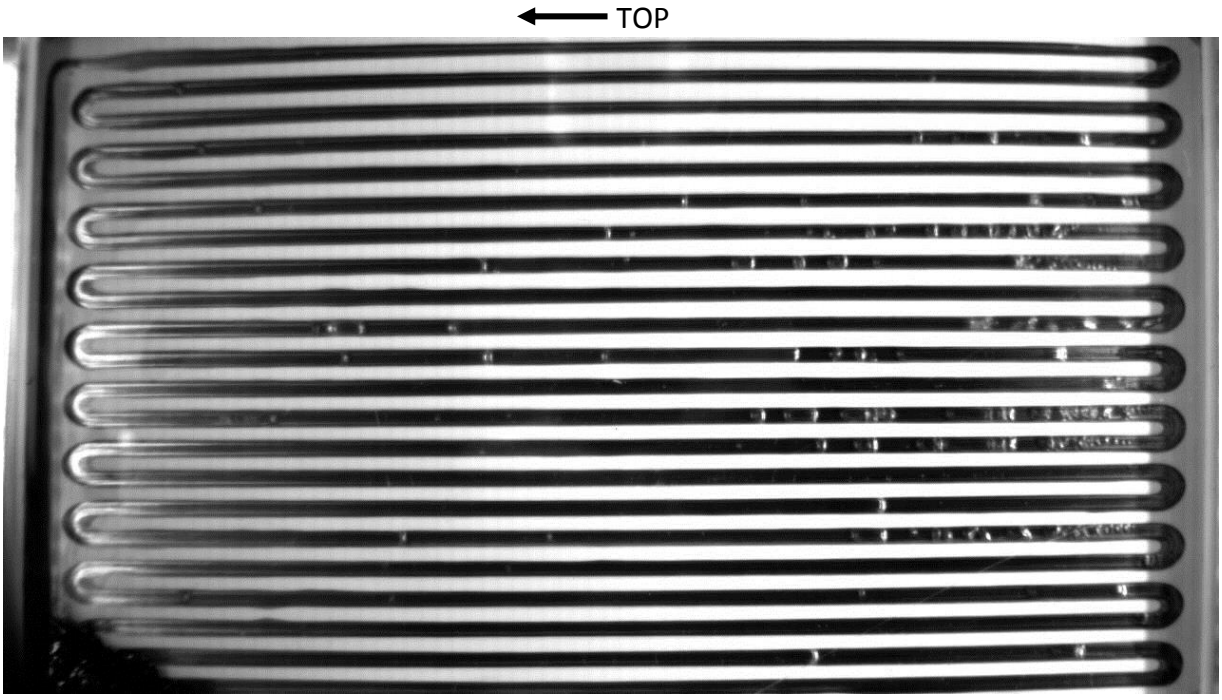

Figure 5.9: Frame of the functioning of the PHP after 6 hours at 20W (Vertical, bottom heated).

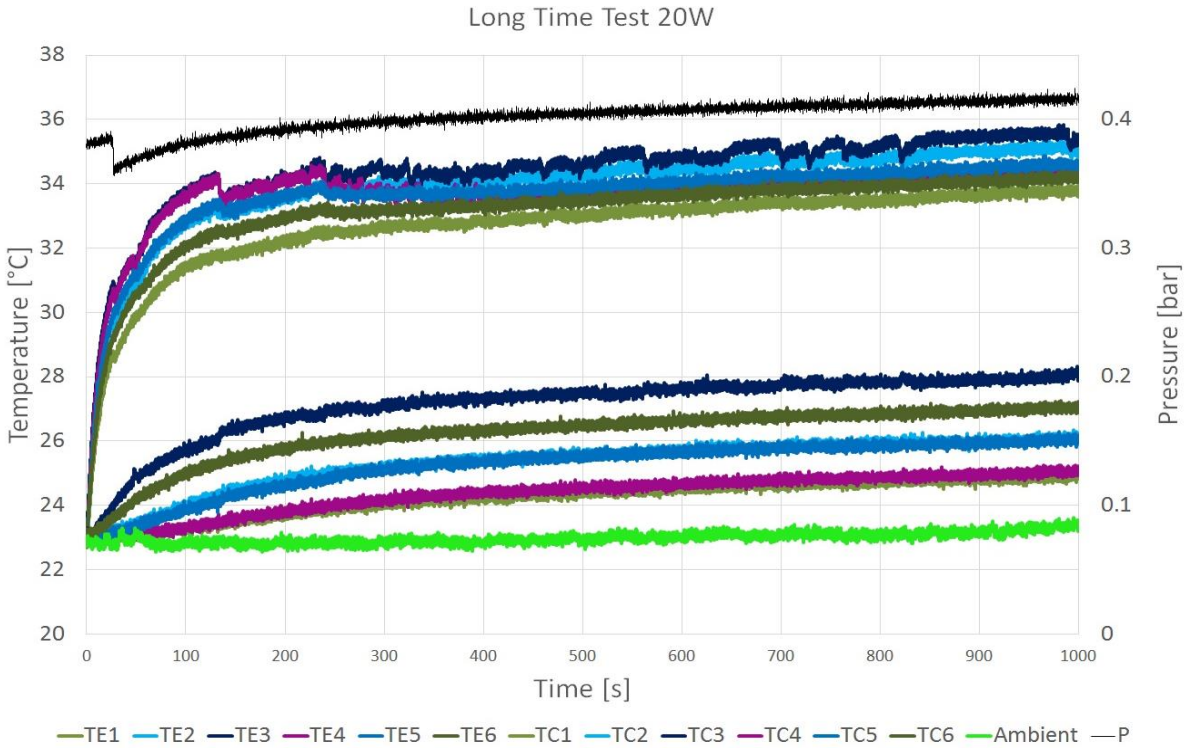

Figure 5.10: Diagram of the first 1000 seconds of the long time test at 20W (Vertical, bottom heated).

5.2 Test in horizontal position

The horizontal test was performed with several power steps, up to the software evaporator temperature safety limit set at 120°C.
The power step chosen for this test was: 0 – 40 – 60 – 80 – 100 – 120 – 130 [W].

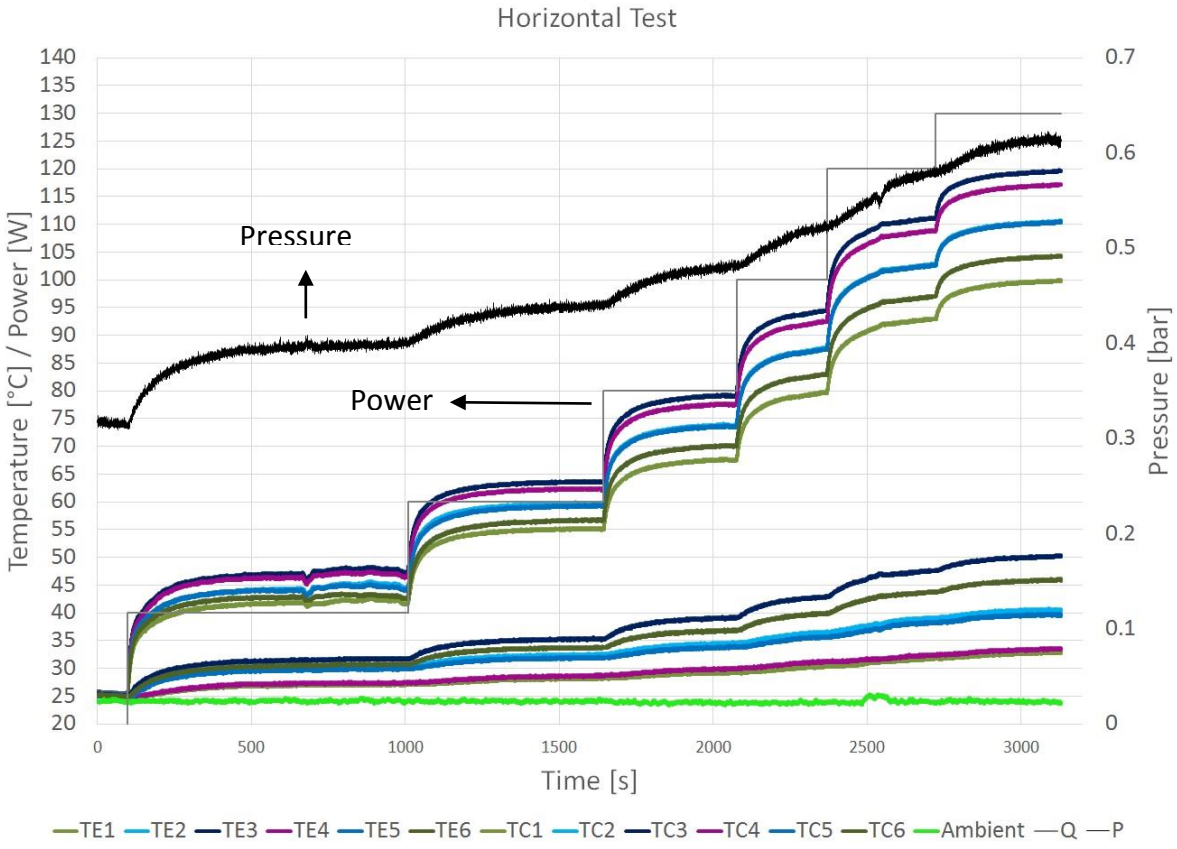

Figure 5.11: Diagram of the test in the horizontal configuration. Q= power at the evaporator.

Immediately after giving power to the heater, the fluid moved through the condenser leaving the evaporator in a nearly complete dry out.
That was due to the different orientation of the gravity, which does not assist the returning of the liquid on the evaporator zone.
However, due to the high dimension of the channel, it was established a liquid flow due to the different pressure between the top and the bottom of the channel around 41Pa and also with a capillary pressure around 9Pa, considering the liquid properties at a temperature of 30°C (see figure 5.12). The pressure due to gravity force is calculated as follows:

$$\Delta P_{gravity} = \rho g \Delta z$$

Where:

- ρ: Volumetric mass density of the working fluid in liquid phase
- g: Gravitational field
- Δz: Thickness of the channel

Capillary pressure is calculated by means of the Young-Laplace equation as follows:

$$\Delta P_{capillarity} = \frac{2\sigma}{R_{eff}} \cos\theta$$

Where:

- σ: Surface tension
- R_{eff}: Hydraulic radius of the meniscus
- Θ: Apparent contact angle between copper and liquid

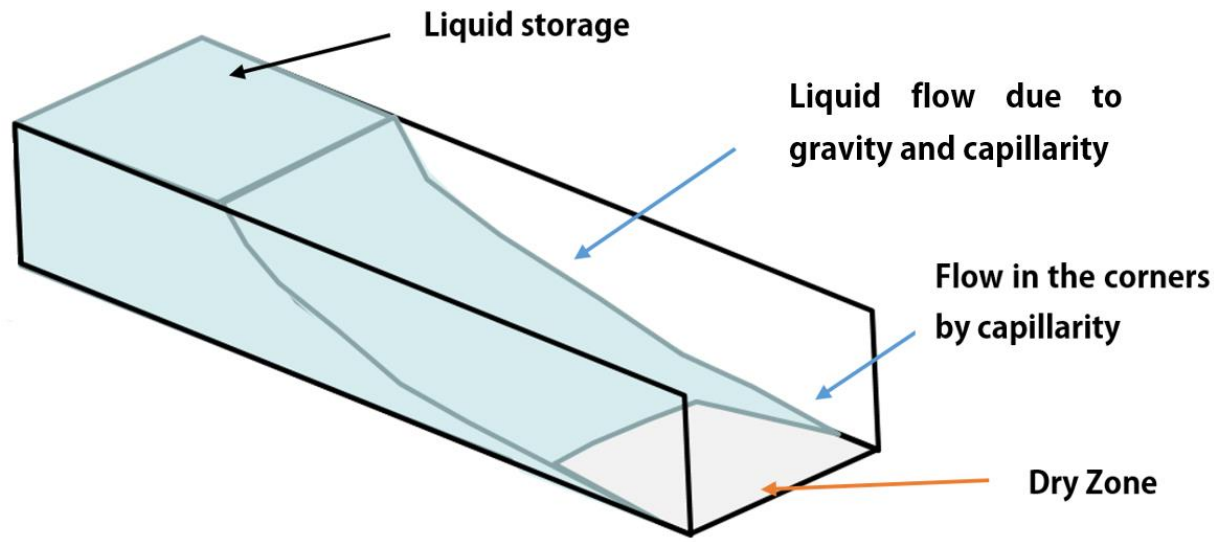

Figure 5.12: Scheme of the fluid disposition inside the channels.

Thanks to that difference of pressure, the fluid was able to return to the evaporator zone. It was also noticed a capillary pumping on the edges which, even if in a small amount, assisted the fluid to go back to the evaporator.

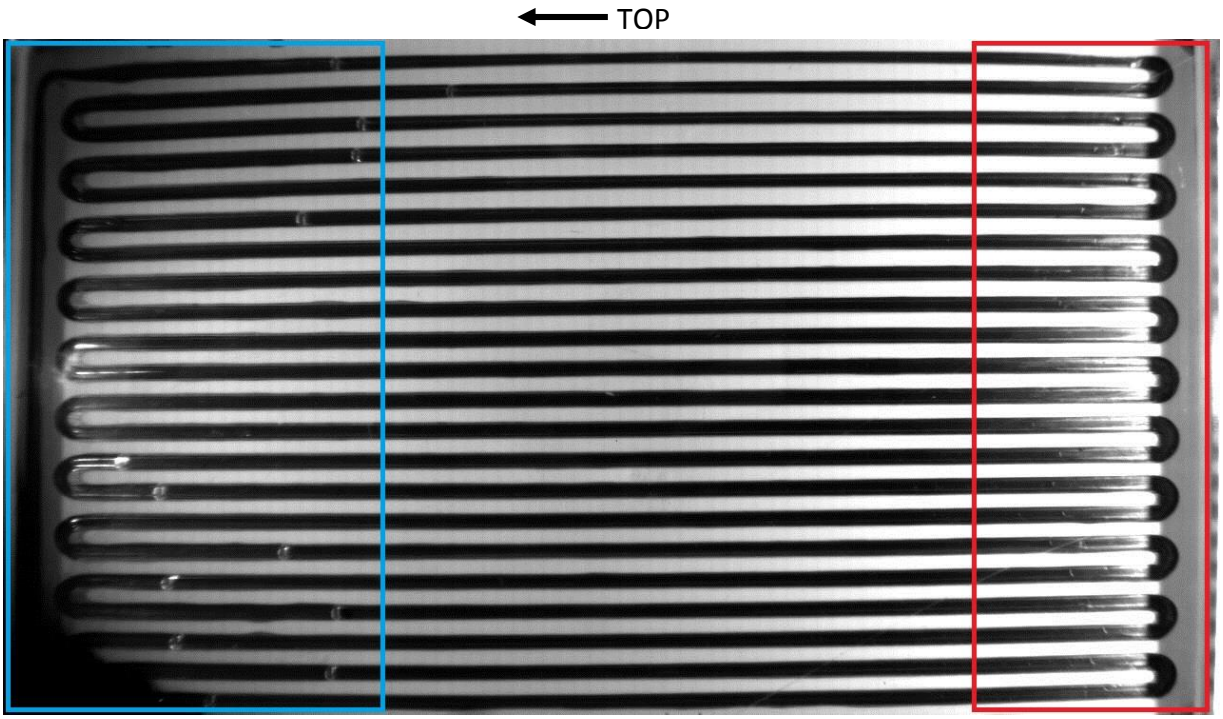

Figure 5.13: Frame of the horizontal test at 40W, on the blue box the liquid storage delimited by the meniscus and on the red box the limit of the liquid film on the evaporator.

Figure 5.14: Zoom on the limit of the liquid film of the frame on the Figure 5.13.

With a higher power, the distribution of the fluid inside the PHP was the same as seen before but with the limit of the fluid film positioned some centimetres up in the direction of the condenser, due to the higher power (figure 5.15).

With this configuration the PHP never activated because of the concentration of the liquid on the upper part of the condenser.

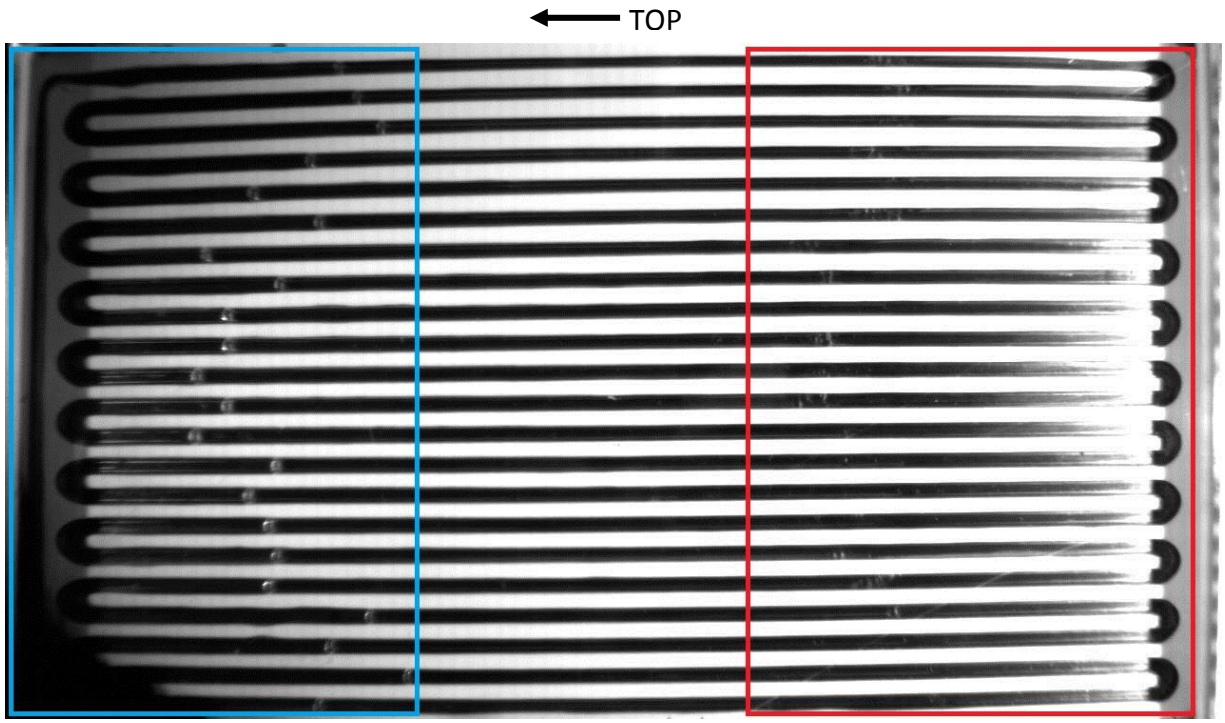

Figure 5.15: Frame of the horizontal test at 130W, in the blue box is the liquid storage delimited by the meniscus and in the red box the limit of the liquid film on the evaporator.

6 The 62nd ESA Parabolic Flight Campaign

In order to see how the microgravity condition influences the functioning of the PHP we had developed, a series of experiments were performed during the 62nd parabolic flight campaign organized by ESA and hosted by Novespace facilities.
The Campaign took place between the 3rd June 2015 and the 12th June 2015 in Bordeaux, France.

6.1 Aircraft ground testing

Before the parabolic flight tests, some preparatory tests were carried out inside the aircraft with all the components in the parabolic flight configuration.

6.1.1 Aircraft “preliminary” ground testing: “Red” PHP

The first test was a power rump-up & rump-down with the red PHP in vertical position.
This test was useful to check the correct functioning of all the devices after the mounting inside the aircraft and to check the maximum power at the heater before the power cutting off by the software security control, due to the high temperature or high pressure.
The power sequence was:0 – 10 – 20 – 30 – 50 – 80 – 100 – 120 – 140 – 100 – 50 – 20 – 0[W].
Each step had a minimum time length enough to reach a pseudo-steady condition.

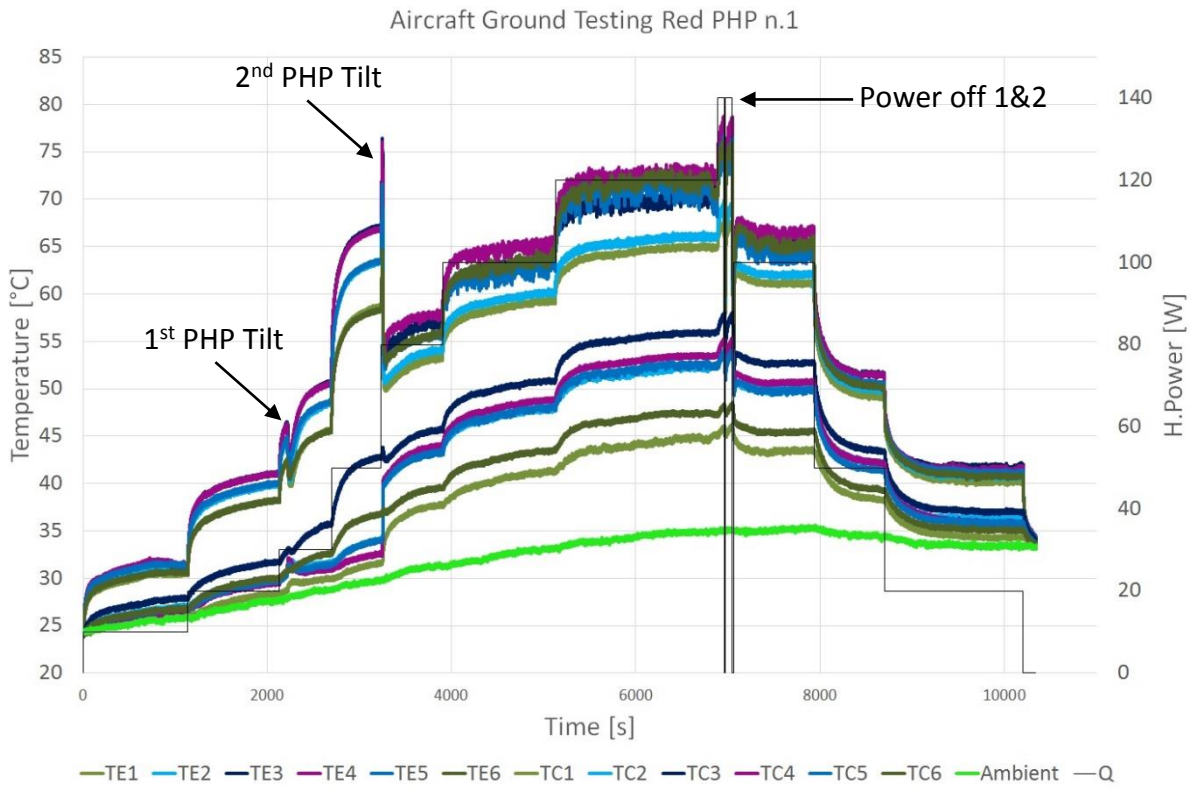

Figure 6.1: Diagram of the aircraft ground test n.1 with the red PHP. (Vertical, bottom heated).

During the first part of the test, the fluid distribution inside the PHP was mainly organized as a liquid storage on the two side and dry out on the central part, so it was necessary to tilt manually the PHP in order to have a better fluid distribution and obtain more significant test results. This operation couldn't be performed during the parabolic flight because all the racks were securely attached to the aircraft.

After the tilting operation, the PHP behaviour was similar to the one seen during the long time test at 100W (Paragraph 5.1). On the centre it is an annular flow and on the side, due to the lower temperature, liquid storage or pool boiling (see figure 6.2).

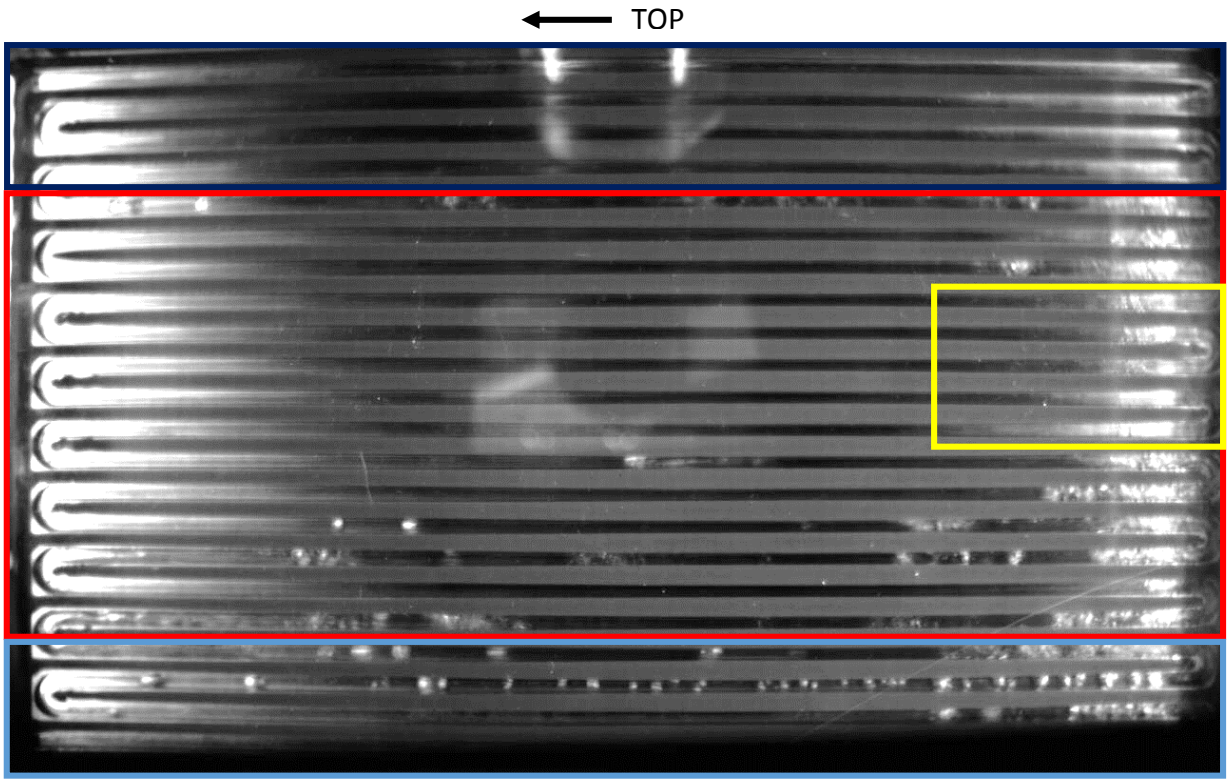

Figure 6.2: Frame of the Aircraft ground test at 100W. In the blue box the liquid storage, in the red box the annular flow, in the light blue box the pool boiling and in the yellow one the liquid film evaporation. (Vertical, bottom heated).

The little concavity on the copper side of the PHP probably reduced the thermal exchange with the aluminium heat sink even with the thermal pad between them. This caused a higher dry out phenomenon in the central channels with just a liquid film evaporation.

At 140W the security system intervened cutting off the power twice because the pressure exceeded 1.1bar (before the second shut down the power was manually reactivated).

The temperature recorded by the ambient thermocouple followed a little bit the trend of the other thermocouples because it had been positioned too close to the heated zone. After the test it was repositioned far from there.

A second test performed with the red PHP was a ground simulation of the first parabolic flight test.

The test was intended to start directly with a power at the evaporator of 100W without an accurate preheating in order to see how fast the PHP reacted.

The reaction was circa 30 seconds after this power input with an immediate activation, as it is possible to see in the figure 6.3.

Two other relevant decreases of temperature happened circa 1300 s and 2350 s after the beginning of the test, due to a decrease of power input to 50W the first and 0W the second.

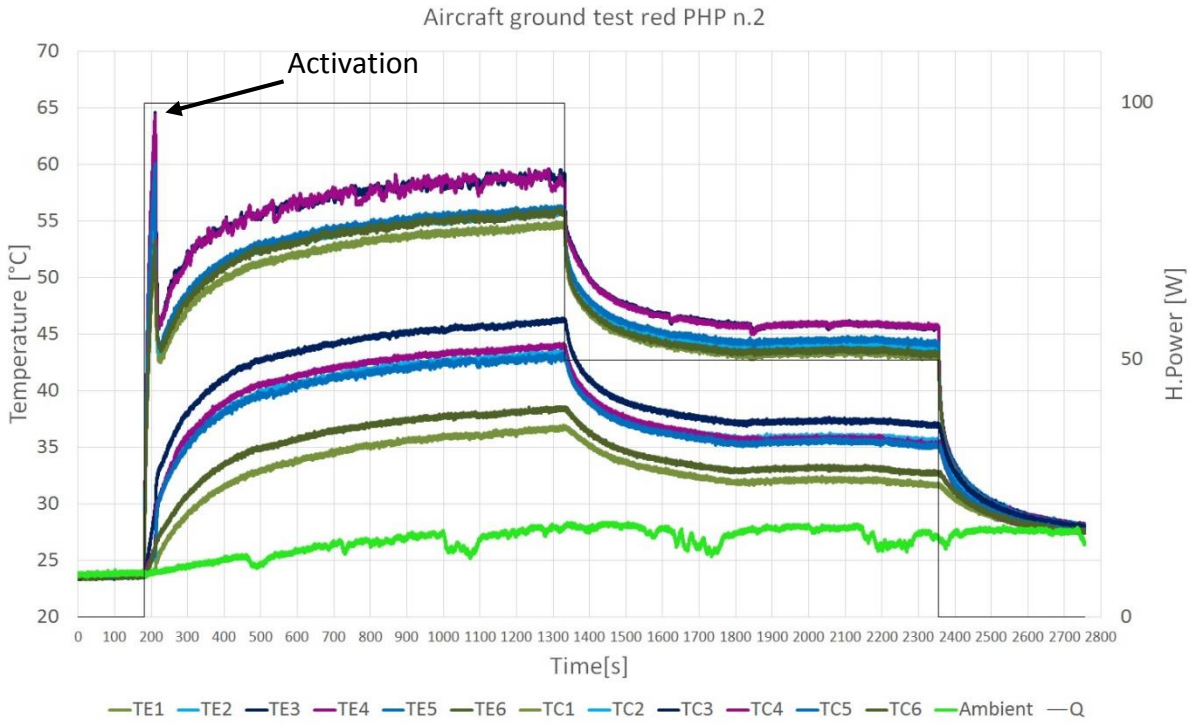

Figure 6.3: Diagram of the aircraft ground test n.2 with the red PHP. (Vertical, bottom heated).

Unfortunately, few seconds after the end of the test, the glass of the red PHP broke.
That was probably due to a thermal shock, starting from the centre of the evaporator the crack propagated to all the length of the glass, making it useless.
The original idea was to test both PHPs during the three days of parabolic flight.
Both of them, as described in the previous chapter, revealed a small defect. The red PHP, the one built using the Loctite glue, showed a little concavity on the copper face and it caused a non homogeneous heat exchange with the heat sink also after putting a thermo conductive pad.
The white PHP, the one built using the Nusil glue, presented a non perfect leakage proof ability and this caused a small leakage of non condensable gasses inside the PHP which could involve a worst functioning of the PHP.

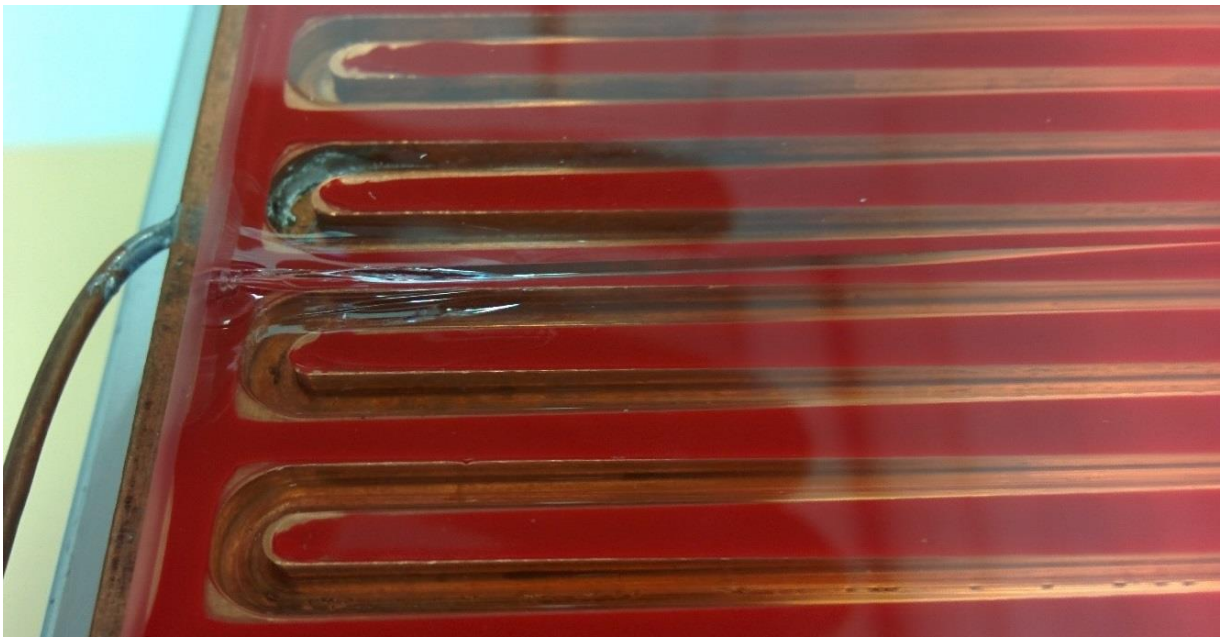

Figure 6.4: Detail of the glass broken during a ground test, the crack propagated to all the length of the glass.

Due to this, it had been decided to test the red PHP for the first two days of parabolic flight and the white one only on the last day, by substituting only the PHP and leaving all the other components of the rack unchanged. We couldn't carry on with this project because of the glass breakage so, during all the three days of parabolic flight only the white PHP was tested, monitoring the amount of non condensable gasses inside the channel after each flight and in case of a high presence of them, they were removed by changing the working fluid.

6.1.2 Aircraft ground testing: "White" PHP

Due to the limited time available, it was possible to perform only one ground test with the white PHP in the parabolic flight configuration inside the aircraft.
In order to avoid any risk of failure (we didn't have any more PHP to substitute in case of failure) the test was performed at a medium-low heat power and with smooth ramp-up and ramp down. The power sequence was: 0 – 20 – 40 – 60 – 80 – 60 – 40 – 20 – 10 – 0 [W].
The PHP reacted well to the thermal input with several activations.
The flow motion behaviour was the same as the one seen during the long time tests, due to the fact that the PHP was the same.

Just a hitch occurred with a thermocouple. The TC2 recorded a wrong temperature because of a problem with the connector. Since we were short of time, it was not possible to repair it before the first day of parabolic flight.

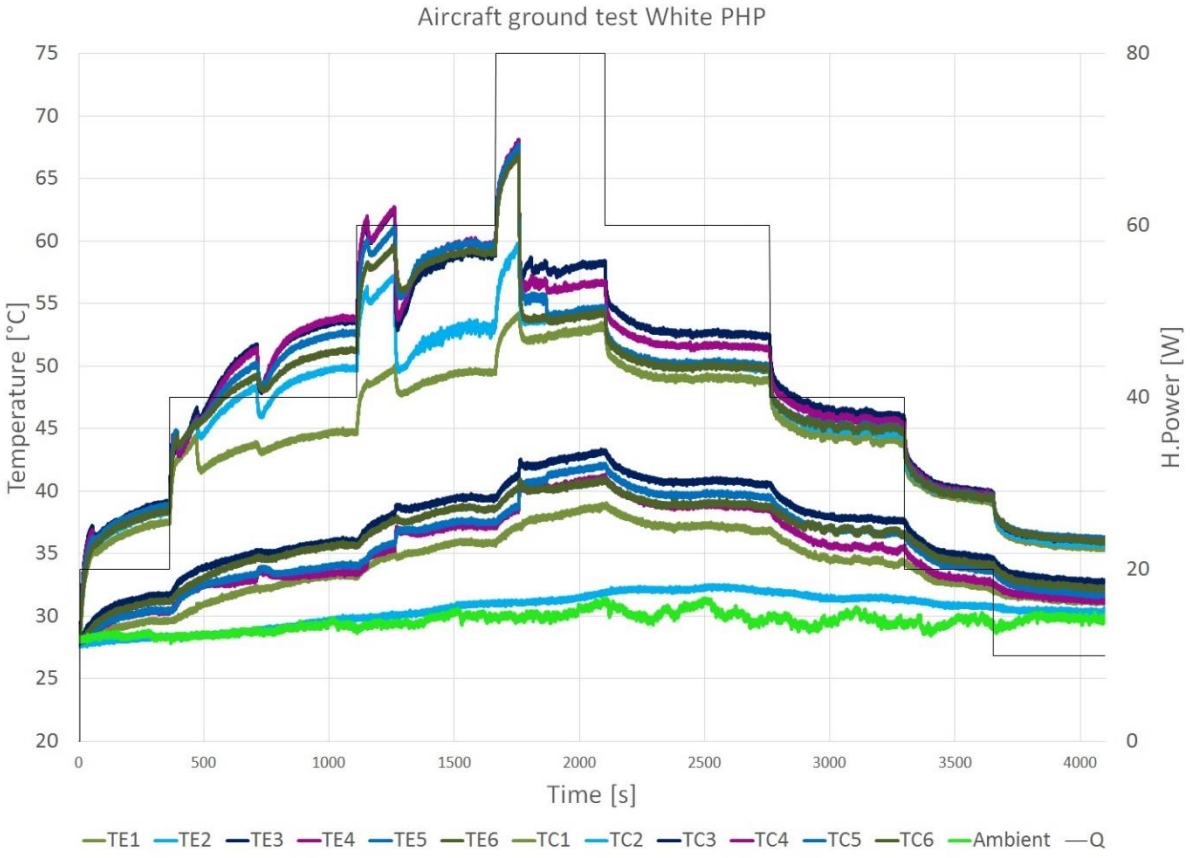

Figure 6.5: Diagram of the aircraft ground test with the white PHP. (Vertical, bottom heated).

6.2 Parabolic flight testing: "White" PHP

The experiment was performed during three days with 31 parabolas each day. It was decided to divide the three days of experiment in the following way:

- Day 1: the PHP was tested at medium-low heat power.
  To the first series of parabolas it was applied a power of 80W to decrease with the following series with a power of 60W for the second, 40W for the third, 30W for the fourth, 20W for the fifth while for the last series the power was increased each parabola from 10W to 20W,40W,60W and 80W.
- Day 2: the PHP was tested at medium-high heat power.
  To the first series of parabolas it was applied a power of 50W to increase with the following series with a power of 70W for the second, 90W for the third, 100W for the fourth, 110W for the fifth and the last at 120W.
- Day 3: the PHP was tested at medium-high heat power once again but it was reached the highest power which the PHP is able to stand.
  During this flight the power was changed every second or third parabola. From the first to the third at 50W, from the fourth to the sixth at 70W, the seventh and eighth at 80W, from the ninth to 11th at 90W, 12th and 13th at 100W, 14th to 16th at 110W, 17th and 18th at 120W, 19th to 21st at 130W, 22nd and 23rd at 140W, 24th to 26th at150W and for the last series from 130W to 50W with a step of 20W each parabola. A scheme is reported in the following table 3.

		Day 1	Day 2	Day 3
	Parabola N	Power [W]		
Series 1	0	80	50	50
	1	80	50	50
	2	80	50	50
	3	80	50	70
	4	80	50	70
	5	60	50	70
		5 minutes break		
Series 2	6	60	70	80
	7	60	70	80
	8	60	70	90
	9	60	70	90
	10	60	70	90
		5 minutes break		
Series 3	11	40	90	100
	12	40	90	100
	13	40	90	110
	14	40	90	110
	15	40	90	110
		8 minutes break		
Series 4	16	30	100	120
	17	30	100	120
	18	30	100	130
	19	30	100	130
	20	30	100	130
		5 minutes break		
Series 5	21	20	110	140
	22	20	110	140
	23	20	110	150
	24	20	110	150
	25	20	110	150
		5 minutes break		
Series 6	26	10	120	130
	27	20	120	110
	28	40	120	90
	29	60	120	70
	30	80	120	50

Table 3: Detail of power steps for each parabolic flight day.

In order to have the best results and limit the possibility of human error leading to PHP failure it was defined a procedure for the days of the flight. It is important to warm up and cool down the PHP before the first parabola and after the last one to avoid a thermal shock which can break the glass.
It was chosen to start the video acquisition at the command "ten" (10 seconds before the pull-up procedure) and to stop it 10 seconds after the pull-out.
The detailed task sequence must be written and communicated to Novespace technicians before the flight. It is reported in the following table 4 and 5.

ON GROUND – PRE-FLIGHT		
# Tasks	**Description**	**Operator #**
1	*Check that 220V is NOT connected* *Switch on PC with batteries* *Check correct working of PC on batteries* *Switch-on Novespace multiplug* *Switch-on differential switch on 220V* *Switch-on rack multiplug* *Check/Switch-on Heater power supply* *Switch-on Heater switch* *Check/Switch-on PC power supply* *Check correct working of PC on power supply* *Check/Switch-on Data Logger* *Check/Switch-on Fans and lights power supply* *Optional Verify/power supply switch to remote control* *Check/Switch-on NUC (PC with USB Camera)* *Run on the PC the remote control of the NUC* *Run Labview on PC and check the correct software version* *Run Labview and check the acquisition is correctly running* *Enable Heater PS on remote control* *Test Heater remote control at 10%, 50%, 100%, 0% (OFF)*	*1*
2	*Disable Heater PS on remote control* *Switch-off Heater power supply* *Wait until all temperature are low* *Turn off NUC (USB Camera PC)* *Turn off PC* *Switch-off Data Logger, Fan power supply, PC power supply* *Switch-off rack multiplug* *Switch-off differential switch on 220V* *Switch-off Novespace multiplug*	*1*

Table 4: Test procedure for the parabolic flight. Pre flight.

	IN FLIGHT – BEFORE THE FIRST PARABOLA	
1	*Repeat task 1*	*2*
	IN FLIGHT – BEFORE EACH PARABOLA	
4	*Set proper Heater power*	*1*
5	*Start the camera acquisition 10s before the pull-up*	*1*
	IN FLIGHT – 1.8g PARABOLA ENTRY PHASE	
6	*observe everything is working correctly*	*1*
	IN FLIGHT – 0g PHASE	
6	*observe everything is working correctly*	*1*
	IN FLIGHT – 1.8g PARABOLA EXIT PHASE	
6	*observe everything is working correctly*	*1*
7	*Stop the camera acquisition 10s after the pull-out*	*1*
	IN FLIGHT – AFTER EACH PARABOLA	
6	*observe everything is working correctly*	*1*
	IN FLIGHT – DURING 5-MINUTE BREAKS	
8	*Save data*	*1*
	IN FLIGHT – DURING 8-MINUTE BREAKS	
8	*Save data*	*1*
	IN FLIGHT – AFTER THE LAST PARABOLA	
8	*Save data*	*1*
2	*Repeat task 2*	*1*
	ON GROUND – POST-FLIGHT	
1	*Repeat task 1*	*1*
9	*Back up all data on an external device*	*1*
10	*Stop Ambient Thermo hygrometer recorder, save data*	*1*
2	*Repeat task 2*	*1*

Table 5: Test procedure for the parabolic flight. During and post flight

6.2.1 Parabolic testing at mid-low power

The first day of this parabolic flight campaign was dedicated to see how the PHP reacts in microgravity condition with a medium low heating power.
A different power level was chosen for each series of five parabolas except for the last series which required a different power level for each parabola.
It is important to remind that the parabolas are numbered from 0 to 30, the 0th being a test parabola, the others being grouped 1-5, 6-10, 11-5, 16-20, 21-25, 26-30.
For the first series at 80W the power was changed after the 4th parabola and not after the 5th one because of an error by the operator.
After a ramp up to reach the power level of 80W, this power was maintained for five parabolas (0-4) and then it was decreased to 60W and it was maintained for all the second series (5-10). After that, the power was decreased to 40W for all the third series (11-15). For the fourth series it was used a power level of 30W (16-20) and for the fifth of 20W (21-25). For the sixth and last series (26-30) it was chosen the heating power of 10W for the parabola number 26, then 20W, 40W, 60W and 80W respectively for the parabolas 27, 28, 29 and 30. The details are summarized in table 6. After the last parabola, the power level was slowly decreased and some videos were shot and data recorded for the clock synchronization.
Unfortunately, on the day of this test, the thermocouple on the condenser number 2 did not work and so a wrong temperature was registered.
In the following paragraph, the results of some series of parabolas will be shortly described, and few single parabola taken as exemplum will be analysed to highlight the behaviours at that power

Series 1	Parabolas	0	1	2	3	4	5
	H. Power [W]	80	80	80	80	80	60
5 Minutes Break							
Series 2	Parabolas	6	7	8	9	10	
	H. Power [W]	60	60	60	60	60	
5 Minutes Break							
Series 3	Parabolas	11	12	13	14	15	
	H. Power [W]	40	40	40	40	40	
8 Minutes Break							
Series 4	Parabolas	16	17	18	19	20	
	H. Power [W]	30	30	30	30	30	
5 Minutes Break							
Series 5	Parabolas	21	22	23	24	25	
	H. Power [W]	20	20	20	20	20	
5 Minutes Break							
Series 6	Parabolas	26	27	28	29	30	
	H. Power [W]	10	20	40	60	80	

Table 6: Detail of power steps for the parabolic flight day number 1.

6.2.1.1 Series number one at 80W

This series includes the parabolas from 0 to 4. In the temperature diagram it is possible to notice the highly different mode of operation of the PHP between normal or hyper-gravity and microgravity.

In normal gravity condition, the temperature on the evaporator side is quite constant, slightly increasing due to the increase of ambient temperature. All the thermocouples are in a range of temperature of 5-6°C with the temperature decreasing from the centre (TC 3 and 4) to the sides (TC 1 and 6) because of the fin effect on the side of the heat sink.

It is possible to notice how the hyper-gravity condition influences only a little bit the temperature on the evaporator with a slight decrease of temperature (of about 1°C) due to the high influence of gravity on thermosiphon functioning.

It was possible to see how in 1,8g the liquid was pushed more rapidly in the evaporator zone so that the bubble velocity was higher than in normal gravity condition.

During the microgravity phase, the temperature started to increase rapidly and with much more oscillation compared to normal gravity condition.

During the normal and hyper gravity, the PHP worked like a thermosiphon with the fluid brought back to the evaporator by the gravity. After the transition from hyper gravity to microgravity, the PHP goes quite immediately to a completely dry out condition on the evaporator and this is the cause of the increasing of temperature. The fluctuations of temperature during the microgravity phase are due to some random instability which brings back the liquid to the evaporator zone followed by another dry out, a kind of stop and start behaviour. This phenomenon was observed during all the parabolas.

The temperature on the condenser was less influenced by the gravity condition with only some fluctuation due to the motion of fluid inside the channel. The temperatures are in a range of 7-8°C and slightly increasing according to the increasing of ambient temperature. It was possible to notice on the figure 6.6 how the temperature was higher moving from the top to the bottom of the condenser (e.g. TC3 compared with TC4 or TC1 with TC6) and from the side to the centre (e.g. TC1 compared with TC4 or TC3 compared with TC6). Generally speaking, due to a non motion of liquid during the microgravity condition compared to the normal gravity, the heat exchange between hot and cold sources was lower, so that the temperatures on the condenser zone were lower.

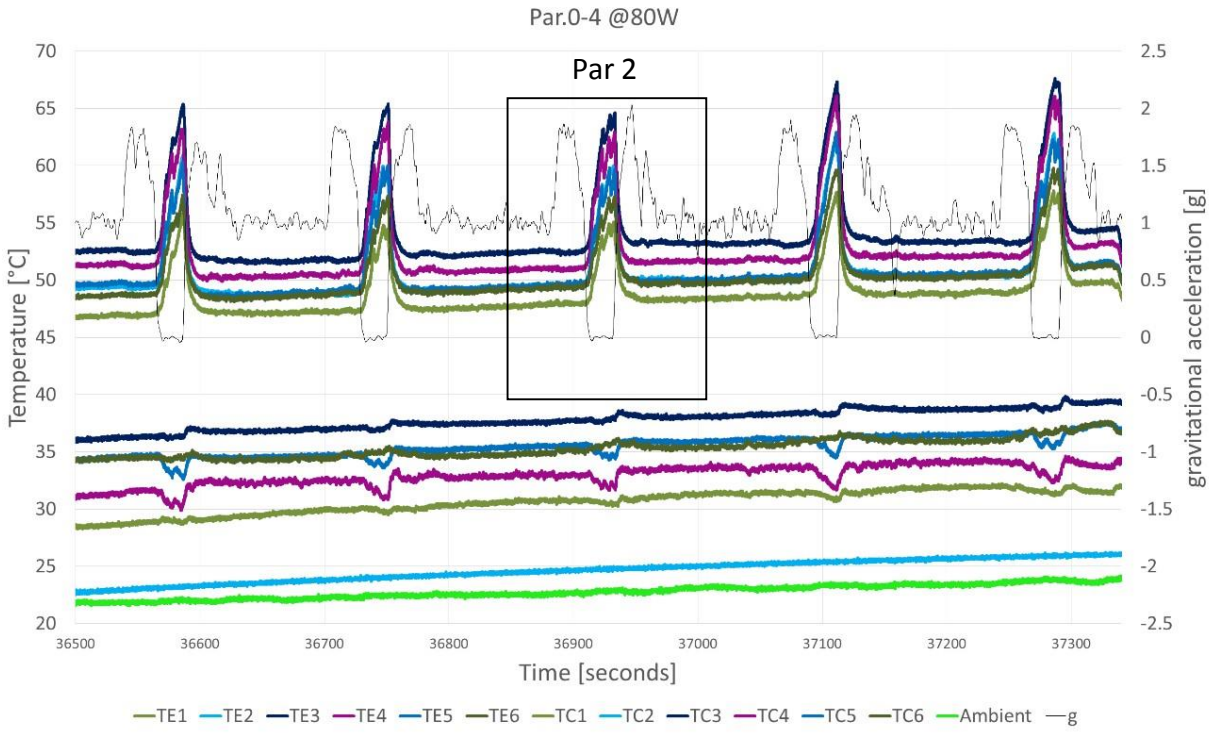

Figure 6.6: Temperature and gravitational acceleration of day 1, series 1 at 80W (parabolas 0 to 4).

6.2.1.2 Focus on Parabola number 2

It was chosen the parabola number two to focus on the functioning during the microgravity phase.

As expected, after the transition in microgravity, the PHP was able to work in a slug and plug configuration as well as with its large channel section.

Just after the transition in microgravity, the functioning mode is no longer assisted by the gravity so, after the evaporation phase, the liquid remains on the condenser zone moving to a full dry out evaporator configuration (see figure 6.8).

In the figure 6.7 it is possible to notice three evident peaks of the temperature of the evaporator during the microgravity condition. These three peaks represent the moments when the instability starts from one channel (showed in figure 6.9) and propagates to the others (figure 6.10), pushing some liquid plugs on the evaporator. This causes a rapid evaporation of the liquid and, as consequence, a flow motion in the whole PHP. Due to this, a decrease of temperature was recorded thanks to a better heat exchange between the hot and cold source.

As a result, it was possible to notice a less evident increase of temperature on the condenser temperature plot, in correspondence of the PHP activation.
Looking at the evaporator temperature plot, just after the injection in microgravity, it was possible to see a continue sequence of rapid increasing and decreasing of temperature. This corresponded to the succession of dry-outs (increase of temperature) and activations (decrease of temperature).
In all the parabolas it was possible to highlight this continue succession of dry out and instability which allowed the evaporator temperature to maintain within a reasonable value.
At the same time, some capillarity pumping through the edge of the channel was observed. Thanks to this phenomenon, some liquid moved to the evaporator zone also when the vapour bubble did not push it.

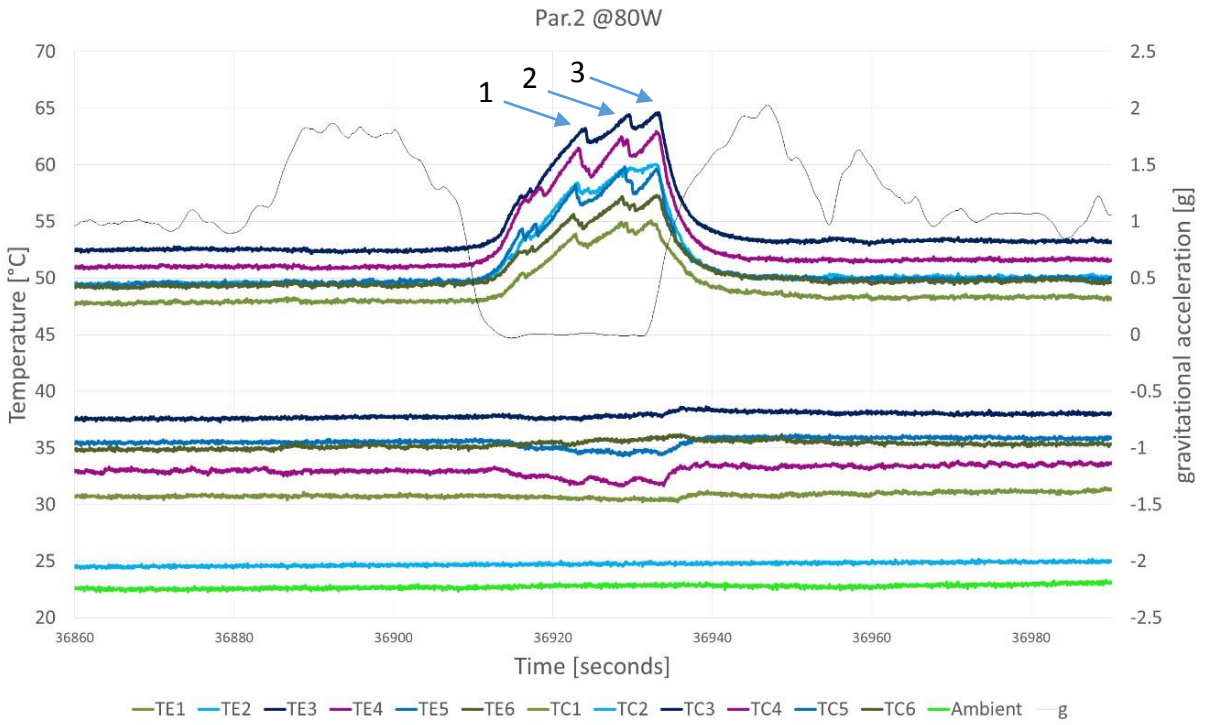

Figure 6.7: Temperature and gravitational acceleration of day 1, series 1, parabola 2 at 80W.

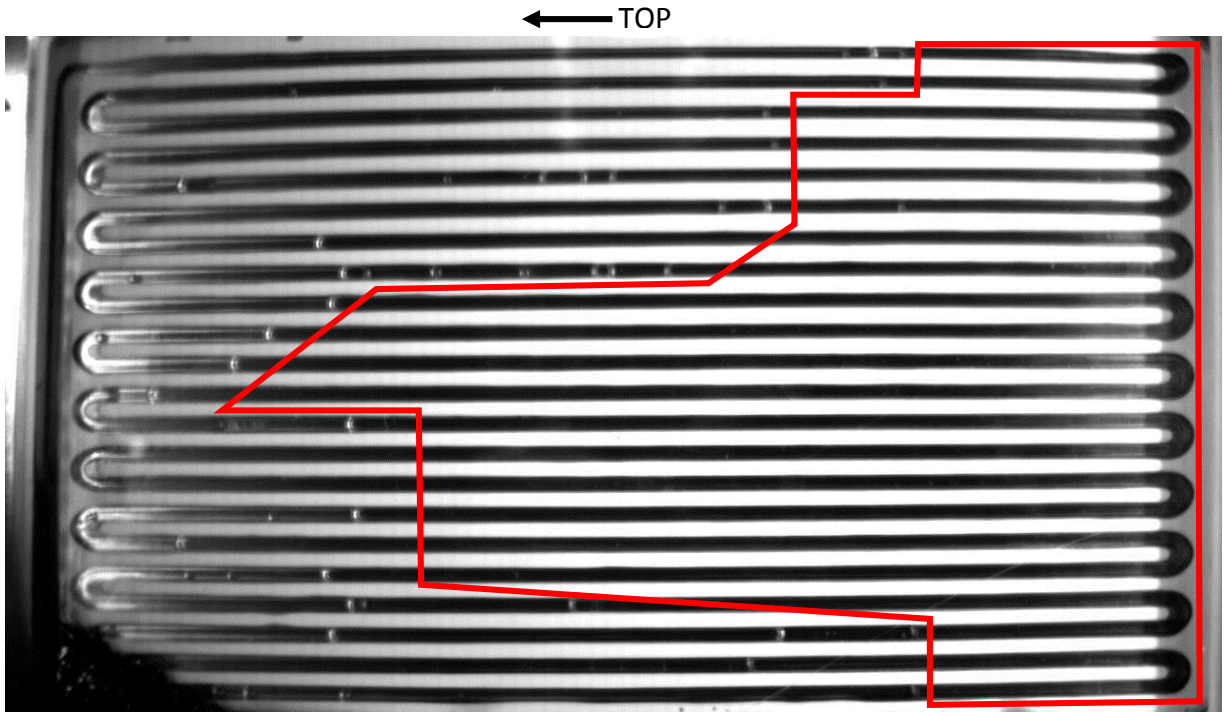

Figure 6.8: Frame of the first dry out region (red polygon) during microgravity in parabola 2.

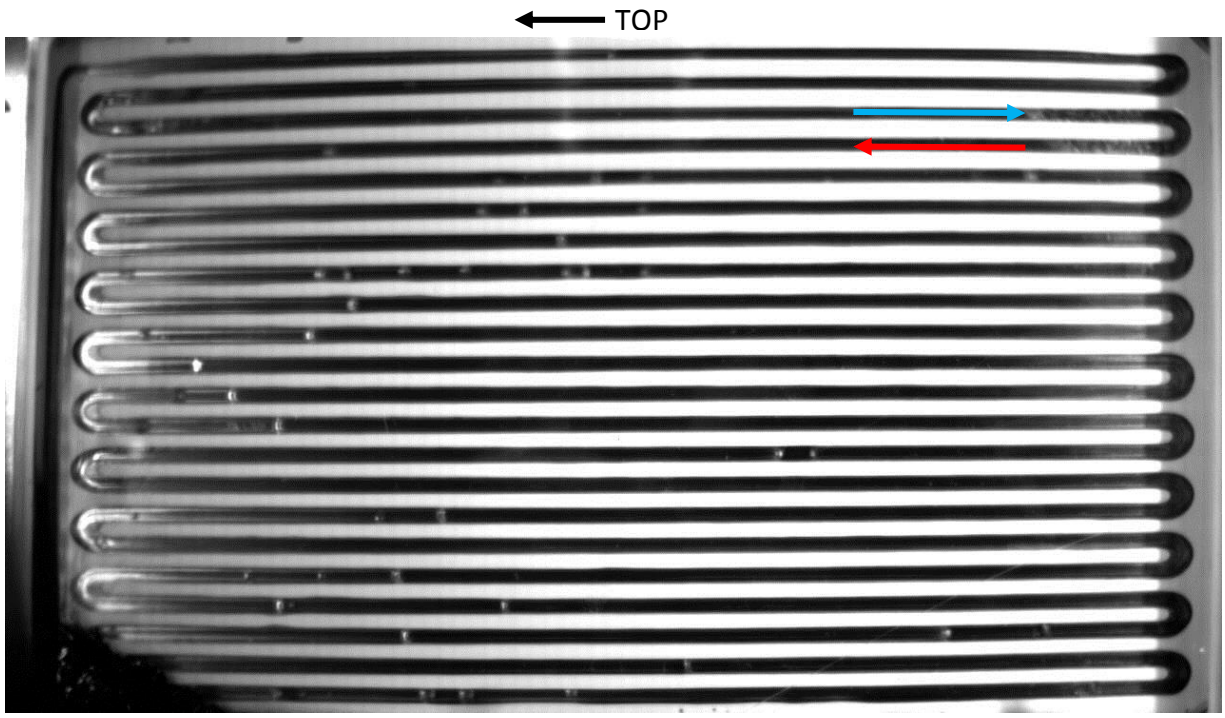

Figure 6.9: Frame of the first activation during microgravity in parabola 2.

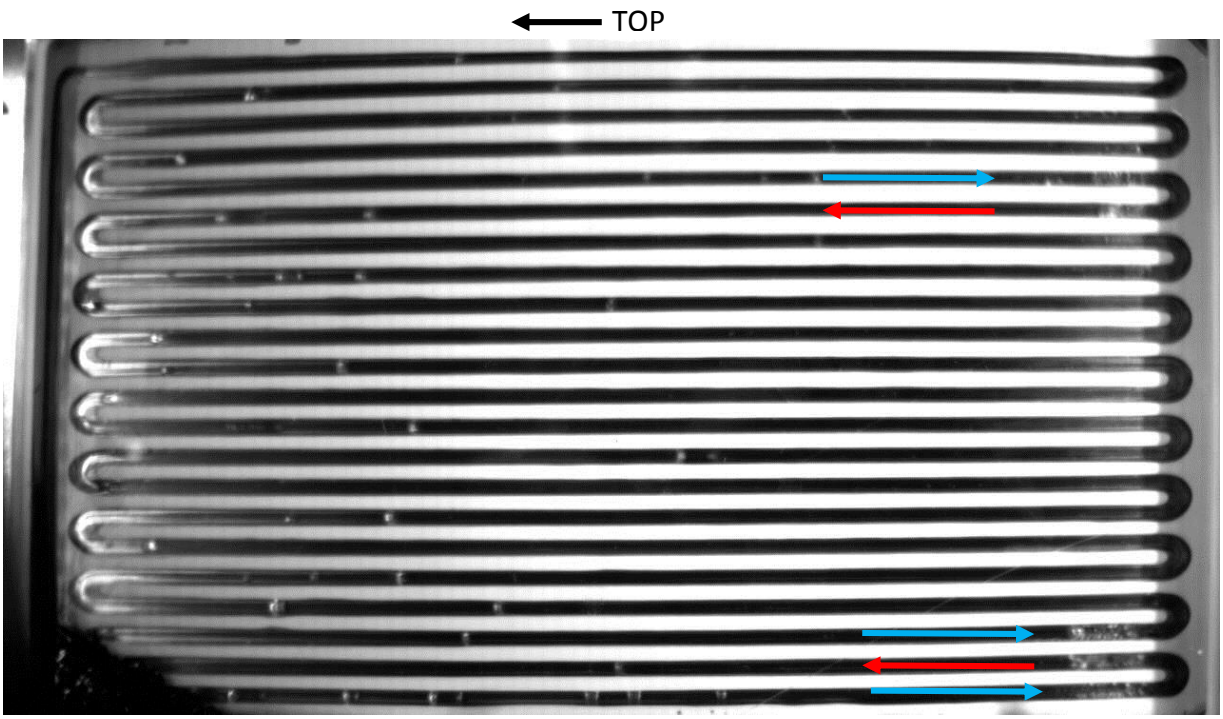

Figure 6.10: Frame of the propagation after the instability on figure 6.5.

6.2.1.3 Series number four at 30W

The forth series includes the parabolas from 16 to 20. At a low heat power, the temperature in the evaporator changed in a restricted range between 38°C to 40°C with the same spreading distribution, which is higher in the centre and lower to the sides.
Due to the low heat power, the pool boiling flow regime replaced the annular flow.
During the Hyper gravity phase it was not possible to notice any change both in the evaporator and in the condenser zone.
During the microgravity phase, there was the same functioning mode as in higher power. A succession of dry out and slug and plug motion was observed. In this case, the transition from pool boiling to the first dry out were much slower due to the lower heat power. When an instability phenomenon happened, the liquid maintained the slug and plug pulsating motion much longer than at high power. It is possible to notice in the figure 6.11 how at low power, the temperature peaks in microgravity are just one or two and are much less sharp.

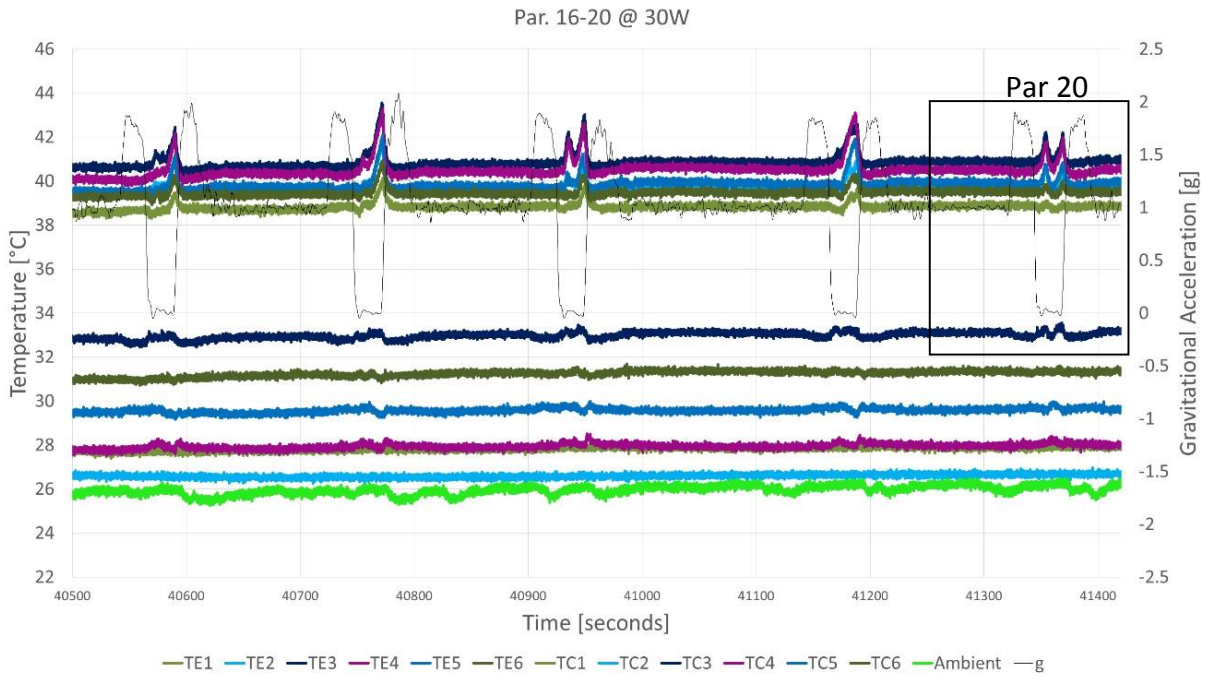

Figure 6.11: Temperature and gravitational acceleration of day 1, series 4 at 30W.

6.2.1.4 Focus on Parabola number 20

During the parabola number 20, it was possible to notice the different thermal reaction on the evaporator at low heat power.

As already registered, during the microgravity phase, there were only two dry-outs followed by two activations. After the first instability phase, the pulsating functioning was much longer compared to the high heating power. This allowed to have a similar temperature between normal or hyper gravity compared to micro gravity (see figure 6.12).

The cause of the dry out could be the breakage of the menisci at high vapour velocities. At high heat power, the fluid velocity is high, leading to the menisci breakage. This causes an accumulation of liquid in the colder part (condenser), whereas at low heat power, the fluid velocity is lower, causing less breakage and dry-out than at higher ones.

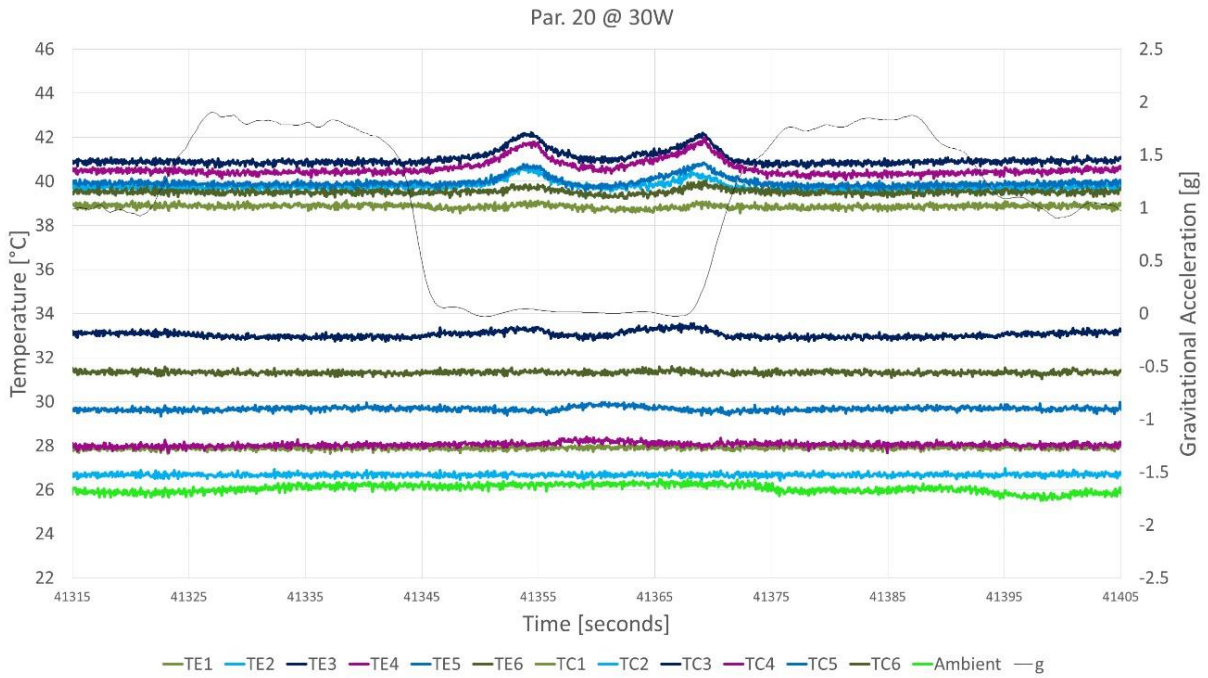

Figure 6.12: Temperature and gravitational acceleration of day 1, series 4, parabola 20 at 30W.

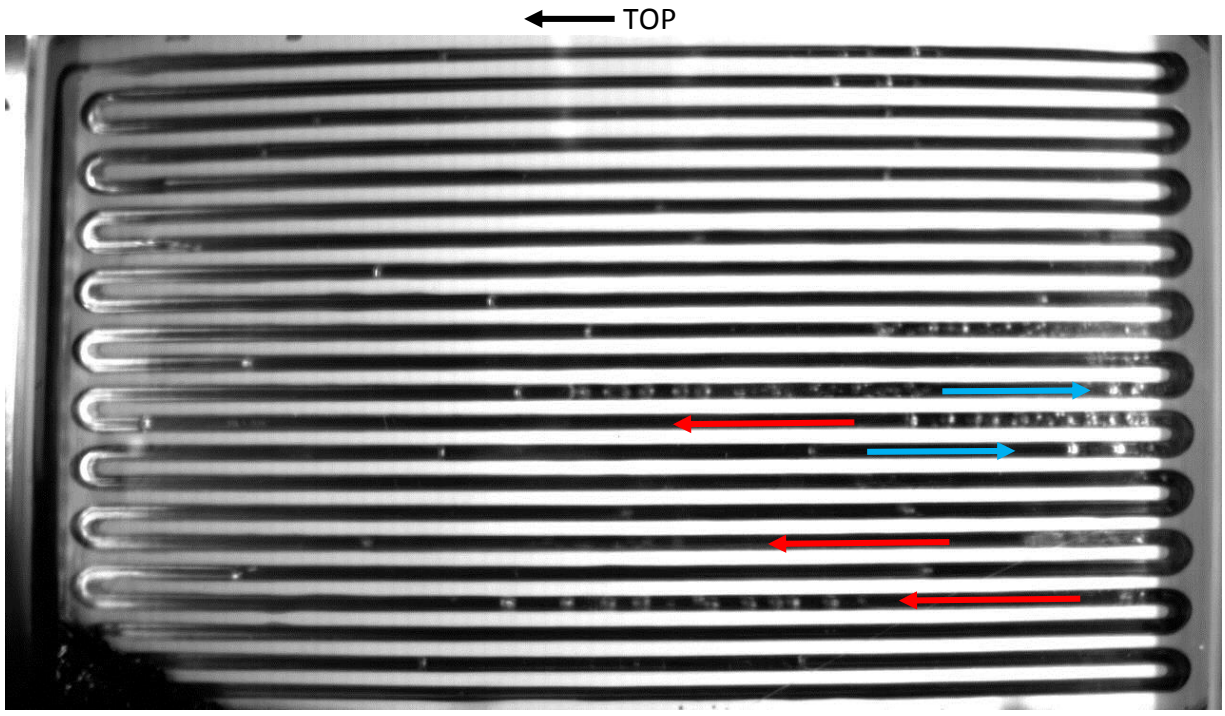

Figure 6.13: Frame of the first activation during microgravity in parabola 20. Due to the low heat power, the menisci was not broken by the vapour and was possible the generation of vapour bubble on the evaporator

6.2.2 Parabolic testing at mid-high power

At the end of the first day of parabolic flight, the pressure inside the PHP was 41.4 kPa at 27°C. That means a partial pressure of non condensable gasses of 9.2 kPa due to the FC-72 saturation pressure of 32.2 kPa at 27°C. That amount of non condensable gasses was irrelevant for the experiment, but, in order to avoid a worst situation on the following day, it was decided to substitute the fluid inside the PHP just after the first parabolic flight.
During the second day of parabolic flight, the PHP was tested at medium-high heating power. One single power was chosen for each series. After a warming up, it was set the power at 50W for the first series. The second was with a power of 70W. The third was with a power of 90W and for all the following series, the power was increased with a step of 10W each so for the fourth it was 100W, 110W for the fifth and finally 120W for the last one. The details are summarized in table 7. During the cooling down phase in this flight, some videos were shot and data recorded for the clock synchronization too (see paragraph 6.3).
The TC2 was fixed so, from this experiment on, all the temperatures were correct.

Series 1	Parabolas	0	1	2	3	4	5
	H. Power [W]	50	50	50	50	50	50
5 Minutes Break							
Series 2	Parabolas	6	7	8	9	10	
	H. Power [W]	70	70	70	70	70	
5 Minutes Break							
Series 3	Parabolas	11	12	13	14	15	
	H. Power [W]	90	90	90	90	90	
8 Minutes Break							
Series 4	Parabolas	16	17	18	19	20	
	H. Power [W]	100	100	100	100	100	
5 Minutes Break							
Series 5	Parabolas	21	22	23	24	25	
	H. Power [W]	110	110	110	110	110	
5 Minutes Break							
Series 6	Parabolas	26	27	28	29	30	
	H. Power [W]	120	120	120	120	120	

Table 7: Detail of power steps for the parabolic flight day number 2.

6.2.2.1 Series number one at 50W

The first series includes the parabolas with number from 0 to 5. The overall functioning was the same as the one we observed during the first day of parabolic flight. That means a very slight reduction of the evaporator temperature during the hyper gravity. The functioning in microgravity is also a sequence of dry out in the evaporator and slug and plug oscillation, which pushes the liquid in the evaporator zone.

During this series, another very important aspect of functioning in microgravity was highlighted.

Looking at the Figure 6.14 it is possible to notice a strong decrease and convergence of temperature on the evaporator. At the beginning, the distribution of the fluid inside the PHP was strongly non uniform with a part in dry out and a part with liquid storage. Just after a couple of parabolas, the situation was better with a more uniform distribution of liquid inside the channels. After five parabolas, there were no more full channels with liquid or completely in a dry out condition. The maximum temperature during the 1g decreased from 47°C recorded on the TE4 and TE5 to 45°C at TE3,and the maximum temperature during the microgravity phase decreased of about 2°C too. During the normal or hyper gravity phase, this PHP is able to work only with an annular flow without any liquid pumping like in the condition of slug and plug motion. This is different during the microgravity phase where the fluid distributes in slug and plug so that the liquid can be pushed to the other channels.

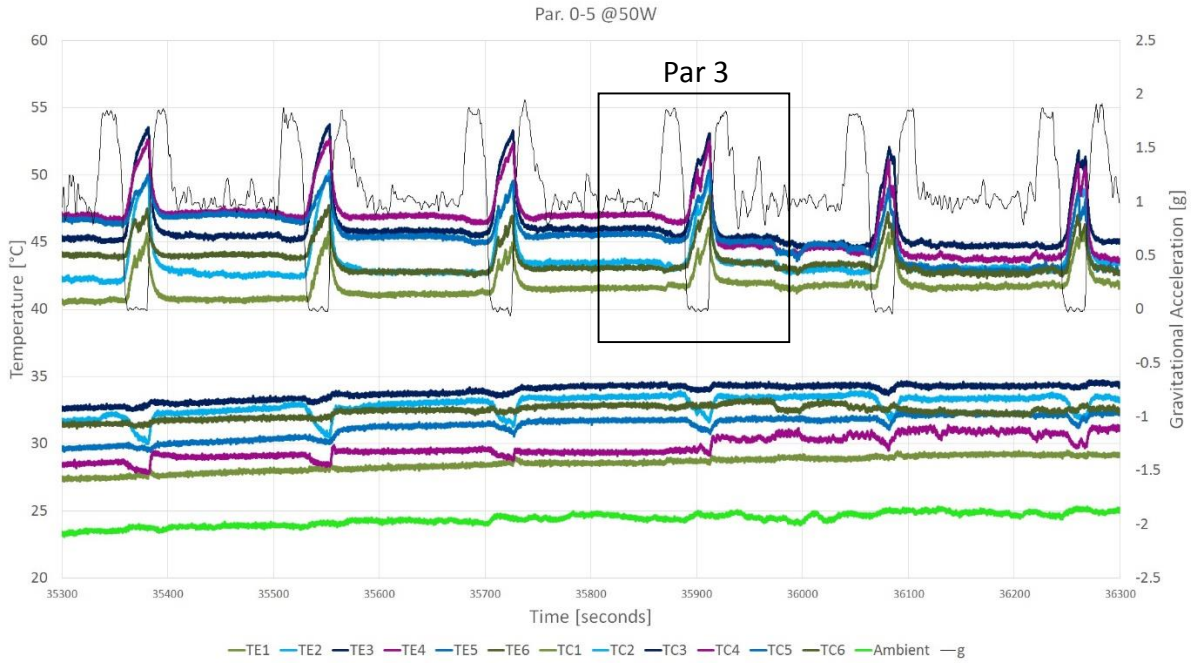

Figure 6.14: Temperature and gravitational acceleration of day 2, series 1 at 50W.

6.2.2.2 Focus on parabola number 3

During the parabola number three it was possible to verify how the microgravity influences the correct distribution of the liquid through the channels.

In the figure 6.15, it is possible to see the disposition of the liquid and vapour at the microgravity beginning. There are some channels with a liquid storage and some in dry out.

After the first instability, some liquid is pushed to other channels from the liquid storage, permitting to fill some of the channels which were in a dry out condition (figure 6.16).

Looking at the figure 6.17 it is also possible to notice that the TE3, TE5 and TE6 do not record any consistent variation of temperature after the first fluid instability inside the PHP. This is because the Slug and Plug motion happens only for few channels, not in the ones in dry out or liquid storage condition.

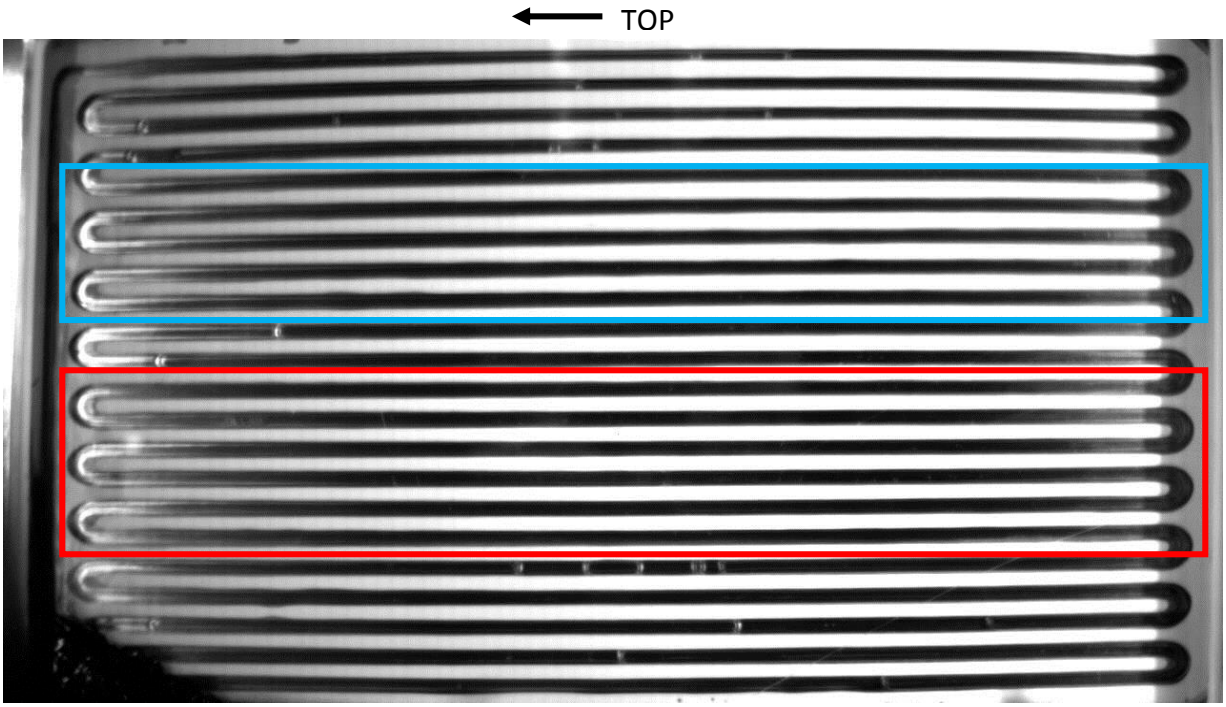

Figure 6.15: Fluid distribution in microgravity. Liquid storage (blue box) and dry out (red box).

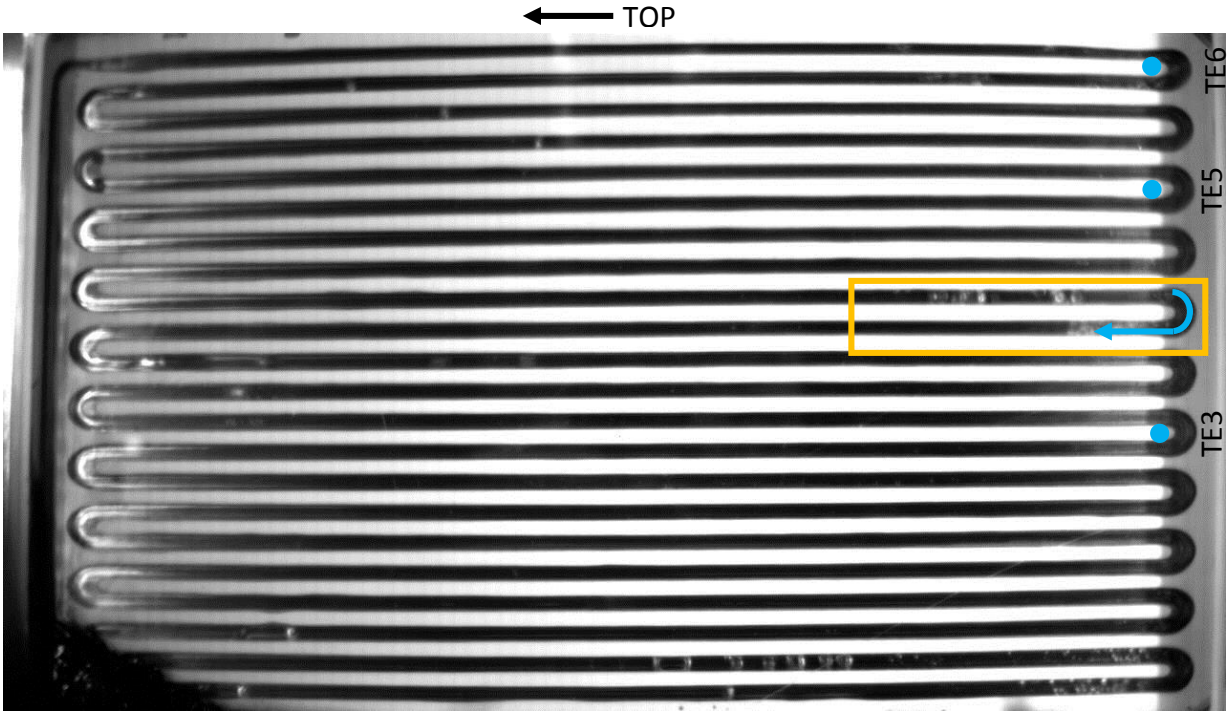

Figure 6.16: Liquid transport to the adjacent channel from the one in liquid storage (yellow box). The blue dot mark the position of the thermocouple TE3, TE5, TE6. No fluid motion was present in that zone

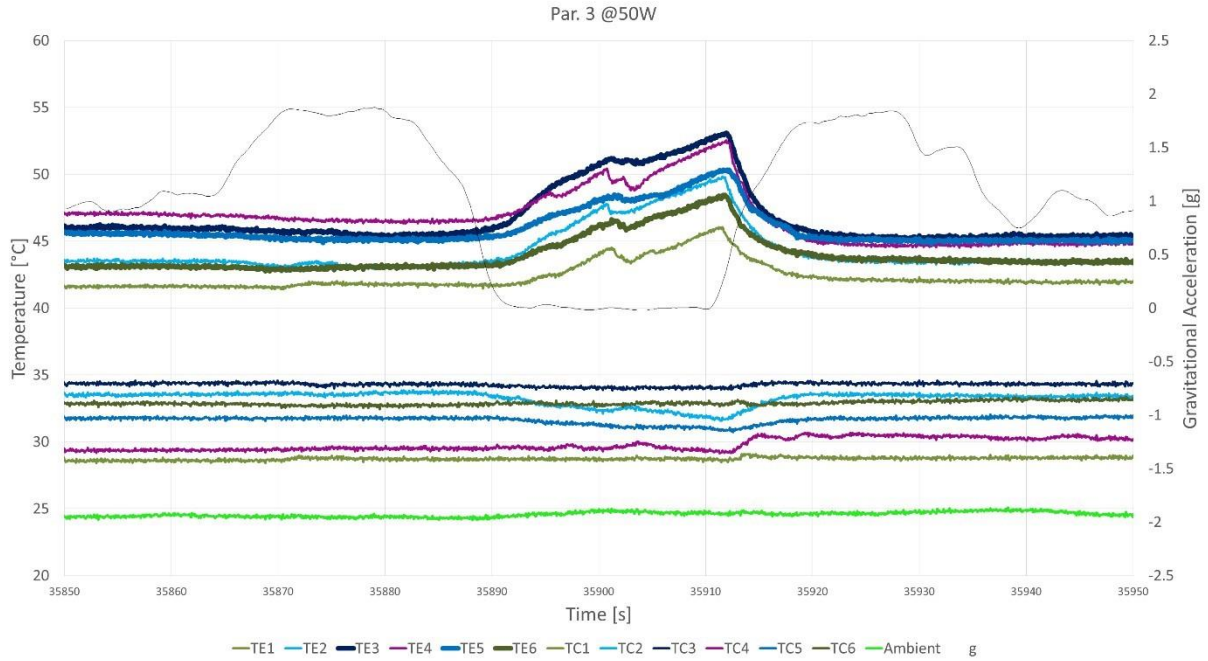

Figure 6.17: Temperature and gravitational acceleration of day 2, series 1, parabola 3 at 50W.

6.2.2.3 Series number six at 120W

The last series of the second day of parabolic flight was performed with a heating power of 120W; higher power were left to the last day of flight, due to the high risk of failure.
During the normal gravity condition, the evaporator temperature was kept within a range between 58°C and 64°C with a little decrease of about 1°C during the hyper gravity phase. On the condenser zone, the temperature was approximately within a value between 36°C and 44°C.
During the microgravity phase, due to the high power at the heater, the evaporator zone went rapidly in a dry out condition, which caused a fast increase of temperature. This is also highlighted by the steep slope of the initial temperature curve on the evaporator side during the first part of microgravity. During all these parabolas, the alternation of the full dry out condition and the reactivation of the pulsating condition was very fast except for the parabola number 27 (the second of this series). During this parabola, most of the time of the microgravity period was in a dry out condition. For all the others, the dry out happened just few seconds after the injection in microgravity. The passage of a liquid plug in the heated zone was followed by the deposition of a thin liquid film (few tens of micrometres) on the walls,

which evaporated and cooled the crossed heated zone locally and momentarily. When the first instability occurred, the fluid inside the PHP started to oscillate. Due to the high power supplied by the evaporator, the fluid motion was divided into two different types: one in the evaporator and one in the condenser. In the evaporator it is an annular flow because the rapid evaporation does not permit the formation of a bubble. In the condenser, liquid and vapour organised in a slug and plug configuration.

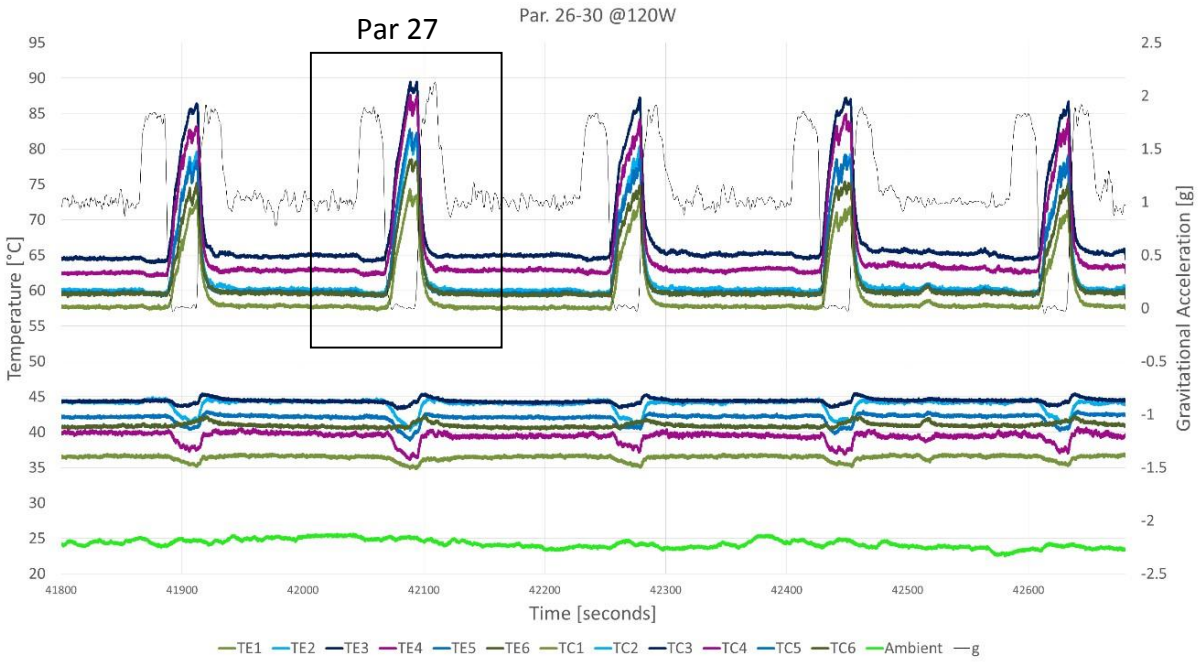

Figure 6.18: Temperature and gravitational acceleration of day 2, series 6 at 120W.

6.2.2.4 Focus on parabola number 27

The overall functioning during this parabola was the same as all the other parabolas seen before.

It was possible to notice three main peaks during the functioning in microgravity. The first two, very close each other, were a rapid succession of dry out – activation – dry out – activation which caused these two peaks. The last one was caused by the returning to the hyper gravity phase.

This parabola was quite interesting for a particular phenomenon: the capillary pumping on the corners of the square channels.

During the first relevant increase of temperature, just after the microgravity begins, it is possible to see on the figure 6.20 how the slope changes inclination. This is due to an important capillary pumping on the corners, which feeds a little bit the evaporator zone with liquid (see figure 6.19). Thanks to this, the temperature on the evaporator side increases slowly compared to a completely dry out condition.

Even if in very small amount, this phenomenon is present in all the parabolas but most of the time it has a negligible effect.

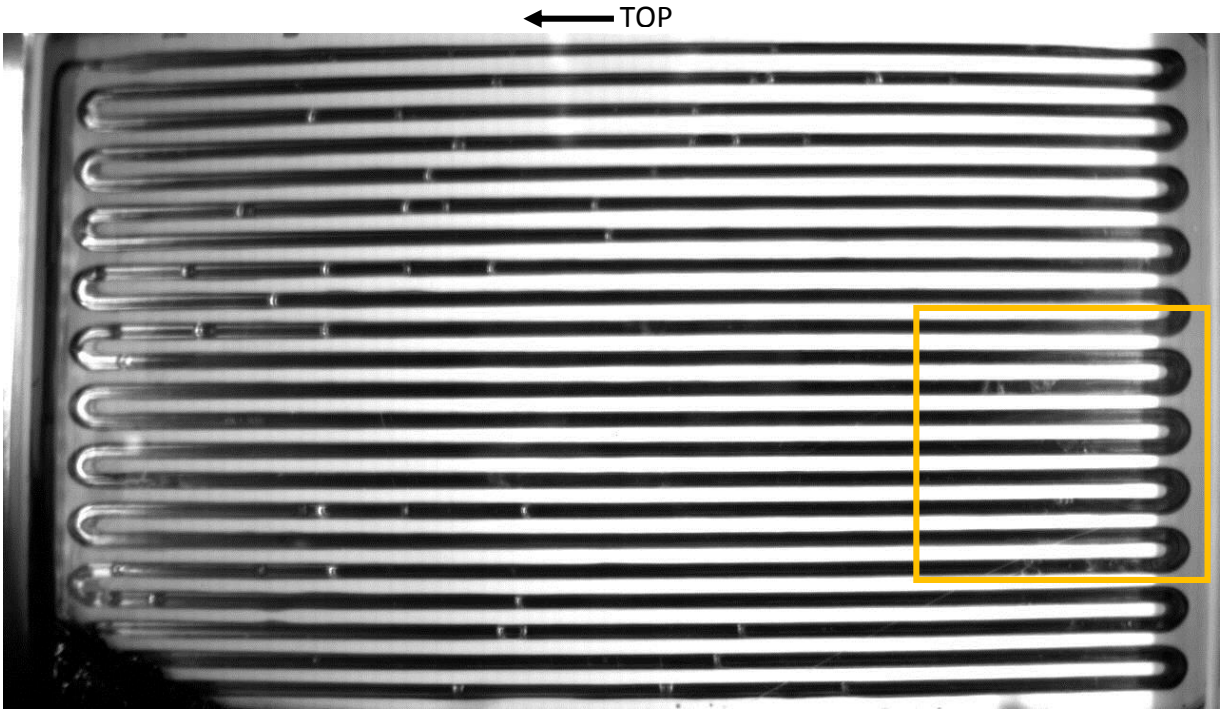

Figure 6.19: Frame of the parabola 27. On the yellow box an evident capillary pumping on the edges of the square channels

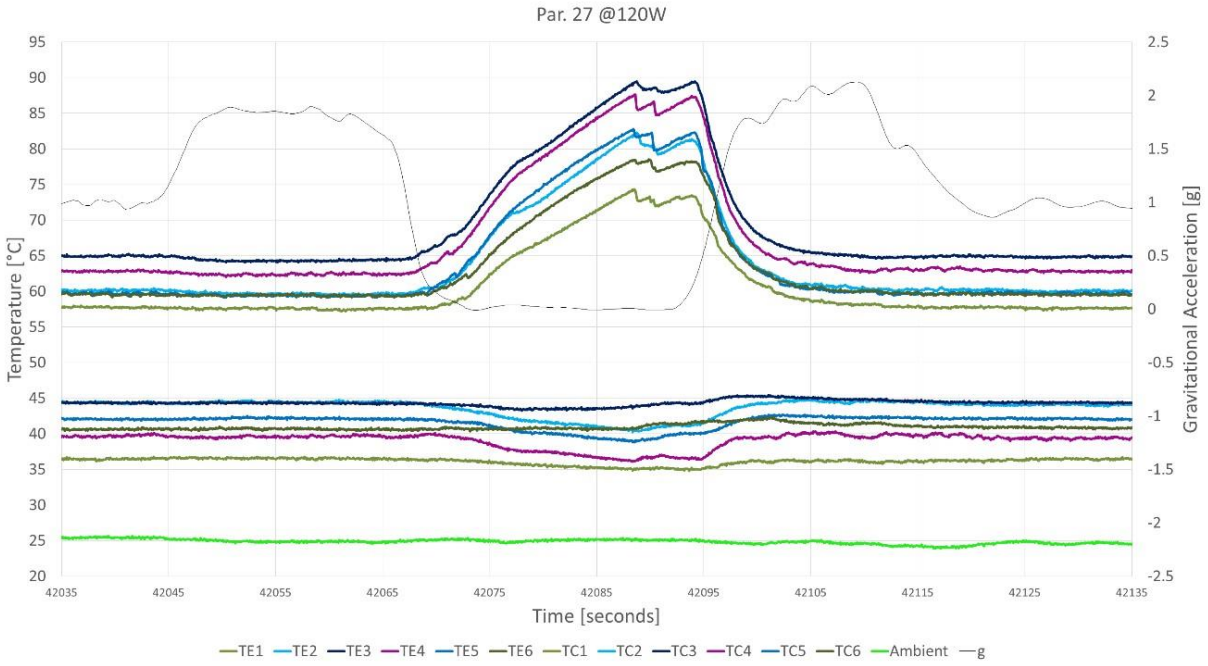

Figure 6.20: Temperature and gravitational acceleration of day 2, series 6, parabola 27 at 120W.

6.2.3 Parabolic testing at the highest power

During the last day of parabolic flight, the PHP was tested at the maximum heat power before the cut down by the security system.

It was decided to start with a power of 50W and increase it after two or three parabolas up to the limit value of 150W. The idea was to test many power levels, with at least two significant parabolas at each level, with the transition after each power increase happening during the pauses between the series, or during the central parabola of a series. The detailed heating power for each parabolas is to be found in the table 8.

Series 1	Parabolas	0	1	2	3	4	5
	H. Power [W]	50	50	50	70	70	70
5 Minutes Break							
Series 2	Parabolas	6	7	8	9	10	
	H. Power [W]	80	80	90	90	90	
5 Minutes Break							
Series 3	Parabolas	11	12	13	14	15	
	H. Power [W]	100	100	110	110	110	
8 Minutes Break							
Series 4	Parabolas	16	17	18	19	20	
	H. Power [W]	120	120	130	130	130	
5 Minutes Break							
Series 5	Parabolas	21	22	23	24	25	
	H. Power [W]	140	140	150	150	150	
5 Minutes Break							
Series 6	Parabolas	26	27	28	29	30	
	H. Power [W]	130	110	90	70	50	

Table 8: Detail of power steps for the parabolic flight day number 3.

One important property during this third day of parabolic flight was the increased presence of non condensable gasses.

In the morning, the pressure inside the PHP was 37.1 kPa with a temperature of 19.8°C. Due to a saturation pressure of 23.5 kPa at 20°C that means a partial pressure of incondensable gasses of 13.6 kPa circa.

Because of the difficulties we found during the replacing of fluid the day before, it was decided not to work on it to avoid any risk of damage before the last day of testing on parabolic flight and also to see the changes on functioning with a larger amount of non condensable gasses inside, that is a parameter always mentioned by many researchers (Henry C.D., 2004) but that has never been deeply investigated.

6.2.3.1 Influence of non condensable gasses

Making a comparison between the parabolas at same power level of day two and day three it is possible to deduce some considerations (see figure 6.21).
The most important one is a considerable increase of temperature in the whole PHP.
At 70W, the temperature on the evaporator side during the 1g was between 49°C and 53°C on the third day (with a higher amount of non condensable gasses) and between 47°C and 51°C on the second day with the same ambient temperature (25°C). During the microgravity phase, the temperature was strictly linked to the motion of the fluid and not predictable.
On the condenser zone, the mean temperature was more or less the same. It was recorded a mean temperature of about 34,9°C for the day two and about 34,7°C for the day three (mean temperature of all the condenser thermocouples for two seconds of sampling). The big difference was the spread of temperature, which was around 6°C for the day two and 9°C for the day three. This was due to the big gap of temperature between the two thermocouples TC1 and TC4 and all the others. These two thermocouples were positioned on top of the condenser where the non condensable gasses were stored for most of the time. Due to this, the heat exchange on the top of the condenser was extremely low and this caused the evident decrease of local temperature.
The results were similar with different heating power too.
The main aspect which is evident in all the diagrams, is the very lower temperature of the two thermocouples on the upper part (TC1 and TC4) compared to the value of the other condenser thermocouples.
The non condensable gasses are mixed with the saturated vapour, artificially increasing the pressure of the vapour bubbles and the corresponding saturation temperature for the fluid to evaporate. In the normal gravity condition, the mixture of vapour/non condensable gasses is accumulated in the highest part of the PHP and acts as describe above. During slug and plug flow motion, it is much more complicated to find out where the non condensable gasses are more concentrated because the quantity of them will be different in every plug, due to the vapour mass transfers during evaporation/condensation processes.

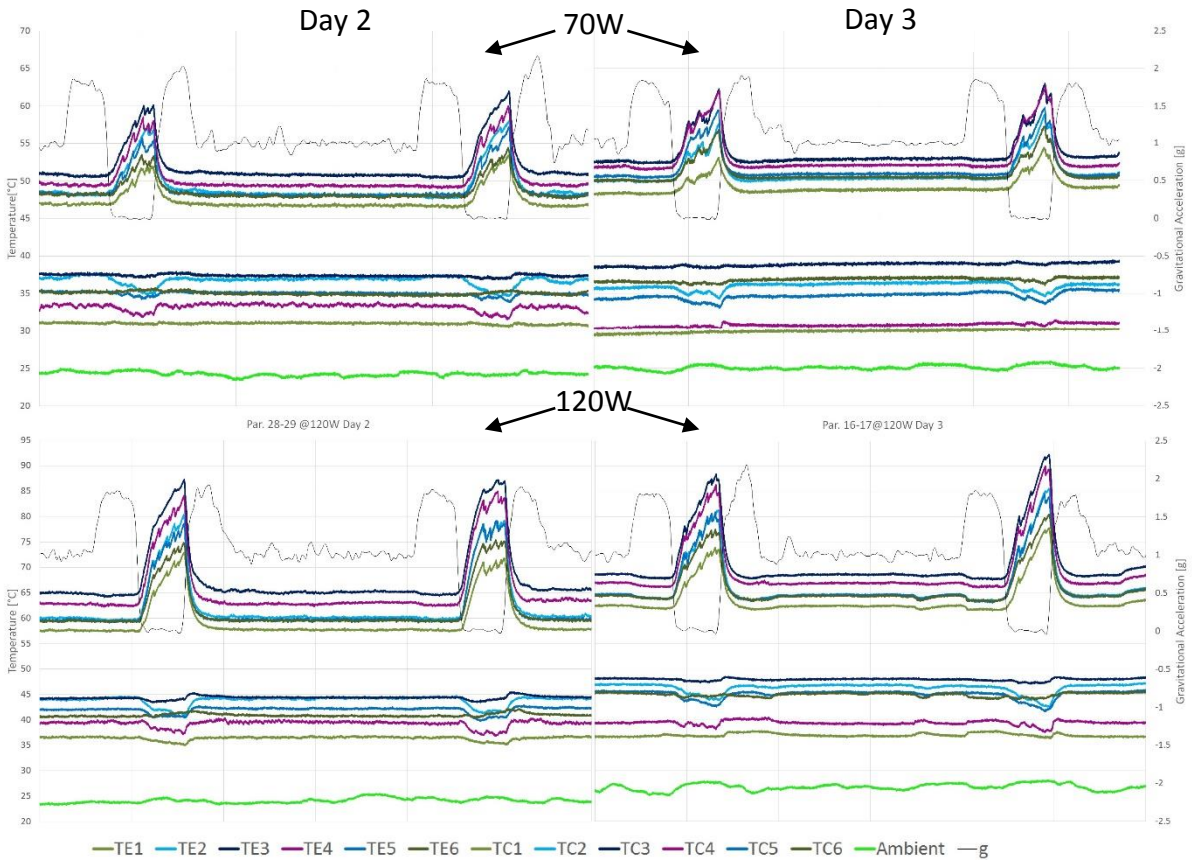

Figure 6.21: Comparison of temperature between Day 2 (on the left) and Day 3 (on the right) with two different power level, up at 70W, down at 120W. During the day 3 there was a higher amount of non condensable gasses.

6.2.3.2 Focus on parabolas 23-24-25

The parabolas number 23-24-25 were the three parabolas at the maximum heat power of 150W tested with this PHP.

During the transition from microgravity to hyper gravity during the parabolas number 24 and 25, a rapid increase of pressure (more than 1.1 bar) caused the cut-down by the software security system. The power was reactivate manually after few seconds.

The functioning was the same as in the previous cases.

For example, the parabola 23 in the microgravity phase, presented six peaks, which corresponded to six different activations, spaced out by six dry outs (see figure 6.22).

In the same way of the parabola 27 on the previous day, due to the high power at the evaporator and during the microgravity, when the liquid goes on the evaporator side, it starts an annular flow which becomes slug and plug on the upper part of the condenser.
In this parabola too, it is highly evident the presence of capillary pumping on the corner which pushes some liquid on the evaporator even without the PHP activation.
Even with a power of 150W, a thermal crisis never occurred thanks to this sequence of dry out and activation which maintained the temperature under reasonable value.

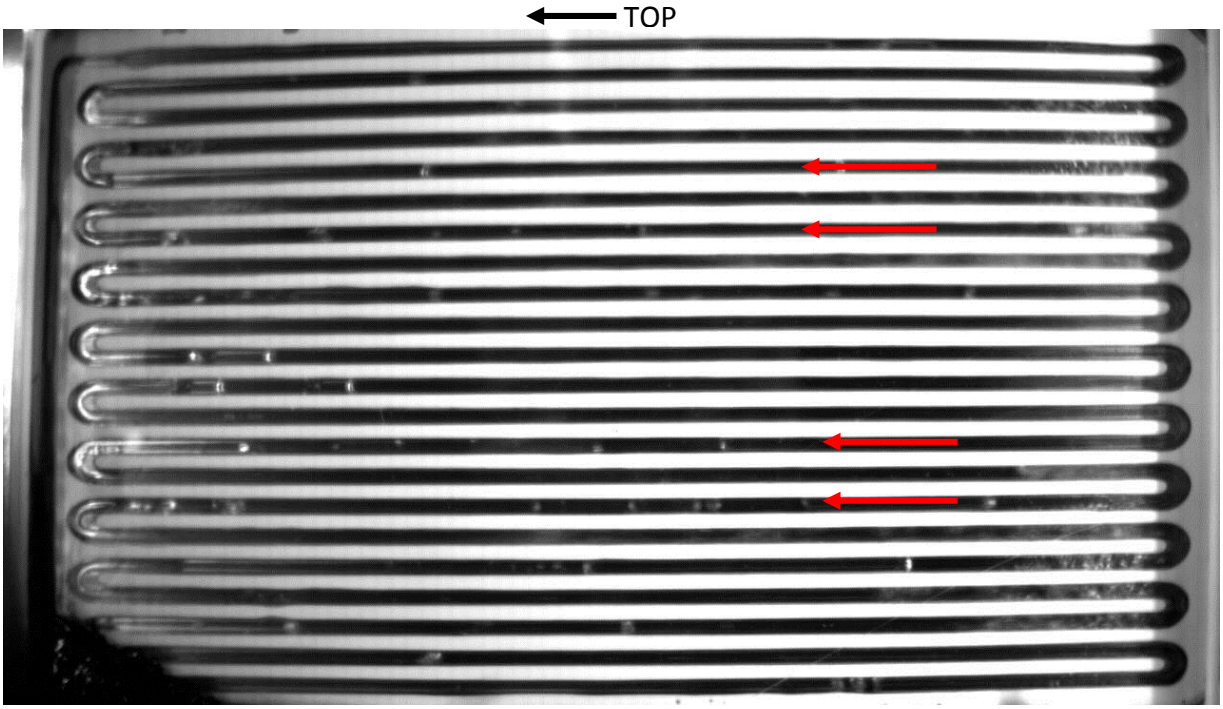

Figure 6.22: Typical fluid distribution and flow pattern during the activation in microgravity at 150W (parabola 23). Slug and plug flow regime on the condenser zone and annular after the evaporation (red arrow)

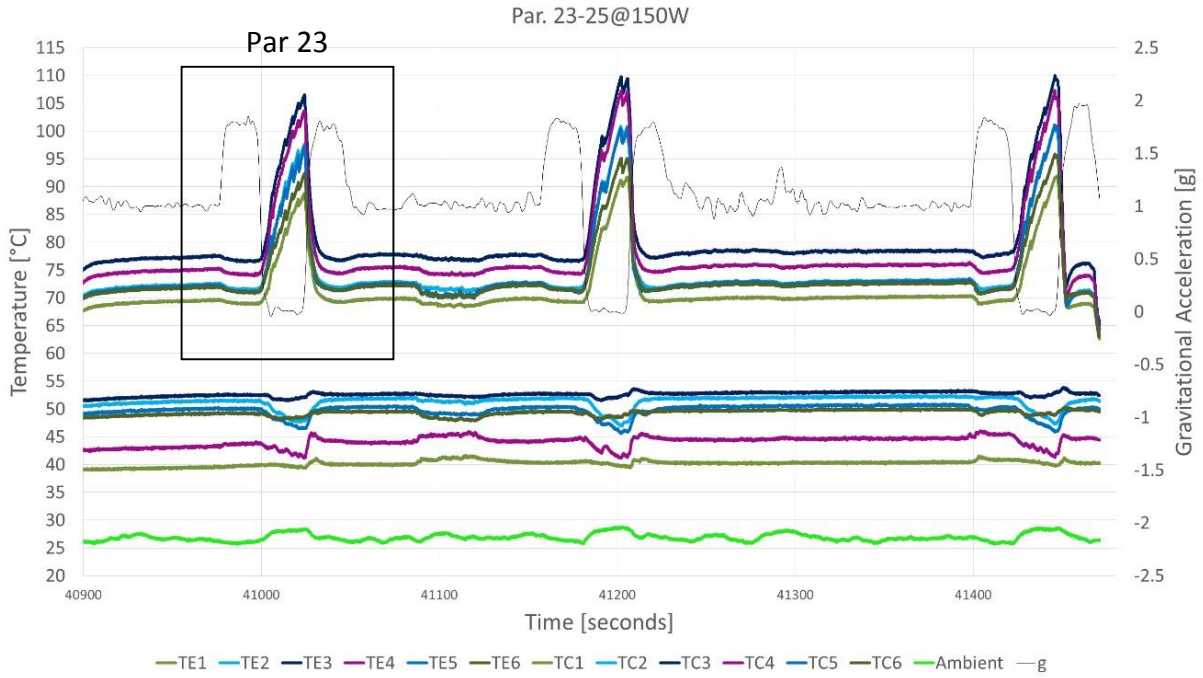

Figure 6.23: Temperature and gravitational acceleration of day 3, series 5, parabola 23-25 at 150W.

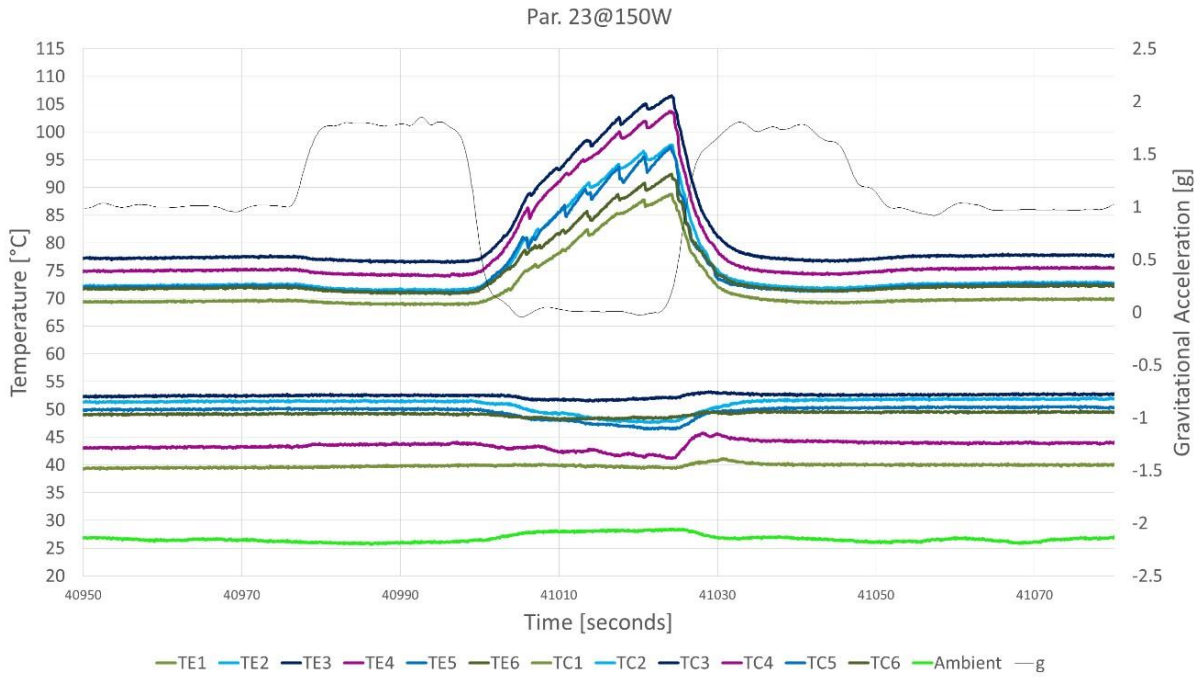

Figure 6.24: Temperature and gravitational acceleration of day 3, series 5, parabola 23 at 150W.

6.3 Clock synchronization

An important data processing step is about the clocks synchronization.
The time data were recorded by three different systems: the compactRIO read the system clock time from the laptop, the camera read the system clock time from the NUC PC and the acceleration data given by Novespace referred to the UTC (Coordinated Universal Time).
At the end of the last parabola of each day, in order to have a correct reference point, some extra video were shot just to have a reference time and marking at the same time a reference on the data by reducing the power. This procedure was repeated five times in order to have the least possible error.
For the synchronization, the time of each video was compared to the time when the power was reduced on the data. The minimum value of delay among the five synchronization records was the one taken in consideration for the analysis.
During the parabolic flight some problems with the g-sensor mounted on the rack occurred. Due to some vibrations the accelerometer connection occasionally failed, causing the loss of the signal at random.
At the end of each parabolic flight, Novespace shared their record of acceleration during the flight. In order to substitute our acceleration value with the Novespace one, a graphic comparison was made.
Due to the different sampling frequency, both acceleration data sets had to be referred to the beginning of the parabola under investigation and not to the absolute time. The acceleration value was in a different scale too. In fact, the g-sensor mounted on our rack gave a value in volt while the Novespace data gave directly the acceleration referred to the standard gravity acceleration.
The two curves were matched on a graphic by shifting the time of one of the two curves. When the matching was nearly perfect, the delay time between the two clocks was the same applied to match the two curves. This procedure was repeated for two parabolas as distant as possible on the same day to verify the value.
The Novespace acceleration data has also the advantage to be easier to read on the graphic, due to its lower sampling frequency compared to the data given by our sensor.
All the procedure of synchronization were repeated for all the three days of parabolic flight.

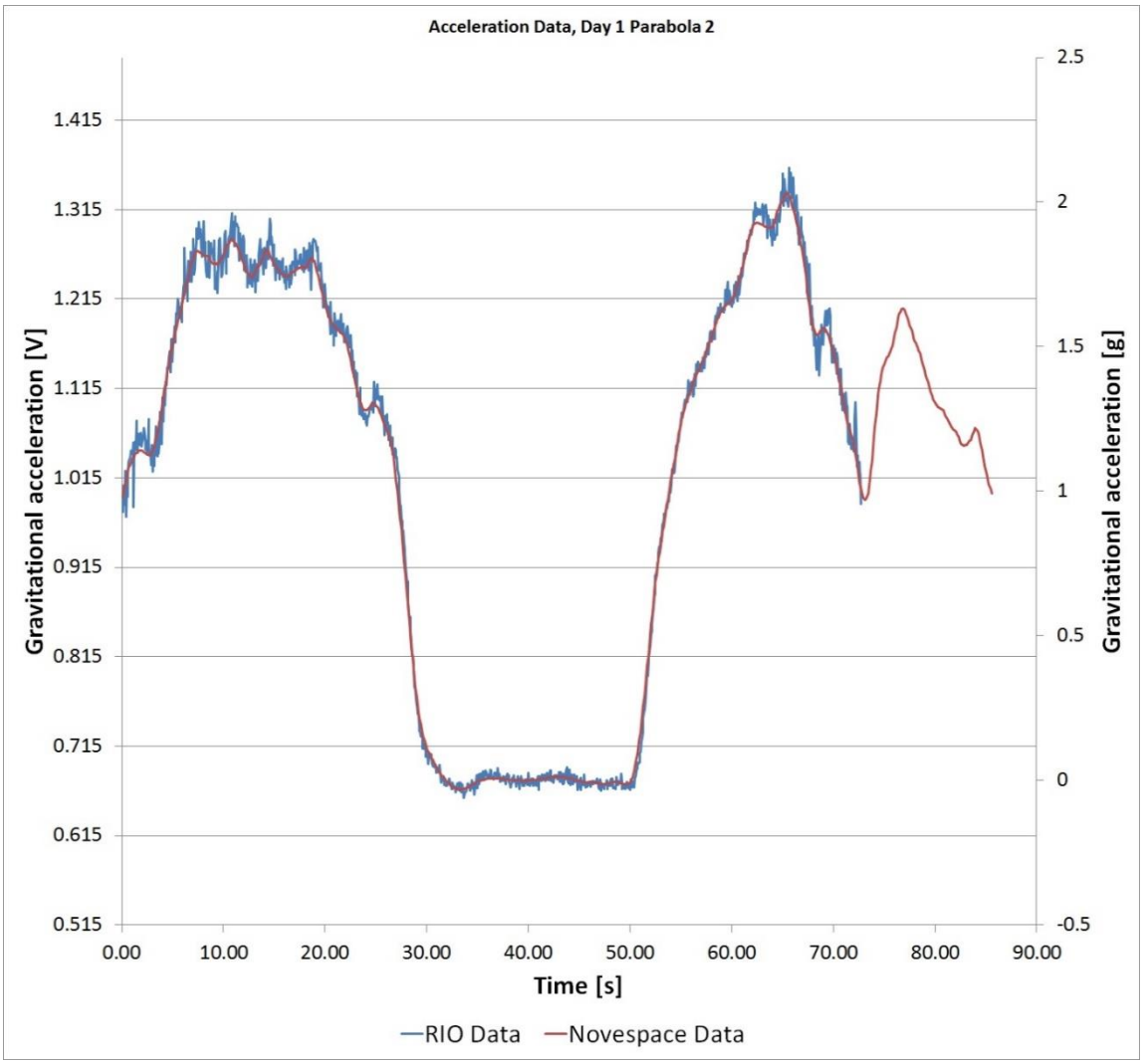

Figure 6.25: Synchronization between the two gravitational acceleration. One, was recorded by the sensor mounted on the experimental rack (RIO Data) the other was given by the Novespace.

6.4 Parabolic flight results

During this parabolic flight campaign, some important data were collected.
As seen during the ground tests, in normal gravity and hyper gravity, the PHP behaved like an interconnected two-phase thermosiphon.
In microgravity condition the situation was different, because a series of dry out and activations occurred.
The video recorded data show that the flow pattern in microgravity condition was different depending on the heating power level.
With low heat power, the flow pattern was slug and plug for all the channels, as it is possible to see in figure 6.26 or figure 6.13. This kind of fluid motion was verified up to 70W.

Figure 6.26: Typical flow pattern in microgravity for medium-low heat power. Frame of the parabola number 9 on the second day of parabolic flight (70W).

With a higher heating power level, the flow regime was different between evaporator and condenser. While in the condenser it continued to be slug and plug, in the evaporator and in the lower part of condenser, it became annular. The cause of this change could be found in the breakage of the menisci at high vapour velocities. With high heat power, the fluid velocity was high, leading to the menisci breakage. Gradually the bubbles moved to the upper part of the

condenser while the vapour condensed and the speed decreased, allowing the re-establishment of a slug and plug motion.
In figure 6.27 it is possible to notice the annular flow in the evaporator zone with a heat power level of 90W in microgravity condition.

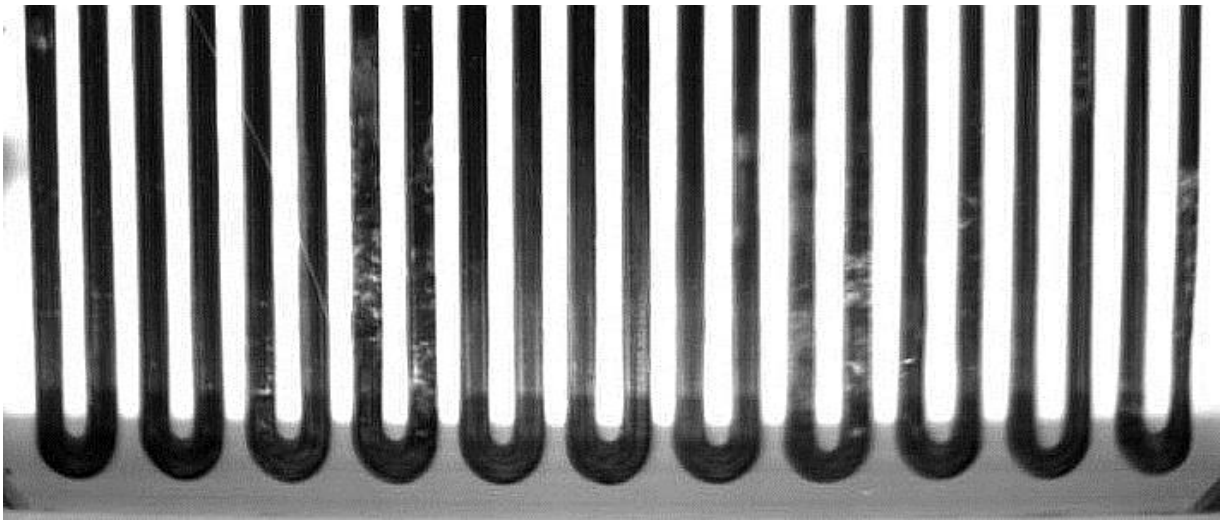

Figure 6.27: Typical flow pattern in the evaporator zone in microgravity for medium-high heat power. Frame of the parabola number 13 on the second day of parabolic flight (90W).

Some dimensionless quantity can be useful to evaluate the fluid motion inside the channels.
The bond number (as already seen in paragraph 1.3.1) is defined as:

$$Bo = \frac{Dh\,(\rho l - \rho v)g}{\sigma}$$

In this way it is possible to evaluate the possibility to maintain the slug and plug configuration and avoid the breakage of the liquid slugs caused by the body forces.
It does not consider the inertial forces nor the viscosity effect leading to transversal velocity profiles, thus limiting its evaluation possibilities to a stagnant or very slowly fluid motion.
The ratio between inertial and capillary forces is indicated by the Weber number:

$$We = \rho_l u_l^2 \frac{D}{\sigma}$$

Where u is the fluid velocity. In this case, in presence of We>>1 the inertial forces dominate the capillarity ones and the breakage of the menisci could happen causing the annular flow inside the channel. In the We number does not appear the gravitational acceleration, so it is impossible to understand the different functioning between microgravity and normal gravity condition.

A dimensionless quantity which can link all the interesting parameter is the criterion proposed by Garimella (2013) defined as:

$$Ga = Re_l\sqrt{Bo}$$

Where Re_l is the Reynolds number for the liquid phase.

$$Re_l = \frac{\rho_l u D}{\mu_l}$$

Where μ is the cinematic viscosity for the liquid phase.

It was experimentally found that for a value of Ga≤160 the fluid regime inside the channel could be slug and plug.

The main difficulty is to obtain a value of velocity from the video we recorded. It could be possible in further developments with different video recording devices suitable for quantitative measurements.

The operative temperature collected, when analysed in the light of the video recordings, show clearly how the fluid distribution or flow conditions, namely dry-out, annular flow, slug and plug flow, pool boiling, liquid storage, have a fast and often easy recognizable effect on the temperatures variations.

A more detailed analysis of the temperature data is the subject of the next chapter where a quantitative characterization of the PHP performance is reported.

7 Data analysis

An important parameter to compare the different performances of the tested PHP through the various tests is the equivalent thermal resistance R_{eq}. It represents the capacity of the device to dissipate the heating flux transferred to the fluid on the evaporator zone.
The equivalent thermal resistance is defined as:

$$Req = \frac{Teva - Tcond}{Q} \ [K/W]$$

Where:

- Teva: average temperature of the six evaporator thermocouples [°C or K]
- Tcond: average temperature of the six condenser thermocouples [°C or K]
- Q: heating power level [W]

The average temperature was calculated considering the arithmetic mean temperature of the six thermocouples (evaporator or condenser) during five seconds of functioning with the PHP in a pseudo-steady state.
For each R_{eq} it was also calculated its standard deviation (σ). All the values of standard deviation calculated for each thermocouple were combined by the arithmetic mean. They were not combined using the root mean square because all the σ were not unrelated each other, indeed, it was possible to notice more or less the same variations of temperature for all the thermocouples simultaneously. Therefore, the σ did not show an error but only a distribution of values. The hypothesis of casual combination of errors is not valid in this case, so the total standard deviation is not the root mean square of the standard deviation but it is calculated by the arithmetic mean.

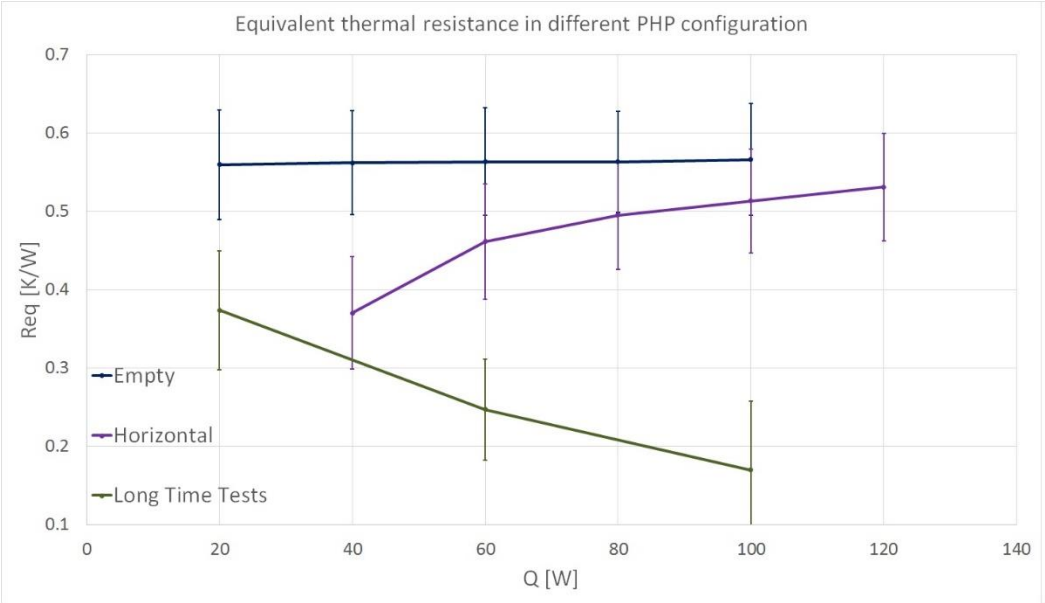

Figure 7.1: Diagram of the equivalent thermal resistance of the PHP in different configurations: empty, horizontal position and vertical position bottom heated. Vertical bars report the data dispersion at 1 sigma

In the Figure 7.1 the variations of the equivalent thermal resistance for different power levels in different PHP configurations are shown: empty, horizontal and vertical bottom heated.
In the "empty" configuration, the PHP was tested in a vacuum condition without the fluid inside the channels (FR of 0%). In this configuration it was checked the performance in a pure conduction mode along the metal walls of the empty fluid channels.
At low heat power, the R_{eq} of the filled PHP was similar both for the horizontal and the vertical configuration, and 35% lower than the empty PHP. As the power at the evaporator increased, in the horizontal configuration (as seen in paragraph 5.2), the evaporator zone went progressively in a dry out condition with all the fluid in the condenser zone. In this situation, due to the low evaporation, the value of the R_{eq} was close to the value with the empty PHP.
With the PHP in a vertical position bottom heated configuration the situation was the opposite. The R_{eq} decreased strongly at less than its initial value with the increase of the power level. During these experiments a thermal crisis never occurred, so the value of the equivalent thermal resistance reached the lower value with the highest heating power.

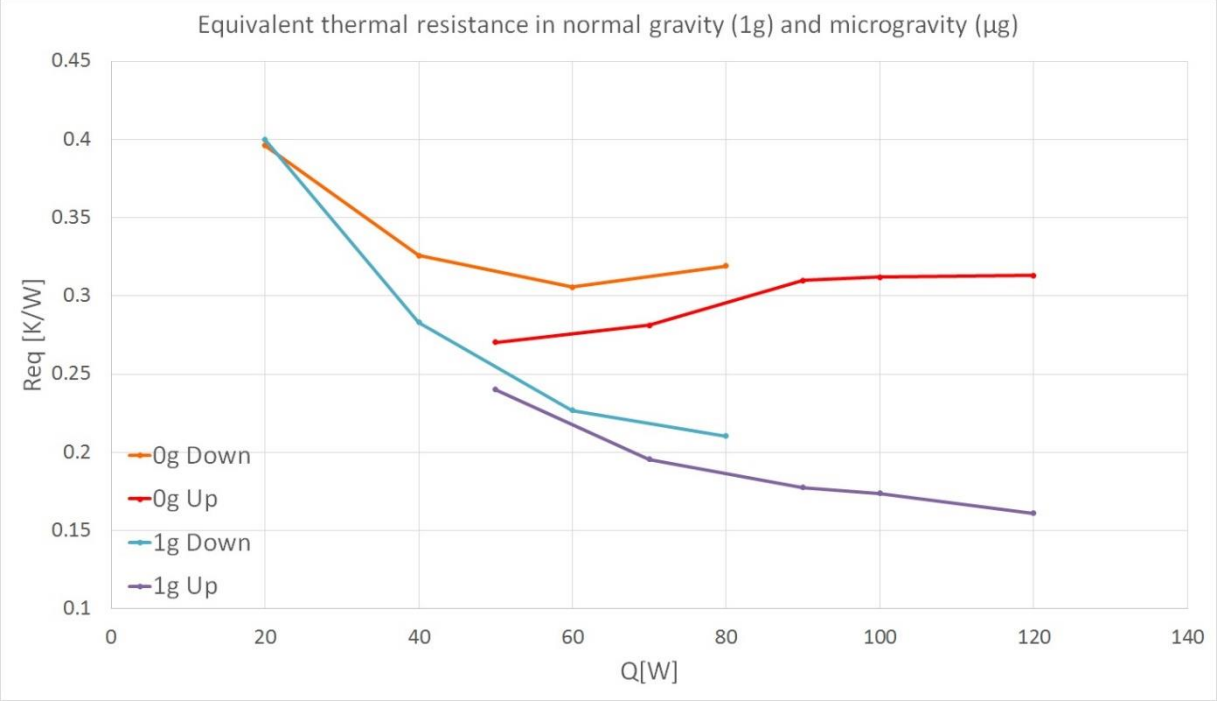

Figure 7.2: Diagram of the equivalent thermal resistance of the PHP during the parabolic flight tests in different gravity condition. Up and Down refers to test performed with increasing or decreasing power levels, to check for hysteresis effects.

In the figure 7.2 the variations of the equivalent thermal resistance for different power input levels in normal gravity condition and microgravity are shown. The graph reports the results obtained during different days of testing, during which the power levels were tested once by increasing steps, and once by decreasing steps, thus allowing also to identify and measure the presence of hysteresis effects.

It is easy to notice how, during the microgravity phase, the performances of the PHP fell down. This was due to the absence of the gravity which did not assist the return of the liquid on the evaporator zone during the microgravity phase.

The difference of R_{eq} between normal gravity condition and microgravity increased for higher power. This happened because during the microgravity phase at higher power, as seen in paragraph 6.2, the PHP was mainly in a dry out condition on the evaporator zone with some short activations. This was different for lower power, where the succession of dry out and slug and plug flow was more homogeneous.

The sigmas are not shown in the figure 7.2 because they are only significant in the presence of a Gaussian distribution and not for a bimodal distribution as in this situation (one temperature is referred to a dry-out condition and one to a liquid temperature).

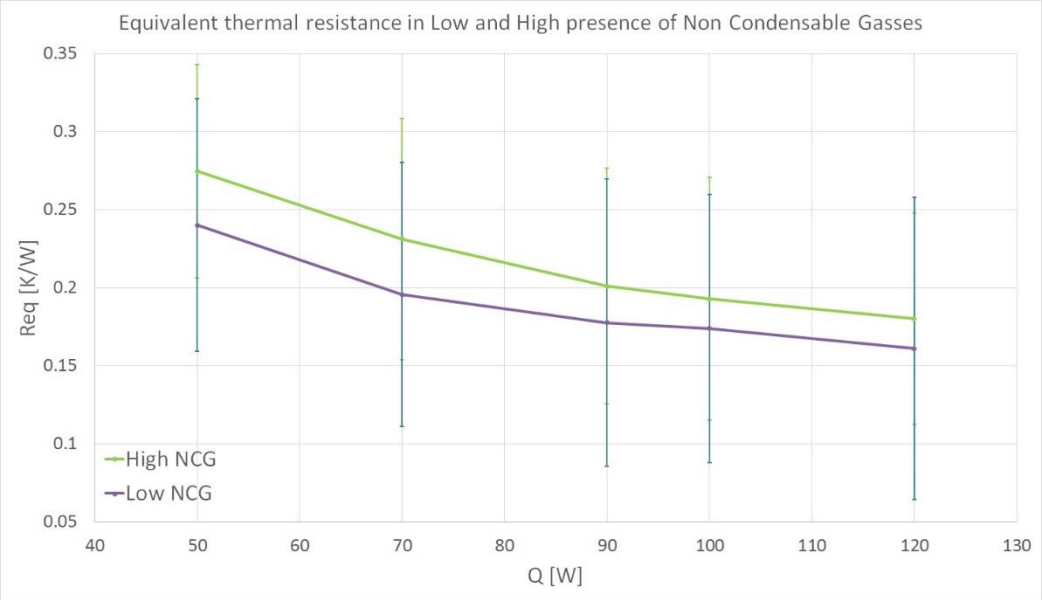

Figure 7.3: Diagram of the equivalent thermal resistance of the PHP during the parabolic flight tests with different quantity of non condensable gasses (NCG) inside the channels

In the figure 7.3 the variations of the equivalent thermal resistance for different power levels in normal gravity condition and different presence of non condensable gasses (NCG) are represented. The data with a low presence of NCG were recorded during the “mid-high test” in parabolic flight (day two), the ones with a high presence of NCG were recorded in the “highest power test” in parabolic flight (day three).

It is possible to notice how the highest presence of non condensable gasses negatively influenced the performance of the PHP causing an higher value of R_{eq}.

The non condensable gasses are mixed with the saturated vapour, artificially increasing the pressure of the vapour bubbles and the corresponding saturation temperature for the fluid to evaporate, which caused the increase of the equivalent thermal resistance.

8 Conclusions

A semi-transparent flat plate pulsating heat pipe has been tested in laboratory and in hyper gravity and microgravity conditions during the 62nd ESA parabolic flight campaign.
The main aim of these tests was to observe the different flow patterns between normal gravity and microgravity at a wide range of heating power. The main peculiarities of this PHP is to have a face completely transparent and to have a channel cross-section with a hydraulic diameter larger than the critical one.
There were just a few minor complications due to the troublesome building process of gluing glass and copper, in order to match all the requirements seen in paragraph 3.2.1.2.
However, the result was satisfactory even if not perfect. The main problem was the small leakage of seal that let a small amount of air penetrate inside the channel. “Thanks” to this problem, it was also possible to notice the different functioning between a condition with and one without the presence of a considerable quantity of non condensable gasses inside the channel.
The main observations to be drawn from this set of results are:

- In a normal gravity condition with the PHP in a vertical position and bottom heated, it behaved like an interconnected two-phase thermosiphon. Due to some thermal heterogeneities in the device, which was hotter in the centre and colder on the sides, the liquid tended to accumulate on the sides, while the central channels were quite dried-out. This phenomenon led to some annular flow with very few liquid in the centre, and pool boiling on the edge channels. The slug and plug flow regime never set up. On hyper gravity the behaviour was similar to normal gravity.
- On microgravity, the fluid immediately organized itself in slug and plug. During this phase it was observed a continuous succession of dry out phases with the stop of the fluid motion and activations which brought the liquid back on the evaporator zone.
  The activations started apparently at random from one channel and propagated to the next one until the next dry out phase.
- It was noticed the considerable positive influence of the microgravity phase for a more homogeneous distribution of the liquid through the channels. Thanks to this, it was possible to pass from a condition of dry out and liquid storage to a condition of annular flow after few passages in microgravity.
- During the horizontal test in laboratory, it was noticed the immediate dry out of the evaporator. The cause of this was the perpendicular direction of the gravity force on

the copper plate together with the large hydraulic diameter. Thanks to the difference of pressure inside the liquid due to the gravity, added to the capillary pressure, some liquid was pushed on the evaporator zone, avoiding the unwanted thermal crisis.

The data collected and post-processed allows to calculate some relevant characteristics of the studied PHP, like its equivalent thermal resistance. When possible, the source of errors and result dispersion are identified, calculated and reported. The visualization of the fluid flow allows to verify some proposed correlation between the fluid pattern ad the leading dimensionless quantity that have been recently proposed in the literature.

8.1 Future Developments

For the future development, there are already some ongoing projects to conduct to test different solutions.

One is to test a similar PHP with the same hydraulic diameter but with water like working fluid. This allow to have a hydraulic diameter largely below the critical one (around 5mm) and allow a disposition of the fluid in slug and plug also in normal gravity condition.

Another PHP will be made in order to have a hydraulic diameter close to critical one.

The influence of different cold source will be also analysed, to investigate also the influence of the activation of nucleation sites. They will be tested different PHP varying the condenser in terms of surface, position (increasing or decreasing the adiabatic zone) or temperature. In order to perform this experiment some Peltier elements will be used.

On the visualization side a new camera will be used in order to have a higher resolution and have the possibility to apply quantitative image analysis on the capillary effects, and flow velocity, to be used also as validation data for CFD simulations.

Annex 1

Here below is reported all the temperature plot of the all series recorded during the 62nd parabolic flight campaign. For the thermocouple disposition see figure 3.5 p.47.

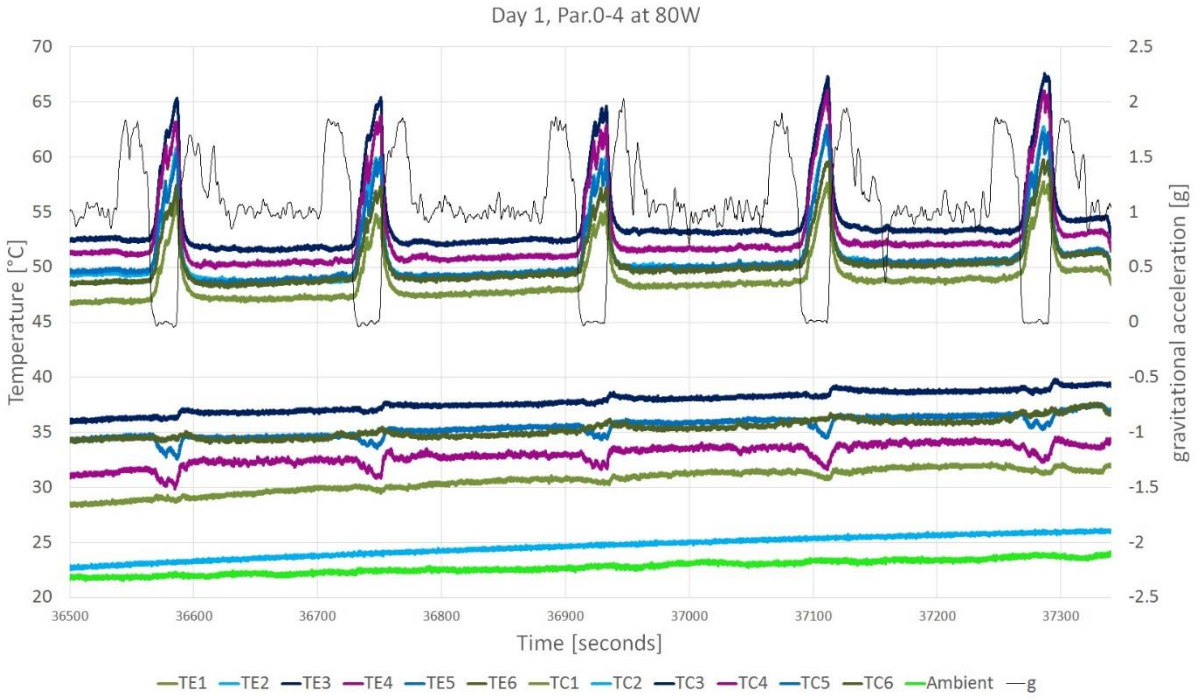

Figure A.1: Temperature and gravitational acceleration of day 1, series 1 at 80W.

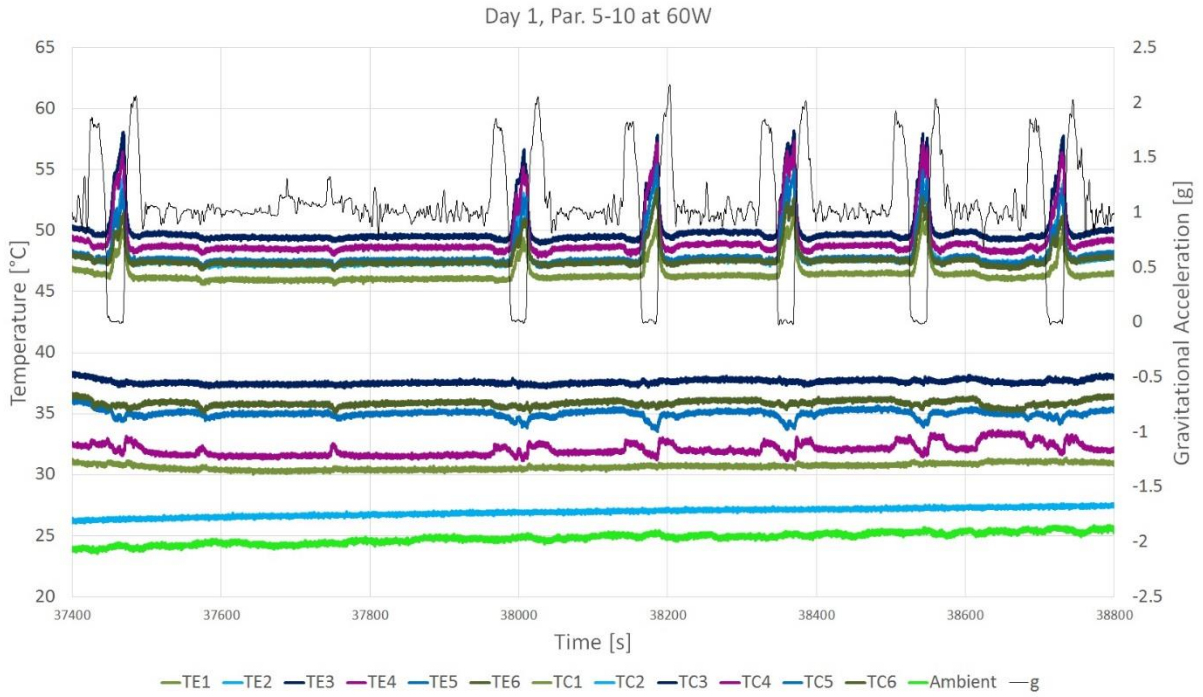

Figure A.2: Temperature and gravitational acceleration of day 1, series 2 at 60W.

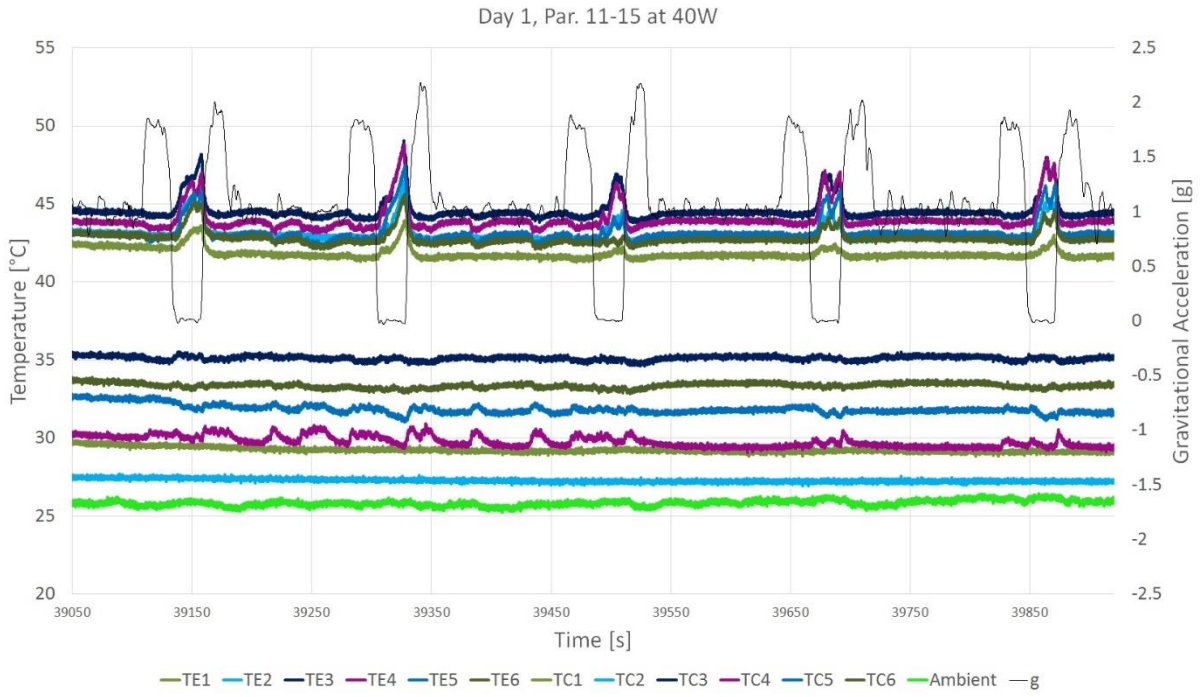

Figure A.3: Temperature and gravitational acceleration of day 1, series 3 at 40W.

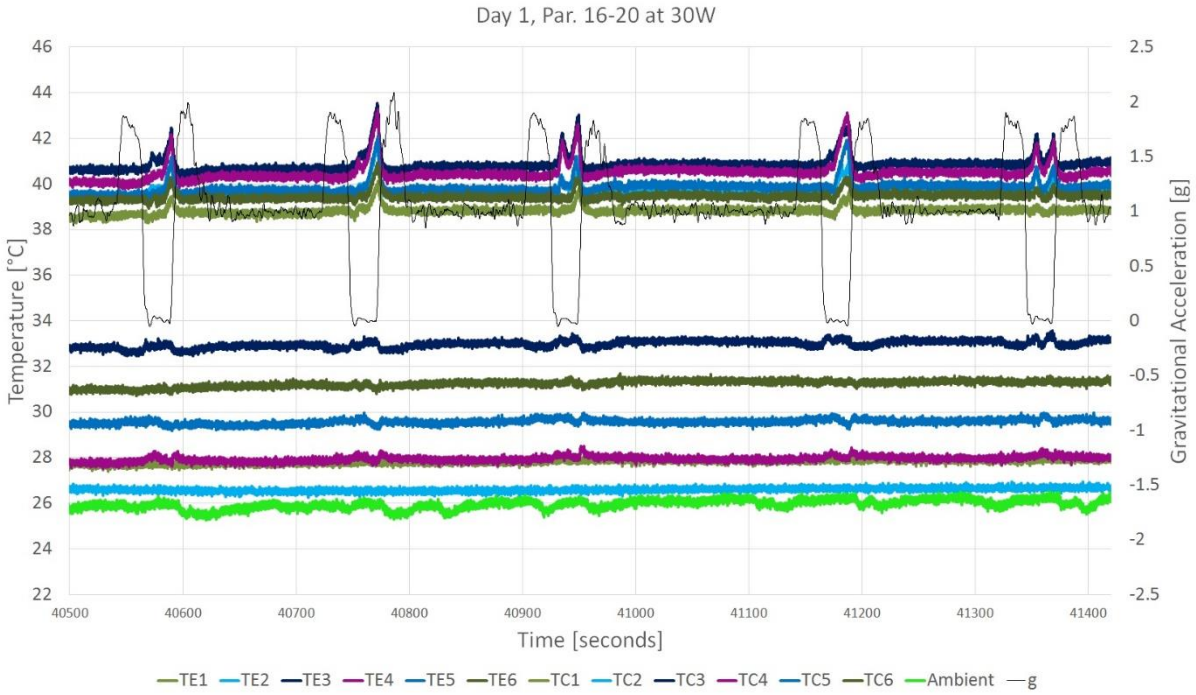

Figure A.4: Temperature and gravitational acceleration of day 1, series 4 at 30W.

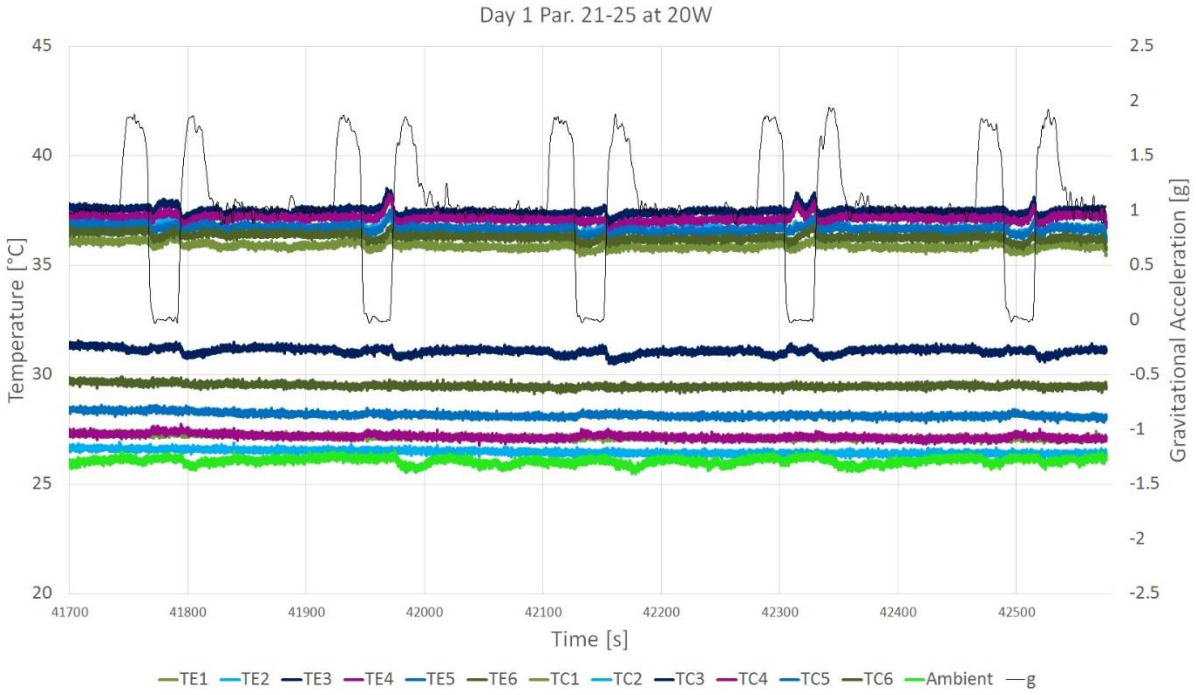

Figure A.5: Temperature and gravitational acceleration of day 1, series 5 at 20W.

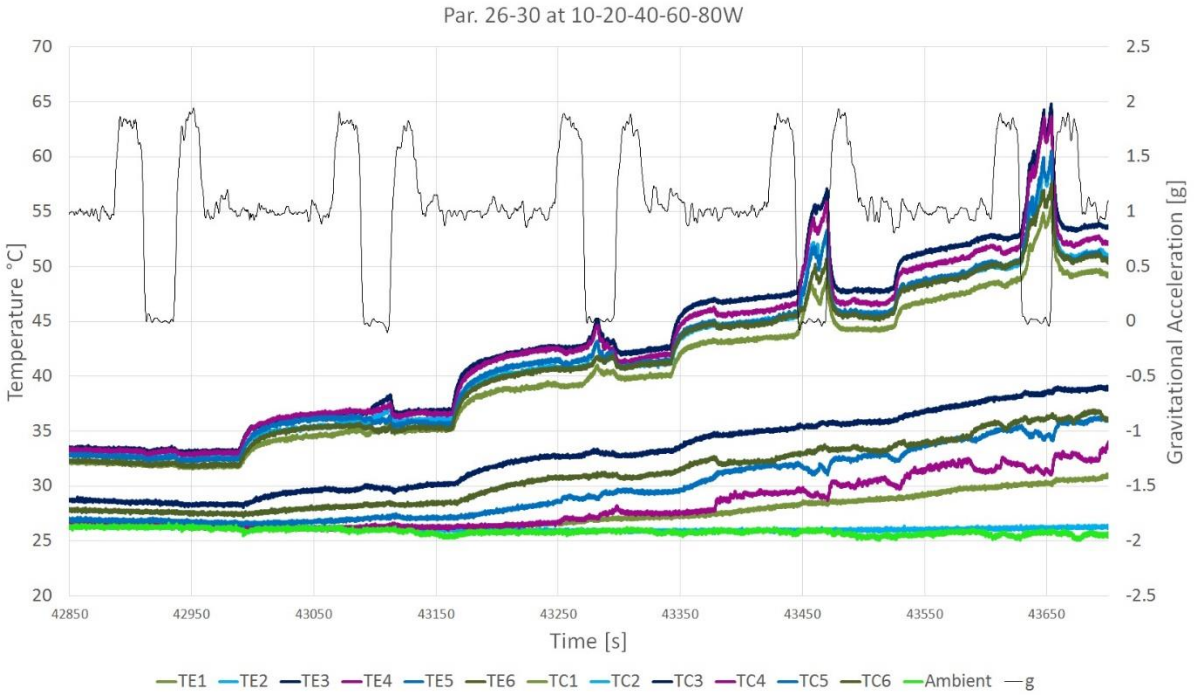

Figure A.6: Temperature and gravitational acceleration of day 1, series 6 at: 10W (Par.26), 20W (Par.27), 40W (Par.28), 60W (Par. 29), 80W (Par. 30).

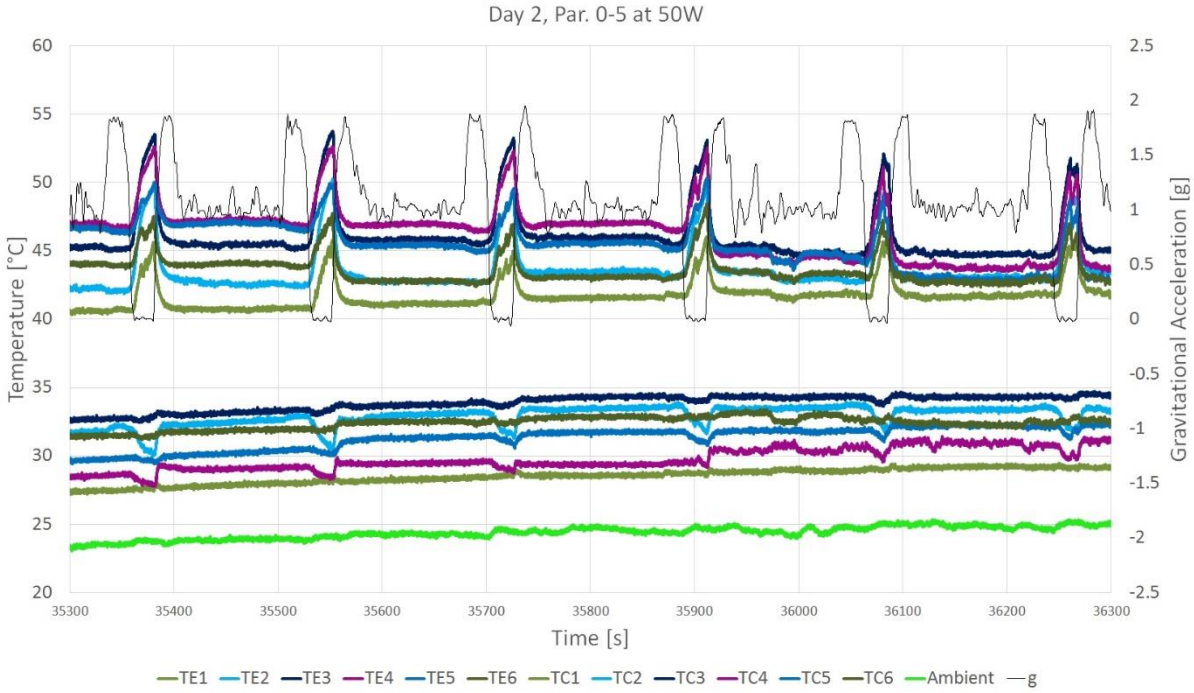

Figure A.7: Temperature and gravitational acceleration of day 2, series 1 at 50W.

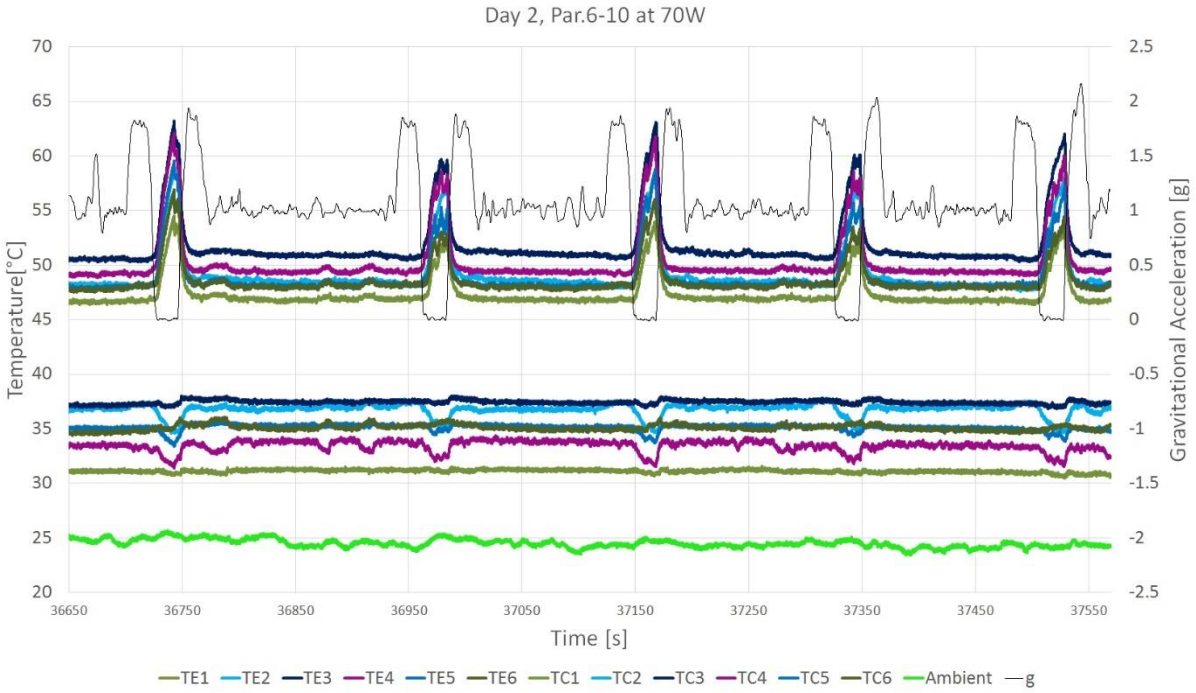

Figure A.8: Temperature and gravitational acceleration of day 2, series 2 at 70W.

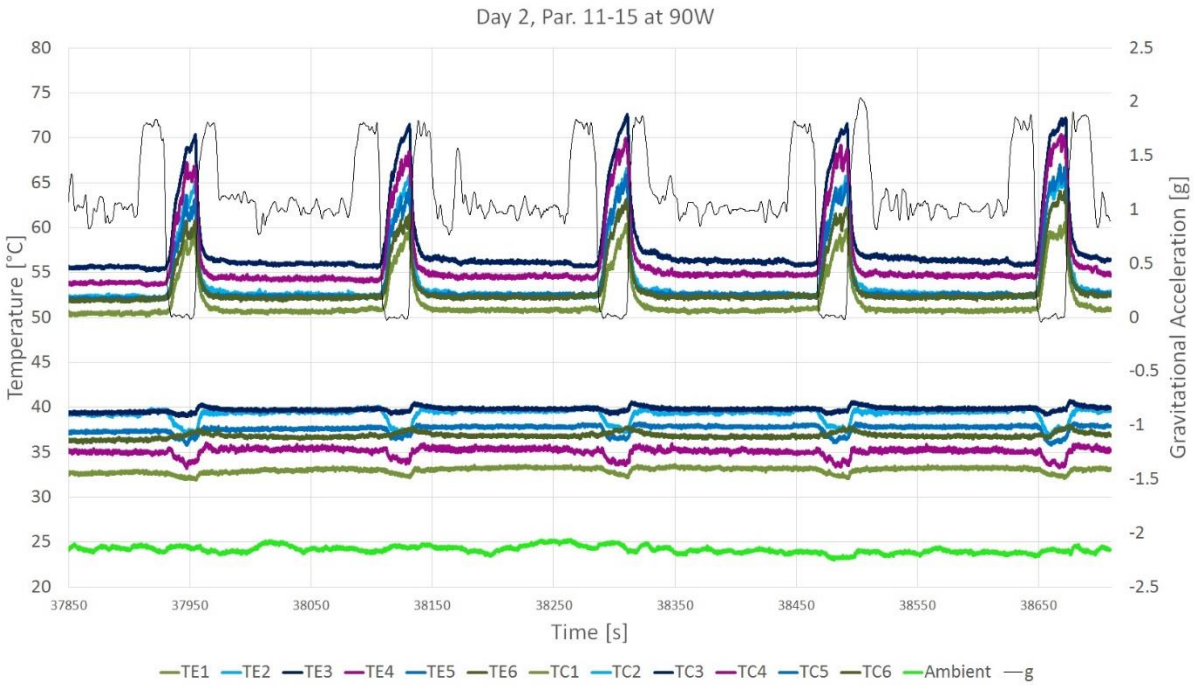

Figure A.9: Temperature and gravitational acceleration of day 2, series 3 at 90W.

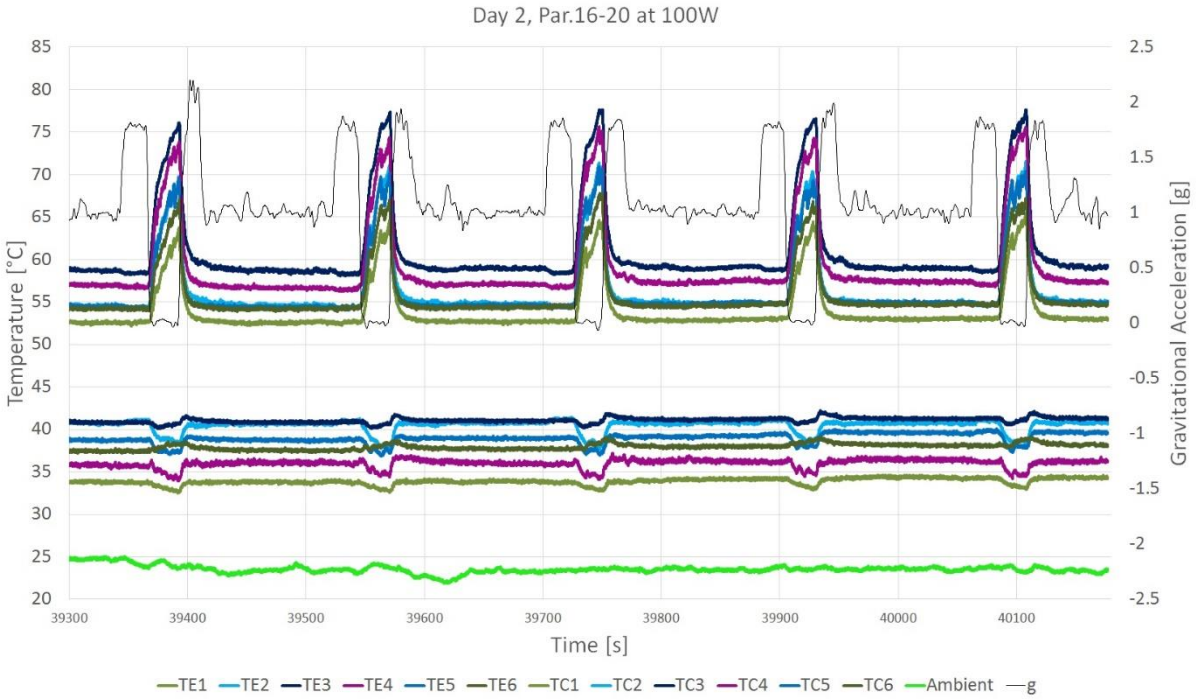

Figure A.10: Temperature and gravitational acceleration of day 2, series 4 at 100W.

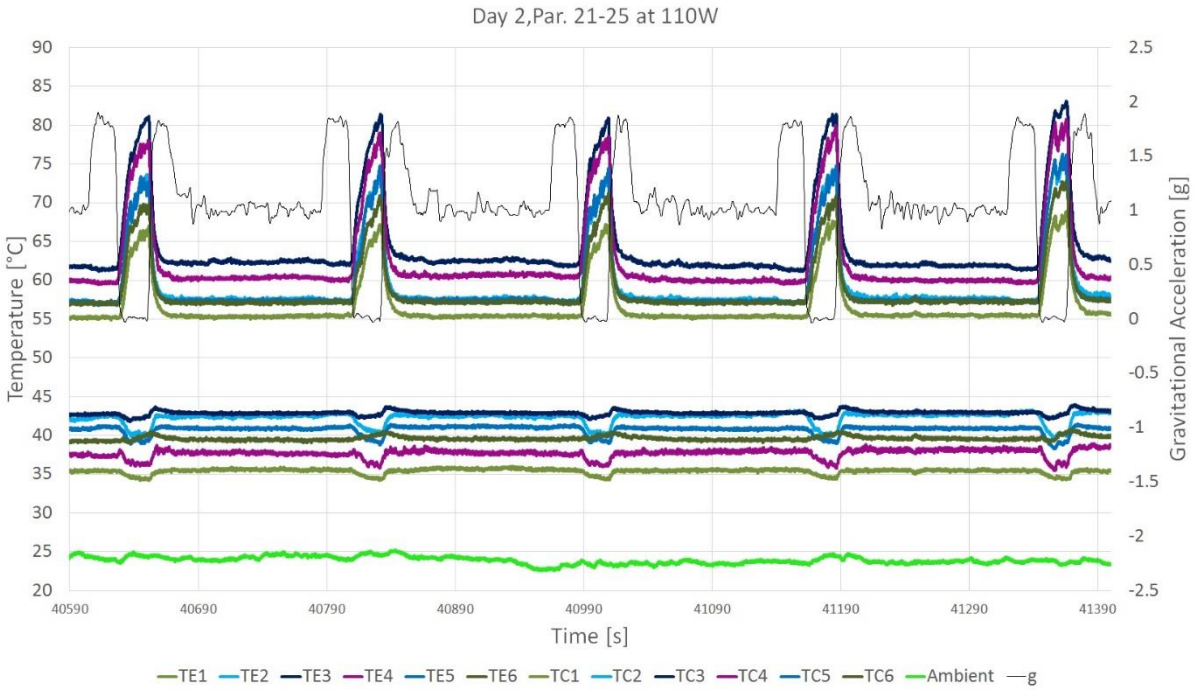

Figure A.11: Temperature and gravitational acceleration of day 2, series 5 at 110W.

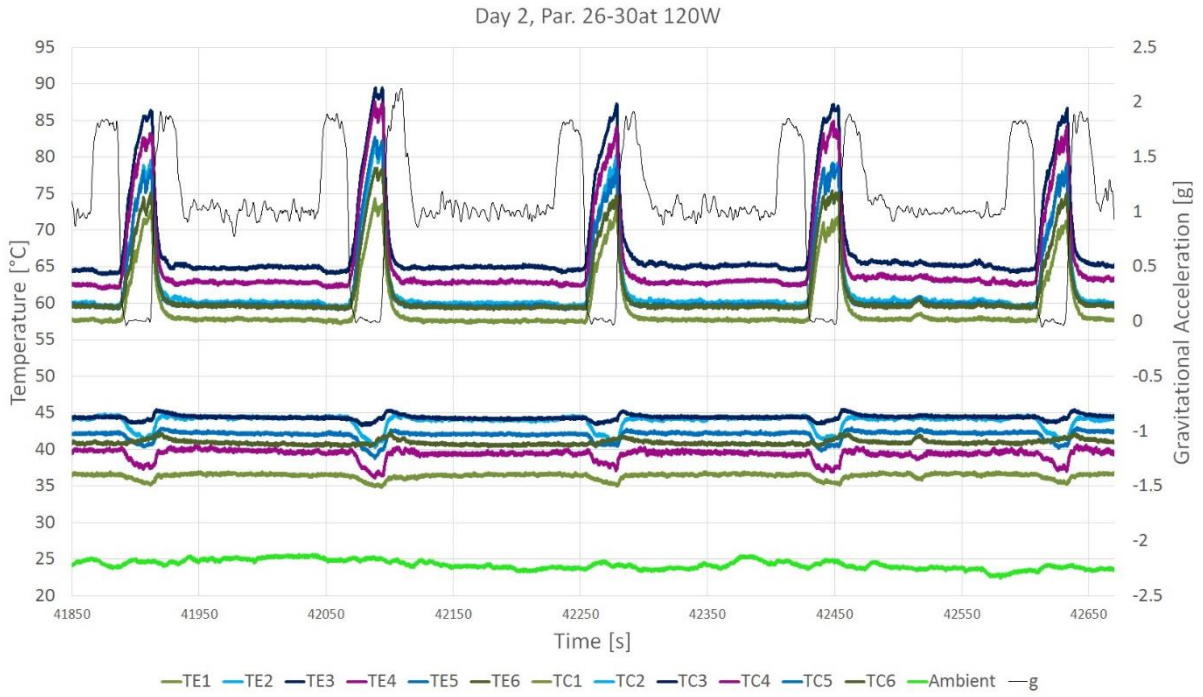

Figure A.12: Temperature and gravitational acceleration of day 2, series 6 at 120W.

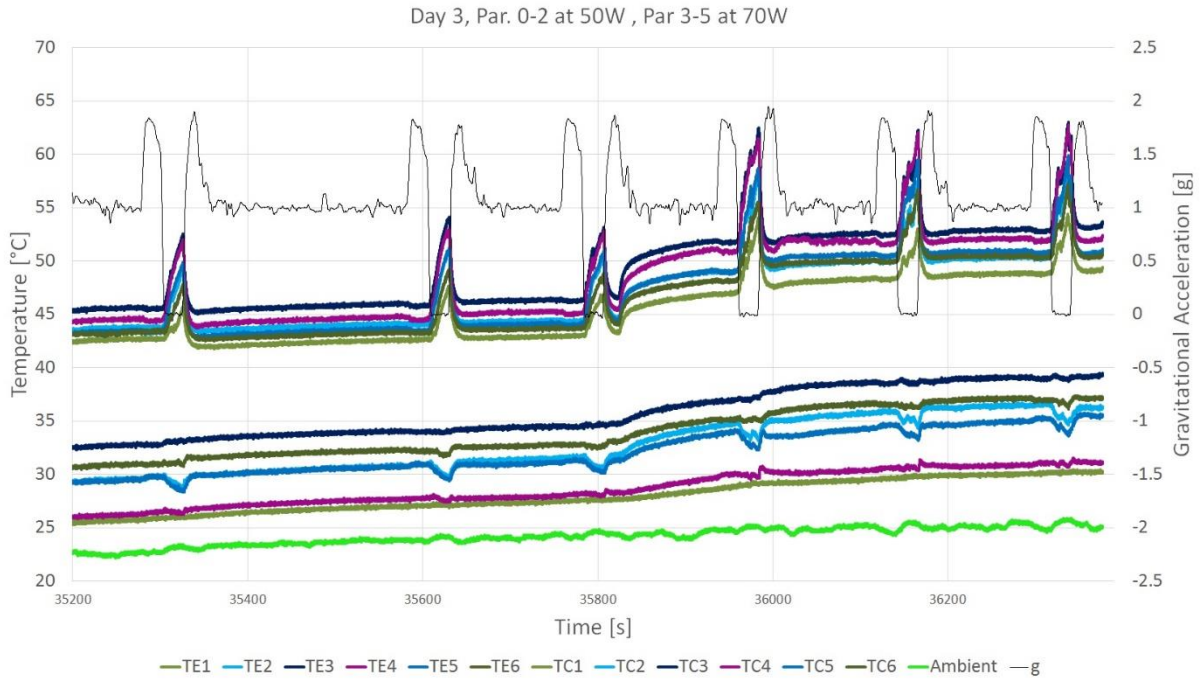

Figure A.13: Temperature and gravitational acceleration of day 3, series 1 at: 50W (Par. 0-2), 70W (Par. 3-5).

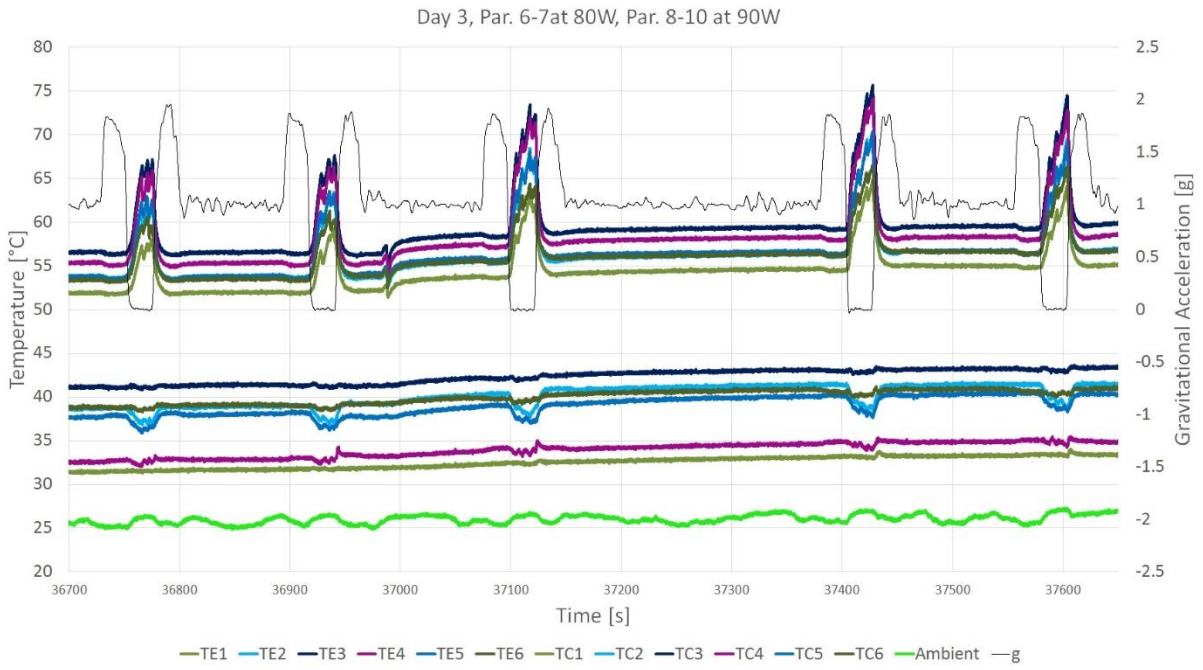

Figure A.14: Temperature and gravitational acceleration of day 3, series 2 at: 80W (Par. 6-7), 90W (Par. 8-10).

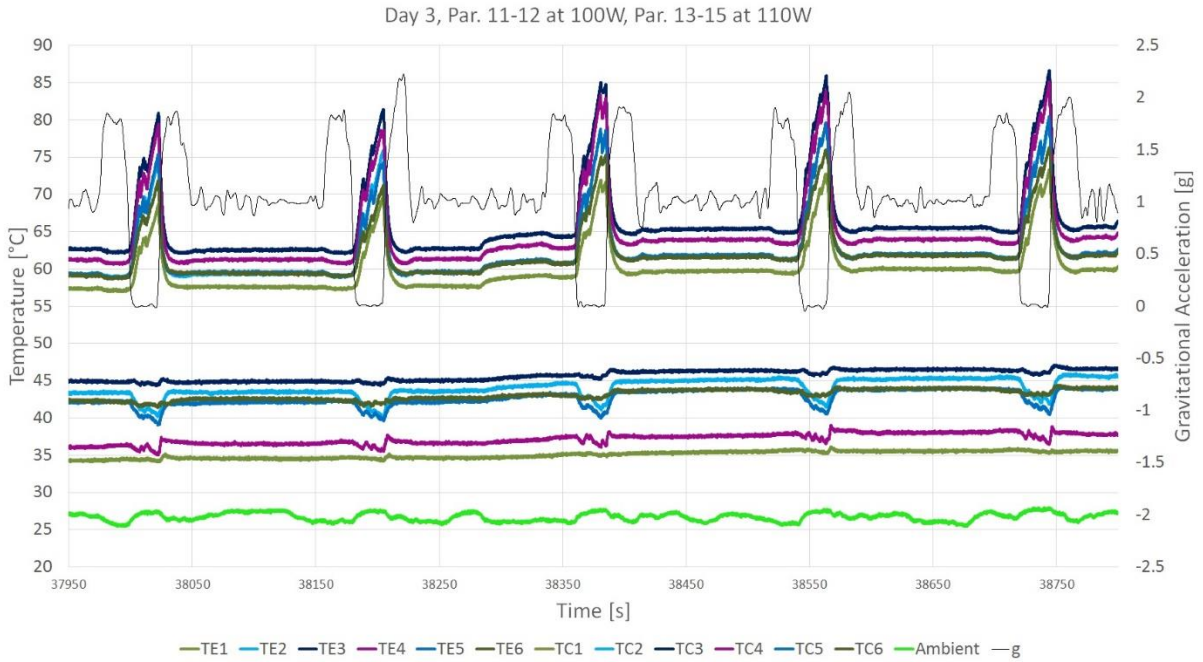

Figure A.15: Temperature and gravitational acceleration of day 3, series 3 at: 100W (Par. 11-12), 110W (Par. 13-15).

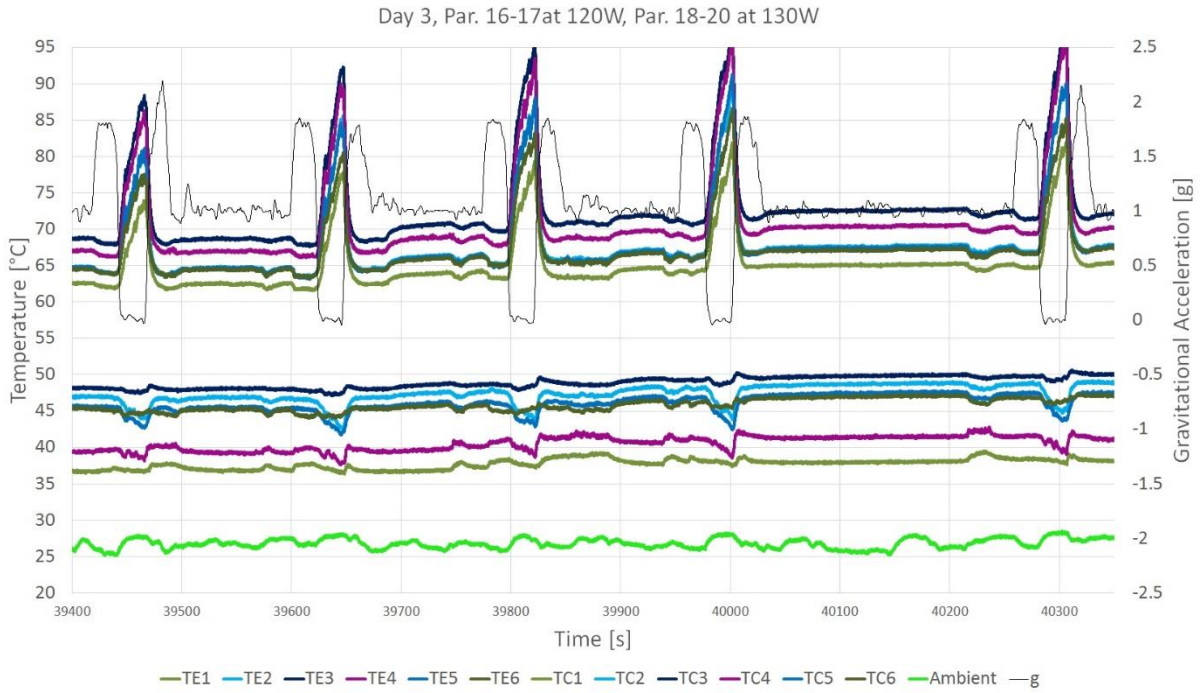

Figure A.16: Temperature and gravitational acceleration of day 3, series 4 at: 120W (Par. 16-17), 130W (Par. 18-20).

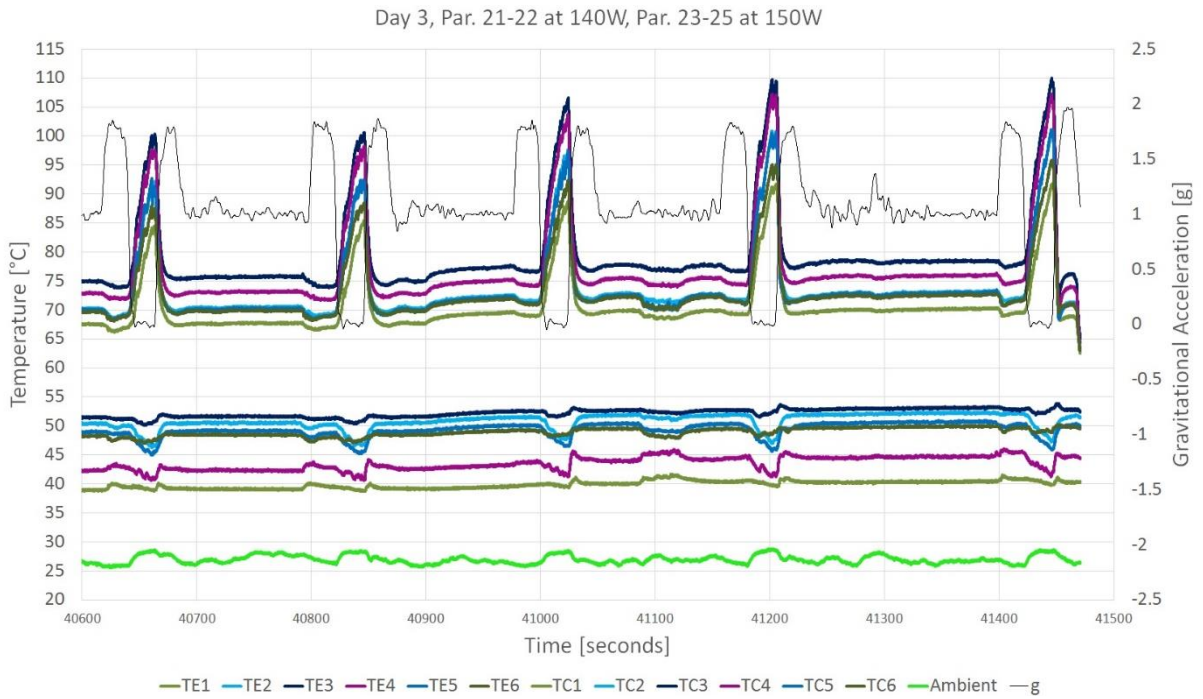

Figure A.17: Temperature and gravitational acceleration of day 3, series 5 at: 140W (Par. 21-22), 150W (Par. 23-25).

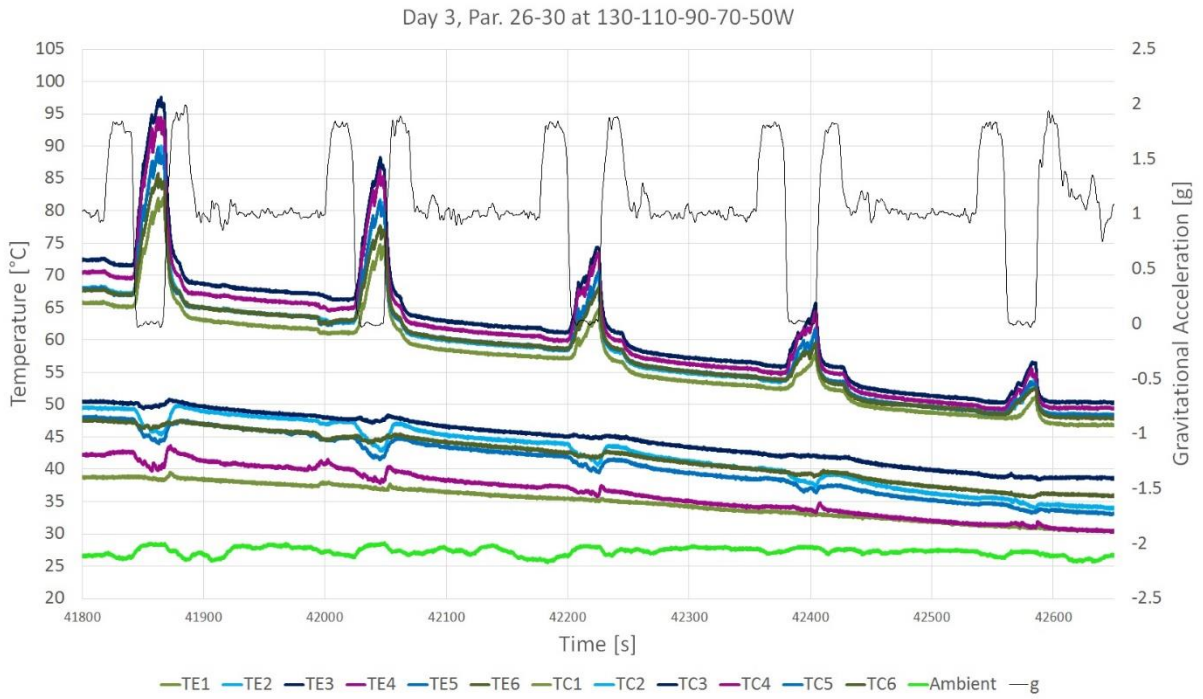

Figure A.18: Temperature and gravitational acceleration of day 3, series 6 at: 130W (Par. 26), 110W (Par.27), 90W (Par. 28), 70W (Par. 29), 50W (Par. 30).

Figure Index

Table index

Nomenclature

P	Pressure	[N/m^2]
g	Acceleration of gravity	[m/s^2]
D	Diameter	[m]
Dh	Hydraulic Diameter	[m]
ρ	Density	[kg/m^3]
u	Fluid velocity	[m/s]
Re	Reynolds number	
σ	Surface tension	[N/m]
Fr	Froude number	
Bo	Bond number	
We	Weber number	
Ga	Garimella number	
μ	Dynamic viscosity	[kg·m^{-1} s^{-1}]
FR	Volumetric filling ratio	
Q	Heating power	[W]
T_e	Evaporator temperature	[°C]
R_{eq}	Equivalent thermal resistance	[K/W]
R_{eff}:	Hydraulic radius of the meniscus	[m]
Θ	Apparent contact angle between copper and liquid	

References

Akachi H., Pola´sˇek F., Sˇ tulc P. (1996). "*Pulsating heat pipes*". Proceedings of the Fifth International Heat Pipe Symposium, Melbourne, Australia, pp. 208–217.

Akachi H., (1990). Structure of a heat pipe. US Patent 4,921,041.

Ayel V., Araneo L., Scalambra A., Mameli M., Romestant C., Piteau A., Marengo M., Filippeschi S., Bertin Y., (2015). "*Experimental study of a closed loop flat plate pulsating heat pipe under a varying gravity force"*. International Journal of Thermal Sciences, Vol.96, pp. 23-34.

Ayel V., Romestant C., Bertin Y., Manno V., Filippeschi S., (2013). "*Visualisation of Flow Patterns in a Flat Plate Pulsating Heat Pipe: influence of hydraulic behaviour on thermal performances"*. 17th international heat pipe conference, Kanpur, India, October 13-17, 2013.

Araneo L., (2015). "*Thermo-hydraulics characterization of a semi-transparent flat-plate pulsating heat pipe in a variable gravity regime"*. Experiment Safety Data Package, Novespace, internal document.

Araneo L., Filippeschi S., Mameli M., Marelli L., Testa R., Marengo M., (2014). "*Thermal Response of a PHP under Varying Gravity*". International Journal of Thermal Sciences, Vol.80, pp.11-22.

Charoensawan P., Terdtoon P., (2008). "*Thermal Performance of Horizontal CLPHP*". Applied Thermal Engineering. Vol. 28, pp.460-466.

Charoensawan P., Khandekar S., Groll M., Terdtoon P., (2003). "*Closed loop pulsating heat pipes Part A: visualization and semi-empirical modelling"*. Applied Thermal Engineering, Vol 23, pp.2009-2020.

Gai F. (2013). *"A300 zero-G user guide"*. Novespace.

Garimella S.V., Harirchian T., (2013). *"Microchannel Heat Sinks for Electronics Cooling*", Vol. 1 in the Encyclopedia of Thermal Packaging, World Scientific, Singapore.

Gu J., Futamata, R. & Kawaji, M., (2004). "*Effects of Gravity on the Performance of Pulsating Heat Pipes"*. Journal of Thermophysics and Heat Transfer, 18(3), pp.370-378.

Henkel, (2014). Loctite adhesive 3609 technical data sheet.

Henry C.D., Kim J., Chamberlain B., (2004). "*Heater size and heater aspect ratio effects on sub-cooled Pool boiling heat transfer in low-g".* Third International Symposium on Two-Phase Flow Modeling and Experimentation Pisa, 22-24 September 2004.

Karimi G., (2004). "*Review and assessment of pulsating heat pipe mechanism for high heat flux electronic cooling in Electronic Systems"*, pp.52-59.

Khandekar S., (2010). "*Pulsating heat pipe based heat exchangers*". In Proc. 21st Int. Symp. Transport Phenomena, Kaohsiung City, Taiwan, 2-5 November, 2010.

Khandekar S., (2004). "*An insight into thermo-hydrodynamic coupling in closed loop pulsating heat pipes*". International Journal of Thermal Sciences, Vol 43, pp.13-20.

Khandekar S., Charoensawan P., Groll M., Terdtoon P., (2003). *"Closed loop pulsating heat pipes Part B: visualization and semi-empirical modelling*". Applied Thermal Engineering, Vol 23, pp.2021-2033.

Lock G.S.H., (1992). "*The Tubular Thermosyphon"*, Oxford: Oxford Univ. Press.

Mameli M., Mangini D., Vanoli G.F., Araneo L., Filippeschi S., Marengo M., (2015). "*Multi-evaporator closed loop thermosiphon"*. 7th European-Japanese Two-Phase Flow Group Meeting, Zermatt, Switzerland, 11-15 October, 2015.

Mameli M., Manzoni M., Araneo L., Filippeschi S., Marengo M., (2014). "*Experimental investigation on a closed loop pulsating heat pipe in hyper-gravity conditions"*. 15th International Heat Transfer Conference, Kyoto, Japan, August 10-15, 2014.

Mameli M., (2012). "*Pulsating heat pipes. Numerical Modelling and Experimental Assessment"*. Università degli studi di Bergamo, ISBN: 978-88-97413-05-9.

Nusil, (2014). Nusil adhesive CV7-2289-1P technical data sheet.

Rosier P., (2014). "*Novespace experiment design guidelines in parabolic flight"*. Novespace.

Scalambra A., (2014). "*Experimental study of a flat plate pulsating heat pipe in parabolic flights"*. Politecnico di Milano, MSc. Thesis, advisor Araneo L.

Verthier B. (2014). "*A310 zero-g interfaces document"*. Novespace.

Yang H., Khandekar S., Groll M., (2008). "*Operational limit of closed loop pulsating heat pipes"*. Applied Thermal Engineering, Vol. 28, pp.49-59.